On the constitutive behaviour of Sandvik Nanoflex™

Modelling, Experiments and Multi-stage Forming

This work was carried out in close co-operation with the NIMR.

Samenstelling van de promotiecommissie:

voorzitter en secretaris:
Prof. dr. ir. H.J. Grootenboer   Universiteit Twente

promotor:
Prof. dr. ir. J. Huétink   Universiteit Twente

assistent promotor:
Dr. ir. H.J.M. Geijselaers   Universiteit Twente

leden:
Prof. dr. ir. R. Akkerman   Universiteit Twente
Dr. J. Beyer   Universiteit Twente
Prof. J.-O. Nilsson   Chalmers University of Technology (Sweden)
Prof. L.-E. Lindgren   Luleå University of Technology (Sweden)
Dr. ir. R.M.J. Voncken   Philips Centre for Industrial Technology
Prof. dr. ir. S. van der Zwaag   Technische Universiteit Delft

ON THE CONSTITUTIVE BEHAVIOUR OF SANDVIK NANOFLEX™

MODELLING, EXPERIMENTS AND MULTI-STAGE FORMING

PROEFSCHRIFT

ter verkrijging van
de graad van doctor aan de Universiteit Twente,
op gezag van de rector magnificus,
prof. dr. F.A. van Vught,
volgens besluit van het College voor Promoties
in het openbaar te verdedigen
op woensdag 29 september 2004 om 13.15 uur

door

Johannes Post

geboren op 18 januari 1960

te Utrecht

Dit proefschrift is goedgekeurd door de promotor:

Prof. dr. ir. J. Huétink

en assistent promotor:

Dr. ir. H.J.M. Geijselaers

Contents

Summary

Metastable stainless steels can be characterised by a good combination of corrosion resistance, strength, formability and a large crack resistance. These properties make these materials highly suitable for various applications. As these materials transform, their behaviour is much more complex than that of conventional steel types. Sandvik Nanoflex™is one of these metastable austenitic steels, but it also includes two extra properties:

- Depending on the austenitising conditions and chemical composition, the material can be unstable to such an extent that stress-assisted transformation occurs as well as strain-induced transformation;

- The martensite phase of this material shows a substantial aging response (more than 1000 N/mm^2).

The behaviour of Nanoflex is characterised by two transformations. The first transforms the material during plastic deformation. This is strain-induced transformation. The second transforms the material without plastic deformation. This is stress-assisted transformation. These transformations may occur simultaneously or consecutively. The degree of stress-assisted transformation depends particulary on the stability of the material. Due to these transformations, the description of the work hardening and the accompanying strains is much more complex than in the case of non-transformable steels. Both transformations depend on temperature and the stress state, which means that heat transport and friction during deformation cannot be neglected.

First, the behaviour of this material was mapped under various conditions. Transformation measurements were largely done by means of inductive sensors. Special attention was paid to the calibration of these sensors. In addition a model was constructed with which the deformation behaviour and the transformation behaviour can be simulated. This model is partly physically based, but macroscopic. The model was implemented in a dedicated FEM solver called CRYSTAL. This solver is an internal Philips code. Implementation involves a flexible approach, in which a material definition file is combined with lookup tables and neural networks, in order to create a proper formal separation between the solver and the constitutive model that allows easy adaptation of the model and material behaviour. The purpose of this setup is that:

- Developments in material behaviour and the solver can be implemented in parallel;

- In various models one executable can be used, which facilitates version management and protection;

- Complex material models can be used by non-specialists.

The implemented model was validated by means of a number of FEM calculations that were compared with martensite and hardness profiles in combination with product contours. A special software program was developed for these validations. With this implemented model various calculations of different metal-forming process were made, including a multi-stage metal forming process consisting of three steps.

   Finally the developed model and solver were used to carry out a process window study of a multi-stage metal forming processes, using standard Design and Analysis of Computer Experiments (DACE) tools. The model includes not only the deformation steps but also the intervals between the steps, as stress-assisted martensite transformation may occur during these intervals and because the temperature changes during the intervals. The product is then austenitised, after which it transforms again due to stress-assisted transformation. The results were processed and analysed with a program called 'Compact'.

Samenvatting

Metastabiele roestvaste staalsoorten zijn te karakteriseren door een goede combinatie van corrosiebestendigheid, omvormbaarheid en een hoge weerstand tegen scheurgroei. Deze eigenschappen maken dit materiaal uitermate geschikt voor allerlei toepassingen. Doordat deze materialen transformeren, is het gedrag echter veel complexer dan van conventionele staalsoorten. Sandvik Nanoflex™is een van deze metastabiele austenieten, echter met nog twee extra eigenschappen:

- Afhankelijk van de austeniteer condities en de chemische samenstelling kan het materiaal dermate instabiel zijn, dat naast een strain-induced transformatie ook een stress-assisted transformatie optreedt.

- De martensiet fase van dit materiaal is precipitatie hardbaar (toename meer dan 1000 N/mm^2).

Het gedrag van Sandvik Nanoflex™wordt gekenmerkt door twee transformaties. Ten eerste transformeert het materiaal tijdens het plastisch vervormen: de zogenoemde strain-induced transformatie. Ten tweede transformeert het materiaal ook zonder te deformeren: de stress-assisted transformatie. Deze transformaties kunnen tegelijk of na elkaar voorkomen. De mate van stress-assisted transformatie hangt met name af van de stabiliteit van het materiaal. Door deze transformaties is het beschrijven van de versteviging en de daarbij optredende rekken veel complexer dan van niet transformeerbare staalsoorten. Beide transformaties zijn afhankelijk van temperatuur en hydrostatische spanning, hetgeen betekent, dat het warmtetransport en de wrijving tijdens omvormen niet verwaarloosd kan worden.

Als eerste wordt het gedrag van dit materiaal onder diverse condities duidelijk in kaart gebracht. De transformatiemetingen worden voor het grootste deel gedaan door gebruik te maken van inductieve sensoren. Speciale aandacht gaat uit naar het kalibreren van deze sensoren. Daarnaast wordt een model geconstrueerd, waarmee zowel het deformatiegedrag kan worden berekend als het transformatiegedrag. Dit model is gedeeltelijk physical based maar macroscopisch.

Het model is geïmplementeerd in een dedicated FEM solver, CRYSTAL genaamd. Deze solver is een interne Philips-code. De implementatie is gedaan op basis van een flexibele aanpak door een materiaal-definitie-file te combineren met lookup tables en neural networks om een goede formele scheiding aan te kunnen brengen tussen de Solver en het constitutief model, zodat wijzigingen in model en materiaalgedrag eenvoudig kunnen worden aangepast. Het doel hiervan is het volgende:

- Ontwikkelingen aan materiaalgedrag en de solver kunnen nu parallel worden doorontwikkeld;

- Er kan met verschillende modellen worden gewerkt met een executable hetgeen versiebeheer en beveiliging vergemakkelijkt;

- Complexe materiaal modellen kunnen worden doorgerekend door niet FEM-specialisten.

Het geïmplementeerde model wordt gevalideerd aan de hand van een aantal FEM-berekeningen, die worden vergeleken met martensiet- en hardheidsprofielen in combinatie met productcontouren. Voor de validaties is een speciaal software programma ontwikkeld.
Met dit geïmplementeerde model zijn vervolgens diverse berekeningen gedaan aan verschillende omvormprocessen, inclusief een meer-staps-omvormproces.

Tenslotte wordt het ontwikkelde model en solver gebruikt om een proceswindow studie te doen, gebruikmakend van een standaard DACE toolbox aan de hand van een multi-stage omvorm proces. Niet alleen de omvormstappen zijn gemodelleerd, maar ook de wachtstappen tussen de verschillende omvormstappen, omdat tijdens deze wachtstappen de stress-assisted martensiet-transformatie kan optreden en omdat de temperatuur zich tijdens de wachtstap wijzigt. Daarna wordt het product geausteniteerd om vervolgens opnieuw te transformeren middels een stress-assisted transformatie. De resultaten worden verwerkt en geanalyseerd met het programma 'Compact'.

Preface

Metal forming is an old trade. People started to melt iron in the Iron Age thousands of years ago. Once they knew how to melt iron, they also started to form metal objects. The early types of iron, however, were not particularly deformable. People soon discovered that the metal could more easily be formed if it was heated first.

This situation continued until the end of the 19th century, especially in the countries, where smiths forged metal objects such as horseshoes and farming tools.

Industrialisation not only led to production on an ever-larger scale but also resulted in the continuous improvement of steel manufacturing methods. Thanks to these improvements, steel types became more ductile, which made cold forming more easy. Until this very day, however, most metalworking companies improve their production processes mainly based on experience.

In recent years experience-based way of working increasingly under pressure. Nevertheless, most companies - the smaller ones in particular - will continue to deal with production problems along these lines for quite some years and perhaps even decades to come.

When I started working at Philips some 20 years ago, I entered just such an experience-oriented world. I was surprised to find that other lines of industry within the Philips organisation ran their production processes in an entirely different way. In my opinion, the clearest example of an entirely different approach is the chip industry. In this line of industry, experience is not always available. That is why these problems are solved with the help of scientific knowledge, i.e. spectator knowledge.

I learned about the concepts of spectator knowledge and experiential knowledge through The Psychology of Science: A Reconnaissance (New York, 1966) [1] by Abraham Maslow. In this book Maslow tells how behaviourism was unable to describe or solve a number of more emotionally related problems. To provide such a description Maslow introduced the concept of experiential knowledge. I don't would chose here for one of them. More strongly: both experiential knowledge and spectator knowledge have to be complemental. Because the spectator knowledge is only a part of reality it will remain necessary to have experiential knowledge in a production environment.

A number of circumstances let move in the opposite direction. Coming from an experiential science, I was faced with a number of problems. Many experienced colleagues retired without being replaced by experienced workers. The new collea-

gues who joined the department needed to be briefly familiarised with the various processes.

Moreover, because of my participation in the introduction of the new material the metastable stainless steel Sandvik Nanoflex™, which has such complex properties that experiential knowledge could never fully describe it and to solve problems within a reasonable time.

Finally, companies have a continuous need to shorten lead times. In innovative processes, metal forming tends to be overlooked. On the one hand it is liked for its low costs, but on the other hand it is rejected because of the complex engineering process as involved.

The above problems can be partly solved by laying down and integrating knowledge in complex calculation packages, although experience will continue to be required, albeit that its importance will gradually decrease. This thesis should be regarded as a step towards integrating spectator knowledge in the experiential knowledge-based world of metal forming engineers, especially when using complex materials.

For many centuries swords were forged on the basis of experiential knowledge. The best sword was made by the best smiths. In 2002 G.B. Olson engineered the hardest sword [2], not on the basis of experience but on the basis of materials science, i.e. on the basis of spectator knowledge.

Voorwoord

Omvormen is een oud vak. In Nederland is de mens begonnen ijzer te smelten in de ijzertijd, wat inmiddels duizenden jaren geleden is. Toen de mens ijzer kon maken is hij vrijwel direct begonnen met het omvormen van metalen onderdelen. We moeten bedenken dat deze vroege staalsoorten niet uitblinken in omvormbaarheid. Door het metaal te verhitten werd het beter vervormbaar.

Eigenlijk heeft deze situatie tot eind 1900 geduurd, althans voor een deel op het platteland, waar de smid het omvormvak bedreef door metalen voorwerpen te smeden.

Daarnaast is door de industrialisatie van de laatste eeuwen de schaalgrootte enorm toegenomen waarbij de processen om staal te maken steeds meer verbeterde. Door deze verbeteringen werden staaltypen ook steeds ductieler wat het koudomvormen steeds beter toepasbaar maakte. Tot op de dag van vandaag is bij de meeste metaalwarenbedrijven ervaring de methode om produktie processen te ontwikkelen.

In de laatste decennia zijn er twee fenomenen die deze ervarings-georiënteerde manier van werken langzaam maar zeker onder druk zijn gaan zetten. Ondanks dit zal het voor de meeste bedrijven, zeker voor de kleinere, nog jaren, mogelijk decennia duren voordat er veranderingen zullen optreden in ervarings-georiënteerde aanpak van problemen.

Toen ik 20 jaar geleden begon bij Philips kwam ik in een dergelijke ervarings-georiënteerde wereld te werken. Tot mijn verbazing waren er ook andere industrietakken in de Philipsorganisatie die op geheel andere wijze hun produktieprocessen tot stand brachten. Het meest sprekende voorbeeld hiervan is in mijn ogen de chiptechnologie. In deze wereld is ervaringkennis niet zonder meer aanwezig. Hier probeert men het probleem met kennis op te lossen, d.w.z. toeschouwerskennis.

De twee beprippen toeschouwerskennis en ervaringskennis heb ik leren kennen uit het boek van Abraham Maslow: 'Psychologie van de wetenschap' [1]. Hij vertelt hierin hoe met het behaviorisme een aantal meer emotioneel gerelateerde problemen niet konden worden opgelost c.q. beschreven. Om dit wel te kunnen introduceerde hij het begrip ervaringskennis. Ik wil hier geen uitspraak doen omtrent welke vorm van kennis meer doeltreffend is, sterker nog ik deel de mening van Maslow dat beide complementair dienen te zijn. Gezien het feit dat de toeschouwerskennis, slechts een deel van de waarheid vertegenwoordigt, zal voor een produktie systeem altijd ervaringskennis noodzakelijk blijven.

Door een aantal omstandigheden heb ik de laatste tien a vijftien jaar de omge-

keerde weg bewandeld. Werkend in een ervaringswetenschap werd ik geconfronteerd met diverse problemen; Veel ervaren collega's gingen met pensioen, zonder dat daar nieuwe ervaren medewerkers voor terugkwamen. Deze nieuwe mensen hadden behoefte om in korte tijd inzicht te krijgen in de diverse processen.

Daarnaast raakte ik betrokken bij de introductie van een nieuw materiaal: het metastabiele roestvaste staal Sandvik Nanoflex™. Dit materiaal heeft dermate complexe eigenschappen dat ervaringskennis niet toereikend is om precies te kunnen begrijpen wat er gebeurt, om zodoende binnen een redelijke tijd de problemen te kunnen oplossen.

Als laatste is er bij bedrijven een voortdurende behoefte om ontwikkeltijden te verkorten. In deze innovatieve processen is het omvormen vaak een stiefkindje: van de ene kant omarmd om zijn lage kosten, van de andere kant afgestoten om z'n complexe engineering proces.

Door kennis vast te leggen en te integreren in complexe rekenpakketten kunnen de bovenstaande problemen deels worden opgelost, er zal altijd ervaring nodig blijven, zij het dat het belang hiervan langzaam zal kunnen afnemen. Deze promotie moet gezien worden als een stap in de richting van het integreren van meer toeschouwerskennis in de ervaringswereld van omvorm-engineers, met name bij het toepassen van complexe materialen.

Honderden jaren werden zwaarden gesmeed op basis van ervaringskennis. De beste smid maakte het beste zwaard. Een aantal jaren geleden (2002) heeft G.B. Olson het hardste zwaard ge-engineerd [2], niet op basis van ervaring maar op basis van materiaal wetenschap, dwz toeschouwerskennis.

Chapter 1

Introduction

1.1   Introduction

Metal forming continues to be a major industrial process. The reasons for this importance are obvious. Metal forming is a technique that is highly suitable for mass production and is also by far the cheapest automated mass production process. However, no matter how many advantages a technique may have, there usually is a drawback somewhere. The disadvantage of metal forming processes is their complexity and, as a result, the long development times, certainly in case of fully automated production processes. The way to tackle this is to create processes that can later be pulled off the shelf. This calls for a proactive approach in the 'Product Creation Process' (PCP), to ensure that the information required is already known before the start of the actual PCP. Virtual engineering is a technique that is eminently suited for this. This technique enables the development of processes in general terms, and shelve them. During the PCP, simulations can be used to test the processes developed, although empirical research will continue to be required. Virtual engineering will, however, limit the amount of empirical research required considerably. Models are increasingly important because the behaviour to be examined is becoming more and more complex. This makes it almost impossible to tackle everything empirically.

This thesis deals with both aspects:

- FEM solver CRYSTAL is nothing but a means to shelve processes. The knowledge of the process and the material is implicitly incorporated in the software. The only further requirement that is needed is design rules, but these are amply available in the literature;

- Material behaviour is described by means of a number of differential equations in a constitutive model.

This method has the extra advantage that process specifications are available on the computer down to the tiniest detail so that the status of the process can be archived. Finally, the results of the simulations can be used to train new employees.

1.2   Multi-stage metal forming

There are clear limits to metal forming processes. One of these limits concerns the fact that the degree of forming per step is not indefinite. These limits have various causes:

- Maximum process forces;

- Elastic compression of the dies;

- Localisation of the deformation;

- Wrinkle formation;

- Tolerances.

As a result, and depending on the final shape, a number of steps will be required to obtain the desired end result. In some cases the material must be annealed to restore the deformation structure. Using different steps is an extra complication. A way of working with different steps is a multi-stage process. In this case different steps of a production process are incorporated in one tool. Multi-stage processes are ubiquitous in the mass production of small parts. The technology required to make tools for multi-stage processes is known as progressive tooling.

The aim of this thesis was not to solve all details concerning the constitutive behaviour of Sandvik Nanoflex™. The aim was to create a major framework in which it will be possible to use the current knowledge on the one hand and improve the model on the other in the same time, so the aim was more to be complete than to be perfect.

1.3   The scope of this thesis

This thesis consists of four parts. A subset of these parts will be published in journals, see appendix C, number 8, 9 10 and 11.

The parts are:

1.3.1   The constitutive behaviour of Sandvik Nanoflex™

In chapter 2 the measured properties of Sandvik Nanoflex™are presented, together with the measuring method used. Next we give our attention to different transformation and deformation models of similar materials described in the literature. Subsequently, a new, two phase, model based on the preceding sections is presented. Special attention is payed to constructing the model in such a way that implementation into the FEM code is relatively easy. The model should also be fittable. The last part of this section consists of a brief presentation of a three phase model, including the epsilon martensite. The latter is not used in the rest of this thesis, but it should be seen as a potential track for future research.

1.3.2   Finite Element implementation

In chapter 3 we focus on the implementation of the model from chapter 2 and the validation. The model is implemented by means of the lookup table approach to ensure flexible implementation. In addition a great deal of attention is paid to the implementation of dilation strain in combination with the stress-state dependence of transformation and to the implementation of transformation plasticity. Subsequently, the model is extensively validated and various exploratory calculations are performed, including heat treatments. Finally the model is checked against a multi-stage process and examined with 3D effects that occur in stress-assisted transformation.

1.3.3 Verification tool for 2D multi-stage metal forming processes

Chapter 4 validation of products or product cross-sections is useful. A measuring setup was created for this purpose. The basis for this setup was a universal image analysis tool combined with a fully automatic hardness tester. This universal system was coupled to a purpose-developed data analysis program, which allows easy measuring of the contour, hardness and martensite profile of a product. This chapter pays a great deal of attention to the numerical solutions required to allow data processing.

1.3.4 Application

Chapter 5 puts all knowledge and software developed into practice by carrying out a process window study on a fictitious product: the Timple. The DACE (Design and Analysis of Computer Experiments) is explained and used to solve a number of engineering problems that play a role in the process choices and the related infrastructure. This analysis also clearly demonstrates how robust the CRYSTAL solver really is, as only a robust solver is capable of making these kind of calculations.

Chapter 2

The constitutive behaviour of Sandvik Nanoflex™

2.1 Abstract

This article presents a model to describe the constitutive behaviour of Sandvik Nanoflex™[3] during metal forming and hardening. The material is metastable, which causes strain-induced transformation during forming. Depending on the annealing conditions, the material will also transform isothermally (as opposed to a-thermal martensite) [4–10]. This transformation can also take place immediately after plastic deformation, as a result of the residual stresses in the material. The martensite phase of this material shows a substantial ageing response (more than 1000 N/mm^2) [11].

In order to understand the behaviour of these transformations, an inductive measuring setup was developed to measure the transformation. This is a known technology, except that calibration of the sensor is complex because the sensor signal is determined by more parameters than only the martensite content.

The results of the various measurements on Sandvik Nanoflex™are discussed. The measurements mainly involved tensile tests and upsetting tests, in which both isothermal transformation and strain-induced transformation were examined. The hardening of the material and the increase in hardness during ageing was also examined.

Finally a constitutive model based on the literature and the measurement results are presented. The transformation part of the constitutive model is based on the work of Olson, Stringfellow and Patel [5–7, 10, 12–15], but redefined in a more general differential equation. The work hardening is based on the approach of Estrin [16, 17] using dislocation densities as internal state variables. Based on this information a new model is constructed that describes the isothermal or stress-assisted transformation, the strain-induced transformation, the work hardening and ageing behaviour. The model has been set up in such a way that it can be implemented in a FEM code.

2.2   Introduction

Table 2.1: Chemical composition

Element	C+N	Cr	Ni	Mo	Ti	Al	Si	Cu
Sandvik Nanoflex™	≤0.05	12.0	9.0	4.0	0.9	0.40	≤0.5	2.0

Sandvik Nanoflex™is a metastable austenitic stainless steel. The martensite phase of this steel is precipitation hardenable [3, 11]. See for the chemical composition table 2.1. Below the M_s temperature, which for Sandvik Nanoflex™is about 83 K, a-thermal martensite will form. This a-thermal martensite formation is outside the scope of this study.

Depending on the stability of the steel, isothermal transformation will occur. The influence of temperature and stress state on the transformation is shown in Figure 2.1 [9, 10]. Transformation occurs below the flow stress of austenite and during plastic deformation. The transformation rate depends on the composition of the material, the austenitising conditions, the temperature and the stress to which the material is subjected [18–21].

There are two possible transformations:
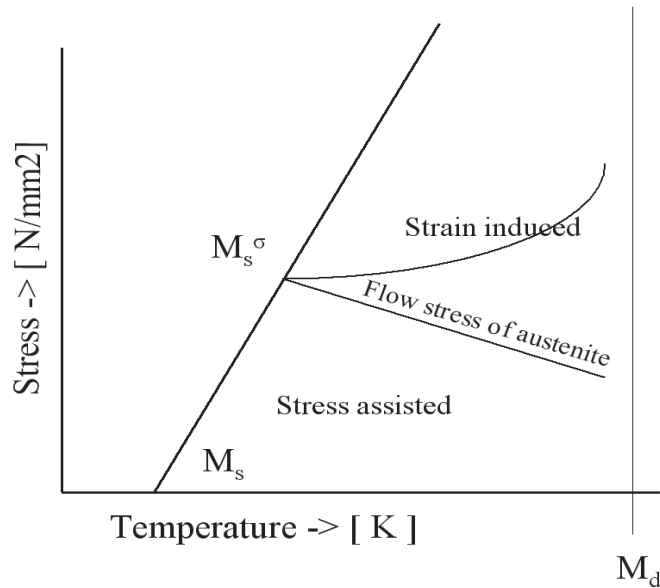
Figure 2.1: Schematic representation of critical stress for martensitic transformation as a function of temperature.

- The transformation below the flow stress of the composite will from now on be referred to as stress-assisted transformation;

- The transformation at the flow stress of the composite, this transformation will occur at higher temperatures above M_s^σ. This transformation is accompanied by plastic deformation. As soon as plastic deformation stops, this transformation also stops. From now on this will be referred to as strain-induced transformation.

When the austenite is deformed, its flow stress rises because of the work hardening. This will affect the transformation behaviour. Depending on the residual stress level, the strain-induced transformation may turn into stress-assisted transformation after deformation.

As a result of the transformation three phenomena occur:

- As martensite has a higher flow stress than austenite ($Re_\gamma = \pm\ 200\ N/mm^2$ and $Re_\alpha = \pm\ 700\ N/mm^2$), transformation will cause extra hardening during plastic deformation. This is referred to as transformation hardening, as opposed to normal hardening, which will further be referred to as classical hardening. This extra hardening leads to a greater attainable strain, because necking is delayed;

- An extra plastic strain component arises as a result of the stress field that accompanies the transformation, this strain component is called transformation plasticity;

- A strain component also develops as a result of the volume change induced by transformation: dilation strain [8, 22].

From the literature it is not fully clear what is meant by the TRIP (TRansformation Induced Plasticity) effect. The fact is that all three effects occur at the same time during the transformation. In this study the combination of these three phenomena are referred to as the TRIP effect.

Strain-induced and stress-assisted transformations depend on temperature, stress state, chemical composition and austenitising conditions.

During metal forming of Sandvik Nanoflex™, both transformations (strain-induced and stress-assisted) occur simultaneously. Mass production frequently uses multi-stage forming processes. Between the various stages, there are waiting times during which stress-assisted transformation occurs, depending on the residual stress distribution. This leads to deformation of the product. Moreover, stress-assisted transformation may also occur after forming.

As austenite is paramagnetic and martensite is ferromagnetic, it is possible to measure transformation in process by means of inductive sensors. To conduct these measurements, sensors and electronics were developed. The main problem that had to be solved was the calibration of the sensors, because the sensor signal is affected by a number of parameters other than just transformation.

This measuring setup was used to establish and quantify the material behaviour, which was already known in broad outlines. Several tests were performed, such as tensile tests, upsetting tests, transformation tests etc.

All the information gathered was used to build a model to make it possible to describe both types of transformation. The model for stress-assisted transformation was based on a model that was frequently used and which was originally proposed by Cohen and Raghavan [23–25]. The model for the strain-induced transformation is based on the model of Olson and Stringfellow [14, 15], which was later modified by others. For implementation in an internal Philips code, the macroscopic physically oriented models were converted into more universal differential equations to keep the implementation as robust and simple as possible.

Finally, a simple empirical model of ageing was also implemented, to predict the hardness after ageing.

2.3 Inductive measurement of martensite

2.3.1 Introduction

To gain insight into the transformation behaviour of Sandvik Nanoflex™, a sensor that can measure both, strain-induced and stress-assisted types of transformation, and a combination of these types was developed. This sensor measures the martensite content inductively [21, 26]. To prevent the magnetic field from disturbing the transformation, a low field strength of 100 μT was selected. In this way a sensor with electronics could be developed relatively easily. The problem concerning inductive measurement is that calibration of the measurement setup is rather complicated. Other parameters besides the martensite content affect the sensor signal. Some of these parameters are known, but others are less easy to detect. The challenge is to separate the various influences in such a way that it becomes possible to compensate for these influences. In this way the measured signal can be explicitly translated into martensite by interpolation.

Austenite is paramagnetic, whereas martensite is ferromagnetic. The difference in relative magnetic permeability μ_r is approximately 100. This is the phenomenon that was used to measure the transformation.

2.3.2 Sensors used

The measurements were carried out with a coil around the material, see Figure 2.2. It is also easy to produce and the position of the specimen does not affect the signal. To be able to estimate the field strength of the material, the sensor was calculated by means of a FEM simulation. Figure 2.2 shows the result of this calculation. The maximum field strength was 10^{-4} T, which is too low to affect the transformation behaviour.

2.3.3 Electronics

For the electronics, a standard IC that is normally used for an LVDT (Linear Variable Differential Transformer) was selected. In it, two coils are compared by supplying an alternating current to both coils and then measuring the voltage across the two coils, see Figure 2.3. A number of adjusting elements can be used to set the voltage, current, frequency and amplification factor. The IC contains an oscillator that generates voltage, a filter and an amplifier. The output is a signal in Volt. A frequency of 10 kHz was selected in order to avoid as much external electromagnetic interference as possible.

2.3.4 Calibration

Various experiments were performed to calibrate the sensor. For this a steel strip was used. This strip had been annealed for 0.5 min at 1323 K and quenched with 1 bar re-circulating inert gas, before the experiments. First, the influence of various parameters was determined, then these data were used to fit simple

models, i.e. polynomials. Next, these models were entered in a general calibration formula as corrections. With this formula it is possible to measure both types of transformation. The following phenomena can affect the signal output and are important for the calibration of the signal:

- Influence of the material volume in the sensor;

- Influence of the plastic strain: tests have shown that plastic strain changes the magnetic properties of the material (martensite);

- Influence of applied stress: elastic stresses in the material influence the output of the sensor. Elastic volume changes cause changes in the magnetic properties, which is known as magnetostriction;

- Influence of temperature: both the self-induction of the coil and the μ_r of the material to be measured are temperature dependent;

- The relationship between martensite and sensor output.

Influence of the plastic applied strain

To be able to measure the effect of the applied strain, a martensitic tensile test bar was needed. This tensile test bar was obtained by annealing the material at 1423 K for 15 min and then quenched using 6 bar re-circulated inert gas to 223 K and keeping it at this temperature for 24 hours. The material transforms isothermally to approximate 89% martensite. As a result, the material hardly transformed during the tensile test, see Table 2.2.

Then, the tensile test bar was pulled at a low speed $\dot{\varepsilon} = 0.001$ in various steps. Between the steps the stress was reduced to 0 N/mm^2. This was done to be able to separate the influence of elastic stress from the influence of plastic deformation. In Figure 2.4 the left-hand graph shows the stress plotted against the strain. The steps are clearly visible. The response of the measurement signal is plotted in the right-hand graph. The ascending loops are caused by the influence of elastic stress on the signal. In this way the influence of plastic strain can be plotted against induction at a reference stress of 0 N/mm^2, which is in fact represented by the tops of the loops. This signal still has to be corrected for the change of the retained austenite, see Table 2.2. The correction for plastic deformation can be expressed as follows, see Figure 2.7d:

$$C_{\varepsilon^p} = f_e(\varepsilon^p) \tag{2.1}$$

where C_{ε^p} is the correction factor and f_e a function that shows the relationship between plastic strain and the correction factor.

Table 2.2: Martensite content versus plastic strain.

Plastic strain [%]	0	1	2	3	4	5
Martensite [%]	89	96	95	95	95	95

Influence of applied stress

Similar to the previous test, the influence of elastic stress on induction was examined [27]. To this end an austenitic tensile test bar was pulled at a low speed $\dot{\varepsilon} = 0.001$ in various steps. Between these steps the stress was reduced to a reference stress of $0~N/mm^2$ By doing this, the influence of the transformation is separated from that of elastic stress. The result can be seen in Figure 2.5. In the left-hand figure the stress has been plotted against the strain. It clearly shows the different steps with the return to the reference stress between the steps. Induction was also plotted in the right-hand figure. This figure shows that the stress has little influence at first, as the martensite content is still too low and the austenite is paramagnetic and therefore has no effect on induction. As the plastic strain increases, the material starts to transform. As a result, the influence of elastic stress on the induction signal will increase. The bottoms of the loops in fact describe the signal change in the loaded condition and the tops of the loops describe the change at reference stress, which was what this test set out to establish. It is clear that there is an interaction between the martensite content and the influence of elastic stress on the sensor signal. This influence can be defined as follows, see also Figure 2.7c:

$$C_{\sigma^{\mathrm{H}}} = f_s(\varphi, \sigma^{\mathrm{H}}) \tag{2.2}$$

where φ is the martensite content and σ^{H} the hydrostatic stress and $C_{\sigma^{\mathrm{H}}}$ the correction factor, with a reference stress of $0~N/mm^2$. We took the hydrostatic stress, as this is related to magnetostriction, because the hydrostatic stress is that part of the stress tensor that is related to the elastic strain and to change in the distances between the atoms.

Influence of temperature

The magnetic properties of both the sensor and the material to be tested were temperature dependent. For the material to be tested, this only applies to the ferromagnetic phase, i.e. the martensite phase. The sensor has it's own induction and electric resistance and both are temperature dependent. The correction of the temperature can be described as follows:

$$C_T = f_T(\varphi, T) \tag{2.3}$$

Relation between martensite and sensor output

In order to establish a direct relationship between the sensor signal and the martensite content, the following tests were performed. Tensile test bars were pre-deformed to different strains, after which the induction was measured without stress. Then, the microstructure of the tensile test bars were revealed and analyzed by image processing to measure the martensite content. The martensite can be measured by ageing the material and then etching it. The material was aged by annealing at 773 K for 30 minutes. Then it was etched with a Lichtenecker and Bloch etchant. For the results see Table 2.3. The last column shows the values corrected for plastic

strain and volume. All the values were recalculated for the reference volume of $4500\ mm^3$, which is the gross volume that can be enclosed by the sensor. These corrected data were plotted in Figure 2.7. See Figure 2.6 for photos of the material structure. This can be described as:

$$U_{ref} = f_\varphi(\varphi) \tag{2.4}$$

Table 2.3: Results of tensile tests at different pre-strains at 323 K, * =mean value of the measured area using image analyzing of 2.5 mm^2

Plastic strain	martensite content*	induction at V_0
0.000	1	0.0
0.013	8	0.4
0.015	9	0.6
0.043	16	1.1
0.071	22	1.8
0.080	26	2.3
0.095	32	3.82
0.103	37	4.2
0.112	48	6.9
0.122	56	8.1
0.128	59	10.4
0.143	61	12.9
0.148	63	14.4
0.151	70	16.3
0.162	71	18.1
0.165	74	19.2
0.174	80	21.4
0.190	86	24.7
0.202	88	27.0
0.209	91	28.6
0.234	95	31.3

Calibration mathematics

The result of the correction tests is shown in Figure 2.7. The output signal of the sensor and electronics must be translated into martensite content. In view of the above, a relationship can be established between the sensor signal and the above parameters:

$$U = U_0 + U(V, \sigma^{\mathrm{H}}, \varepsilon^p, \varphi, T) \tag{2.5}$$

where U is the output of the electronics and the sensor in Volt. V is the volume of the material inside the sensor, σ^{H} is the hydrostatic stress, ε_p is the plastic deformation, φ is the volume fraction of the martensite and T is the temperature in Kelvin. U_0 is the offset voltage of the sensor. The output signal is also known to be linear dependent on the volume of the sensor. The maximum volume enclosed by the sensor is therefore defined as V_0 and the signals were recalculated to the reference volume:

$$U = U_0 + \frac{V}{V_0} f(\sigma^{\mathrm{H}}, \varepsilon^p, \varphi, T) \tag{2.6}$$

Combination of (2.1), (2.2), (2.3), (2.4), and (2.6) results in:

$$U = U_0 + \frac{V}{V_0} C_{\sigma^{\mathrm{H}}} C_{\varepsilon_p} C_T U_{ref} \tag{2.7}$$

or

$$U = U_0 + \frac{V}{V_0} f_s(\sigma^{\mathrm{H}}, \varphi) f_e(\varepsilon^p) f_T(\varphi, T) f_\varphi(\varphi) \qquad (2.8)$$

If φ is to be found from this equation, this must be done numerically. Equation (2.8) can also be rewritten as a potential function of φ:

$$P(\varphi) = U - U_0 - \frac{V}{V_0} f_s(\sigma^{\mathrm{H}}, \varphi) f_e(\varepsilon^p) f_\varphi(\varphi) f_T(\varphi, T) \qquad (2.9)$$

This equation was solved by bisection. With this calibration formula it is possible to explicitly determine the martensite content under any condition as regards temperature, stress and plastic strain. This also holds for a combination of transformations, for example a martensite content of 50% is generated during a tensile test and afterwards an external stress is applied below the flow stress of the composite. Because of this applied stress the specimen will transform further by stress-assisted transformation. This transformation is without plastic deformation. If all the information, stress, temperature, plastic pre-strain is known, the martensite content can be calculated using (2.9)
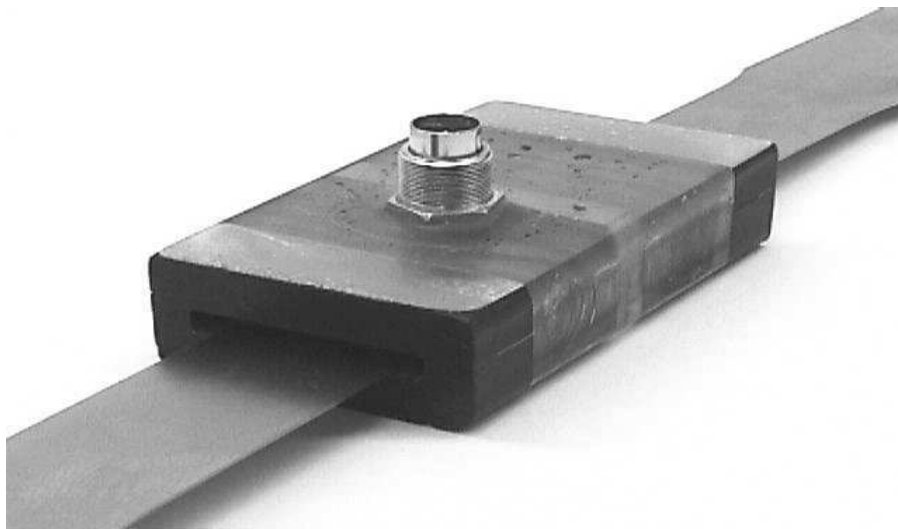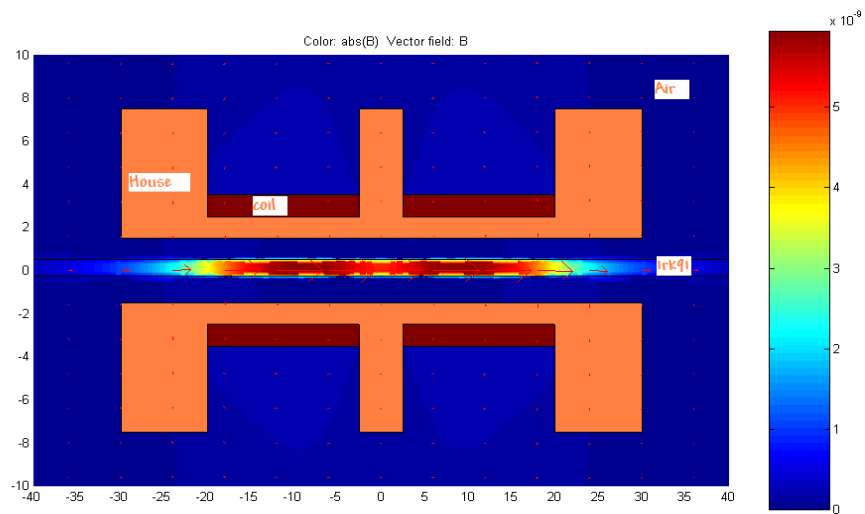
Figure 2.2: The FEM calculation of the magnetic field is shown at the top, while the photograph at the bottom shows the sensor used.
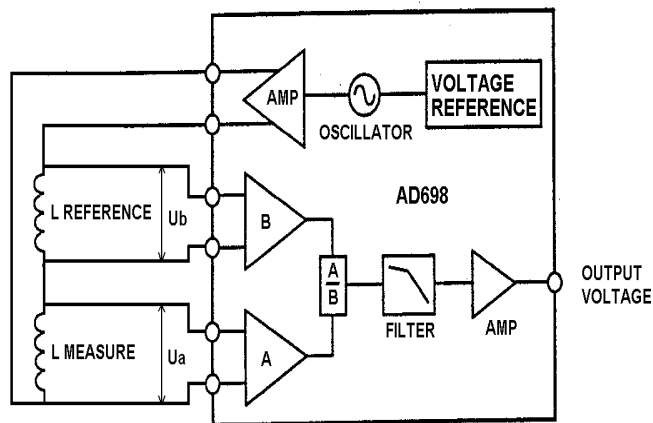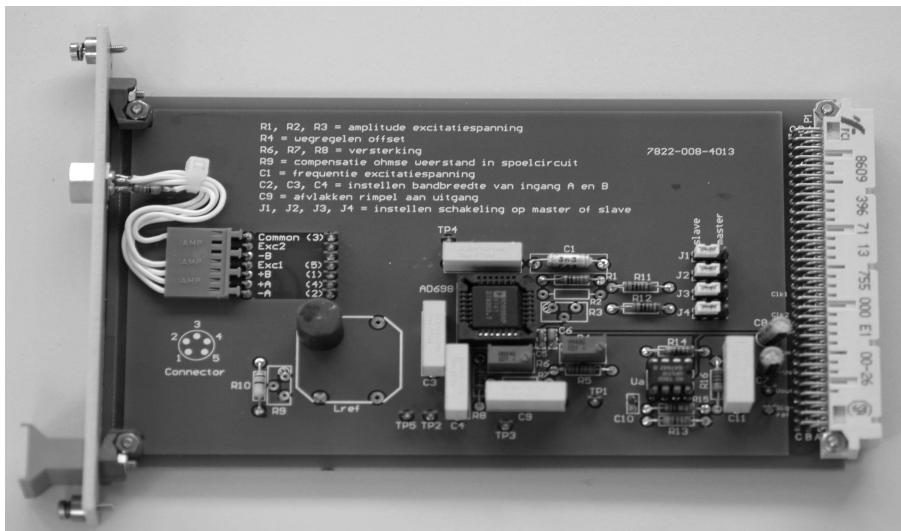
Figure 2.3: The PCB (Printed Circuit Board) is shown at the top and the measuring circuit at the bottom.
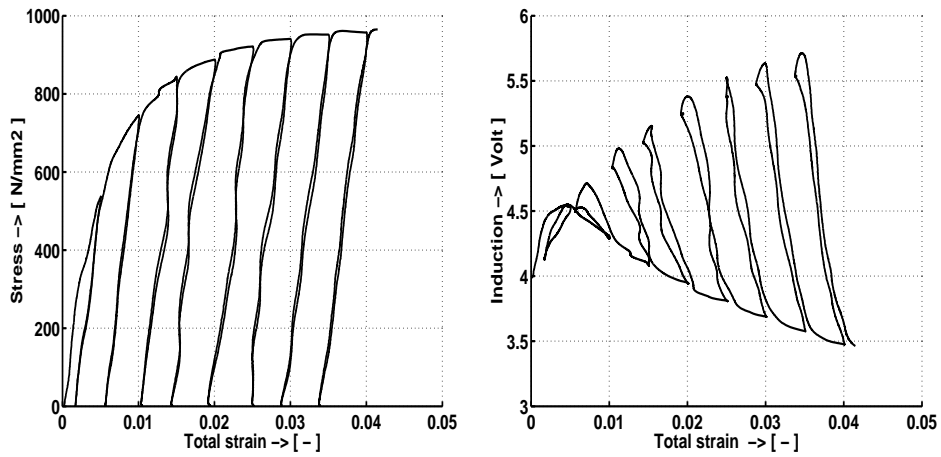
Figure 2.4: The influence of plastic strain on the signal, the stress is shown at the
left-hand site, the sensor signal at the right-hand site.
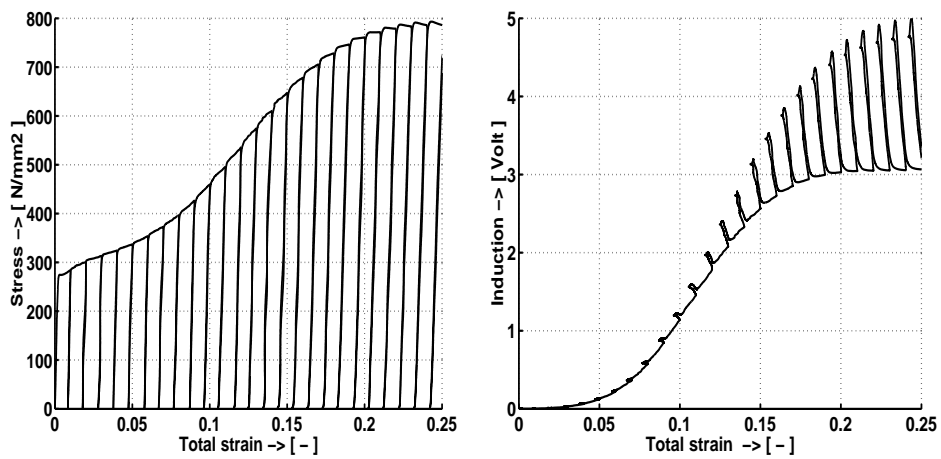
Figure 2.5: The influence of stress on the signal; stress is shown at the left-hand site,
the sensor signal at the right-hand site.

(a) 0.5%   (b) 4.3%   (c) 8.0%

(d) 12.2%   (e) 14.3%   (f) 16.5%

(g) 19.0%   (h) 23.4%
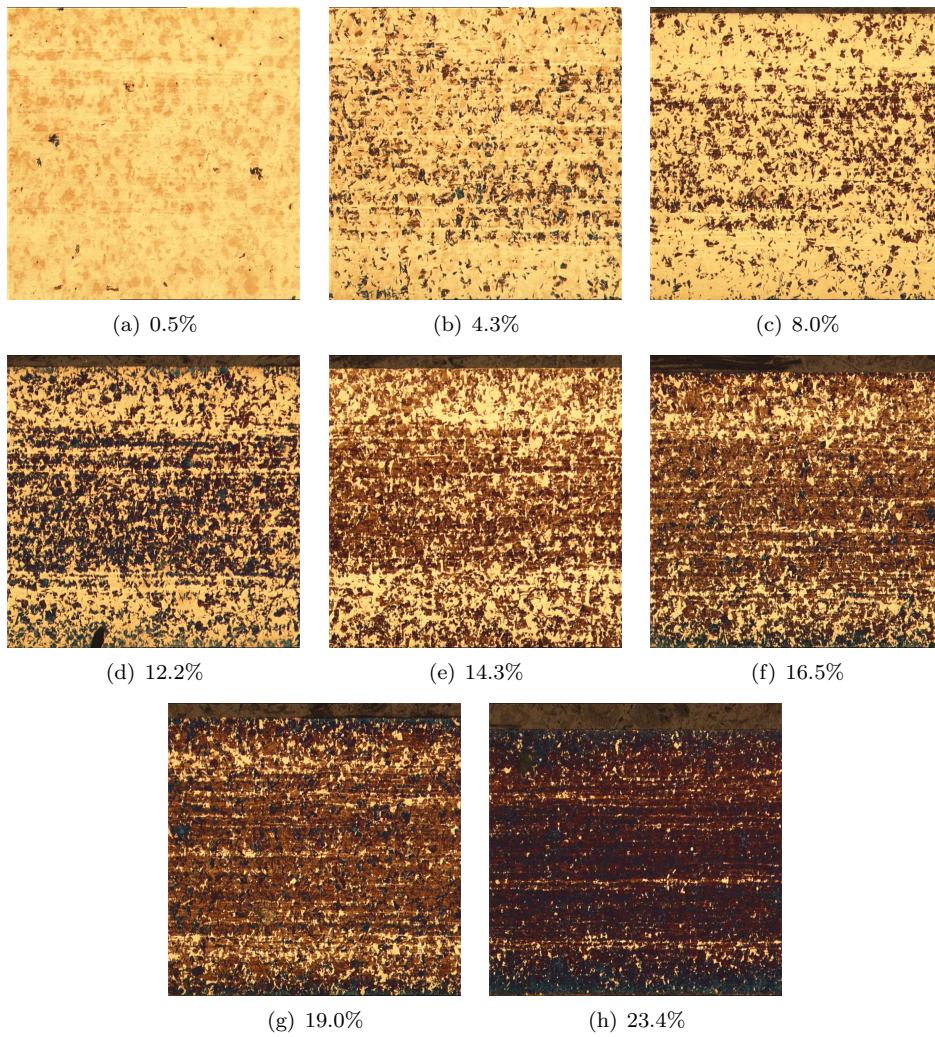
Figure 2.6: The structure of Sandvik Nanoflex™(100X) at different plastic pre-strains, determined from tensile tests at 323 K. (dark=martensite, light=austenite)
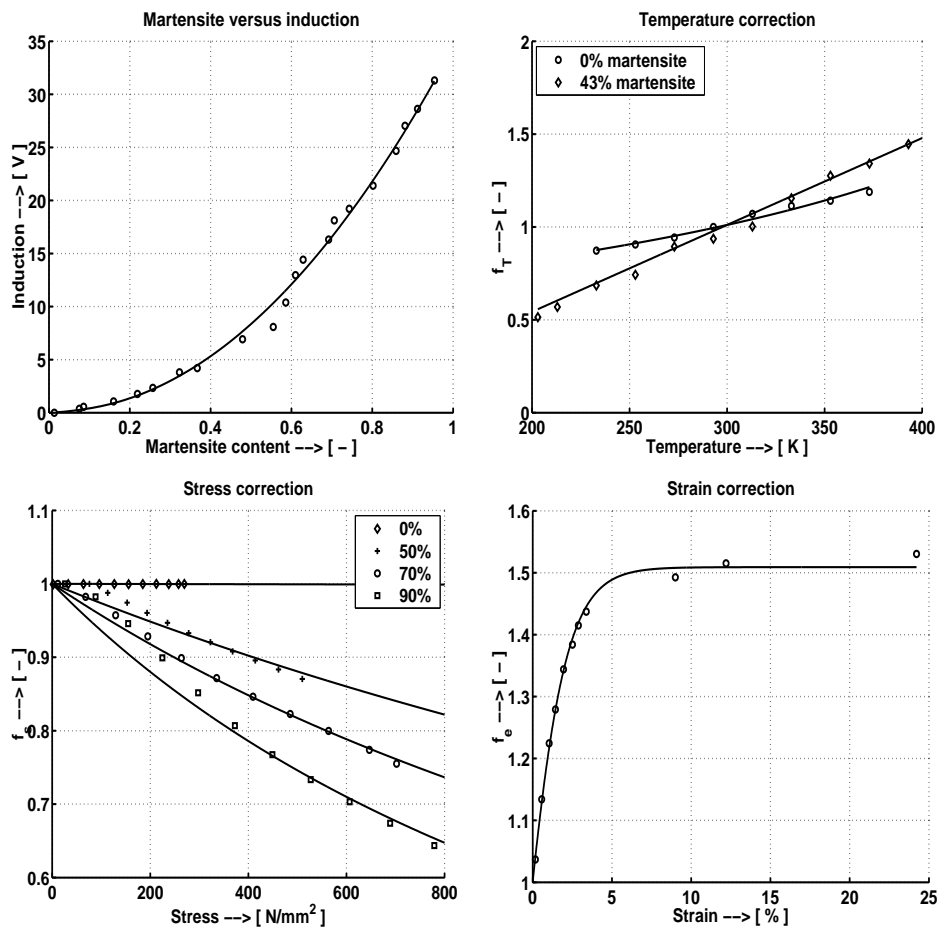
Figure 2.7: Calibration of the sensor: the relationship between signal output and martensite content (a) and the influence of temperature (b), stress (c) and strain (d). Reference temperature is 293 K.

2.4 Experiments

2.4.1 Experimental procedure

This section describes the results of a large number of tests. These tests were carried out to gain insight into the constitutive behaviour of Sandvik Nanoflex™. The material was received in two conditions: a stable condition to examine strain-induced transformation and an unstable condition to examine stress- assisted transformation. The stability of the material is partly influenced by its chemical composition, which is outside the scope of this thesis. The stability is strongly influenced by the austenitising conditions. Two different austenitising conditions were selected:

- a 'stable' treatment, from now on referred to as pre-treatment 1. The material was austenitised at 1323 K for 30 sec and then slowly cooled down to room temperature (quenching 1 bar re-circulating inert gas). This treatment took place in a vacuum furnace.

- an 'unstable' treatment, from now on referred to as pre-treatment 2. The material was austenitised at 1323 K for 15 min and then cooled down quickly to room temperature (quenching 6 bar re-circulating inert gas). This treatment took place in a vacuum furnace.

Unstable refers to the material being in a condition that will cause it to transform spontaneously in time without external energy sources. Stable indicates that this spontaneous transformation does not occur. In this case external energy will have to be added in the form of deformation or stress to generate transformation.

2.4.2 Combined cold rolling tensile testing

To gain an insight into the general material behaviour of Sandvik Nanoflex™under different conditions, a number of tests were performed. Stable strip material (pre-treatment 1) was deformed by means of rolling. The diameter of the rolls was 400 mm. After this the rolled material was subjected to tensile testing. Rolling took place in small steps and at low speed, to keep the strain rate low and the temperature as constant as possible. Despite the low speed, the strain rate still reached a level of about $1/sec$. The material was cooled to room temperature between the different rolling steps. The tensile tests were carried out under isothermal conditions, i.e. with a strain rate of about $0.001/sec$. As a result, the temperature rose by less than 10 K during the test, which means that the results of these tests can therefore be regarded as more or less isothermal.

Two series of 30 tensile tests were carried out. The first series concerned material that had only been rolled. Figure 2.8 clearly shows that the material behaves rather peculiar at small rolling reductions. This is the result of strain-induced martensite formation. The second series of tests was carried out on material that was aged after rolling (30 min. at 773 K) Figure 2.9. At small rolling reductions, ageing will not have much influence, as only the martensite phase can be aged. Figure 2.9 shows the results of the tensile tests. The flow stress R_e and the tensile strength R_m
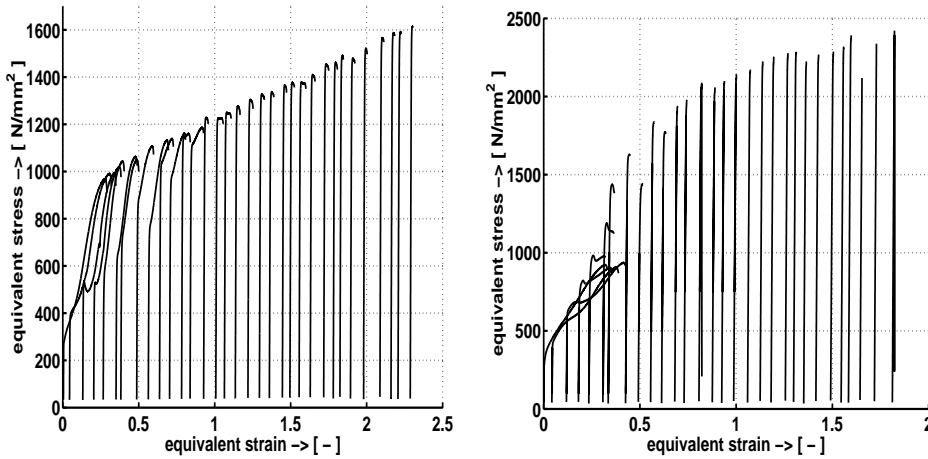
Figure 2.8: Left: the tensile tests in non-aged condition after pre-straining by rolling.
Right: the tensile tests in aged condition after pre-straining by rolling.

have been plotted against the pre-straining due to rolling. The figure clearly shows that non-aged material has a high amount of work hardening at small strains, this is caused by the work hardening of austenite combined with transformation hardening. At large strains, the material will be transformed to martensite, which causes very little work hardening, because of the low carbon content of the martensite. It also shows that ageing results in two effects:

- During cooling down of the austenitising process, stresses in the material are introduced together with fixation of some interstitials. During the ageing process these stresses will vanish and the interstitials will move to grain boundaries etc, this will result in a lower flow stress of the austenite

- The martensite content will precipitate, which will increase the flowstress. Figure 2.10 shows the results of XRD measurements on the test material to establish the martensite and austenite content on the right.

The Vickers hardness (Hv0.2) was measured on the cross-section of the aged as well as non-aged material. The result is shown in Figure 2.10 on the left. In general there is a linear relation between the flow stress and the hardness. Comparing Figure 2.10 and Figure 2.9b shows that relation.

2.4.3 Strain-induced transformation

A major property of Sandvik Nanoflex™is the formation of martensite during plastic deformation. This phenomenon is known as strain-induced martensite and occurs in all metastable austenites, such as AISI 301 en AISI 304. The transformation greatly depends on the temperature and stress state. This transformation is also very useful
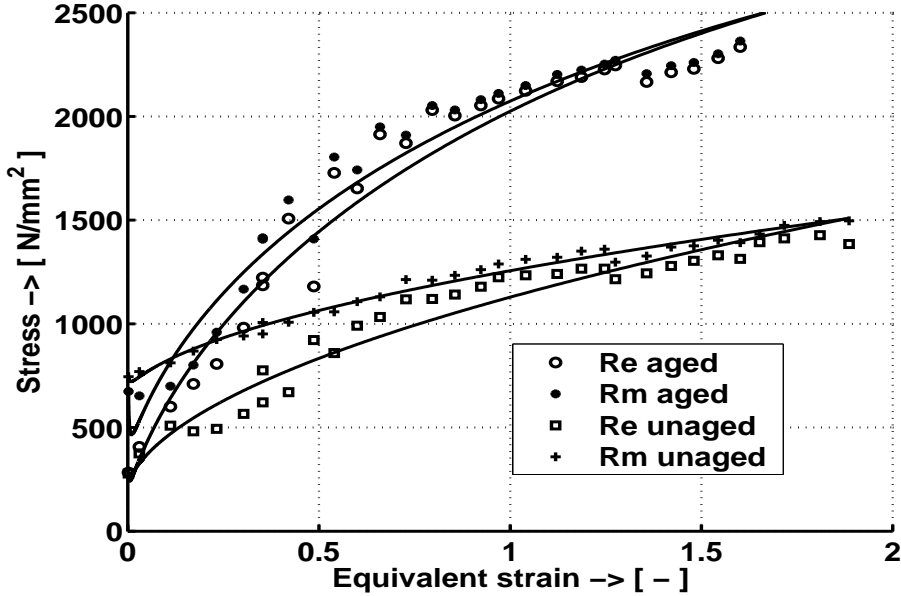
Figure 2.9: The tensile strength (Rm) and flow stress (Re) of Sandvik Nanoflex™after pre-straining by rolling in aged (line above) and non-aged (line below) condition.

from an industrial point of view, as large strains can be obtained during metal forming in this way, i.e. by selecting the correct ratio between classic hardening and transformation hardening, see Figure 2.11. This phenomenon is known as TRIP. This martensite formation was examined by means of a number of tests.

Influence of temperature

To be able to investigate the influence of temperature on the transformation rate, the test setup shown in Figure 2.12 was created. The starting point was a tensile tester with a temperature chamber, in which the tensile tests can be carried out. For the tensile tests strips or bars were used. During the test the force and the displacement were measured, as usual in tensile tests. In addition, the martensite content was measured by means of an inductive sensor, while the temperature was measured with a thermocouple. All these data were logged and the true stress was derived from the data as follows:

$$\sigma^{\mathrm{Y}} = \frac{F}{A} = \frac{FL}{A_0 L_0} \tag{2.10}$$

where A is the cross-section area of the tensile bar and L_0 and A_0 are the original length and area respectively. L is the instantaneous length and F is the force. For
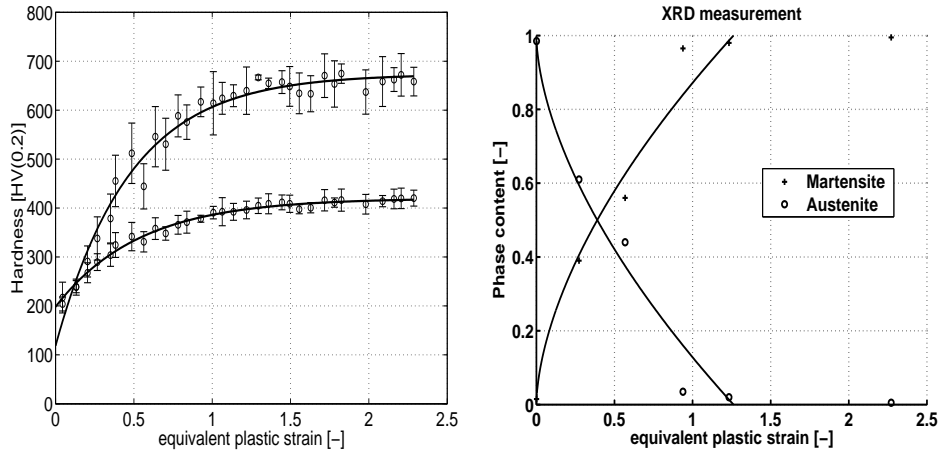
Figure 2.10: Left: Vickers hardness (Hv0.2) of Sandvik Nanoflex™after pre-straining by rolling of aged and non-aged material. Right: the martensite content of Sandvik Nanoflex™after pre-straining by cold rolling.
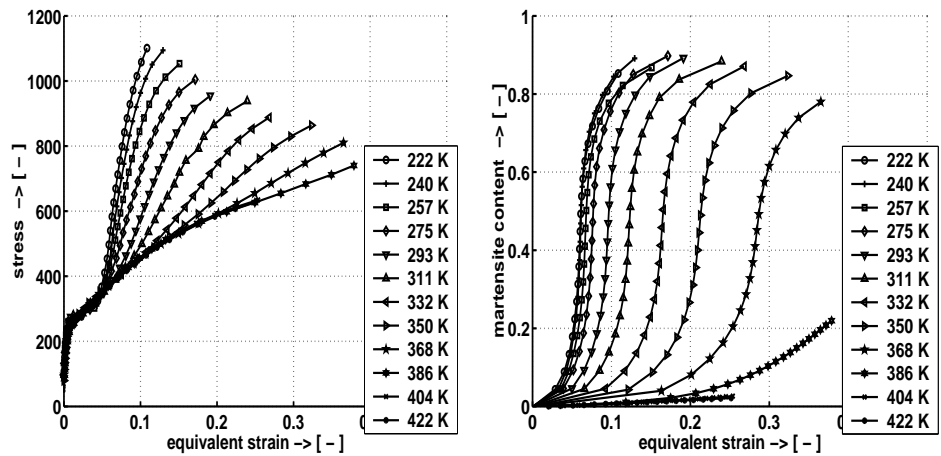
Figure 2.11: The results of tensile tests at low strain rates (0.001/sec) at different temperatures.

the true strain applies:

$$\varepsilon = \ln(L/L_0) \tag{2.11}$$

where ε is the strain in the direction of the tensile bar. The inductive signal at each of the values of strain, temperature and stress was converted to martensite.
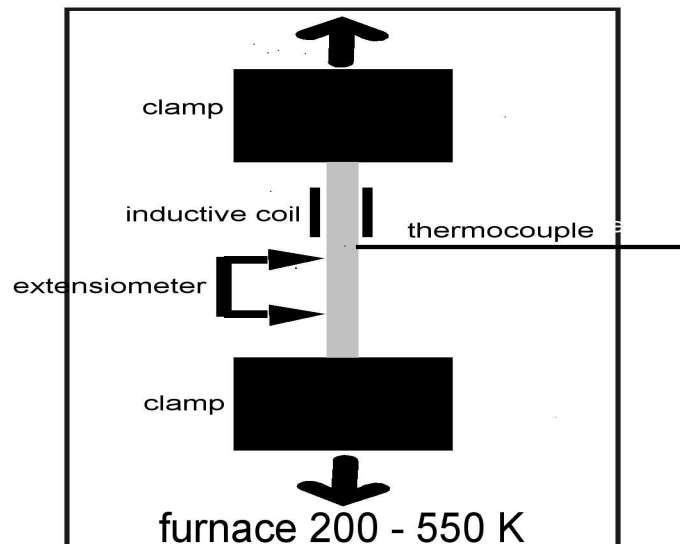
Figure 2.12: Sketch of the tensile test equipment.

This results in two graphs, of which one shows the transformation during tensile tests and the other shows the stress, see Figure 2.11.

Influence of stress state

To be able to establish the influence of the stress state, the following tests were performed:

- a tensile test at room temperature;

- an upsetting test at room temperature;

- tensile tests under hydraulic pressure of 0 to 6000 bar.

These tests were carried out in steps so that the martensite content could be measured at different strains afterwards. The tests under hydraulic pressure were carried out in the following manner. Plugs were inserted into the top and bottom of a tube. These plugs also serve as the chucks that grasp the ends of the tensile bar. The cylinder with the plugs fitted at both ends was mounted on a hydraulic press. It was the pressured by means of a hydraulic pressure unit. Then the traverse was lowered at a constant speed. The pressure in the cylinder pushed the plugs outwards, which caused the tensile bar to be deformed plastically. See Figure 2.13 for a sketch of the measuring setup and the results of the tests. The figure clearly shows that there is an influence of the stress state on the transformation behaviour. The legend shows the estimated hydrostatic stress during test.
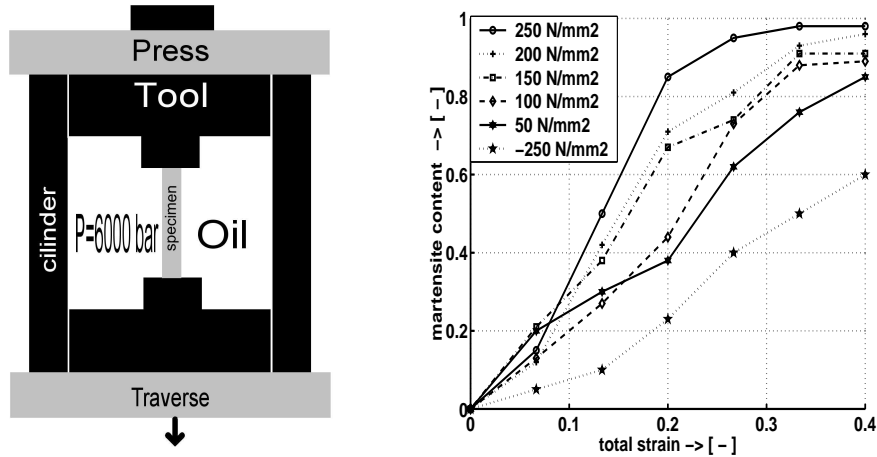
Figure 2.13: An indication of the influence of the stress state on the transformation rate of strain-induced transformation, the test with an estimated hydrostatic stress of 250 N/mm^2 is a normal tensile test, the test with an estimated hydrostatic stress of -250 N/mm^2 is a normal upsetting test.

2.4.4 Stress-assisted transformation

Stress-assisted transformation is an austenite-to-martensite transformation without any plastic deformation or at least without plastic deformation induced by an external energy source such as metal forming. This transformation does not always occur. It depends on the chemical composition and the austenitising conditions.

Due to the change in volume and the influence of the stress induced by the transformation, positive residual stresses will decrease, causing the stress-assisted transformation to stop after some time.

Influence of the austenitising conditions

The stability of the material is largely determined by austenitising conditions. To be able to estimate this influence, various specimens were annealed in different ways. These 24 specimens were followed with an inductive sensor to track spontaneous isothermal transformation. These tests were carried out in a temperature controlled climate chamber at 233 K for 24 hours. The results of these tests are described in Figure 2.14.

Influence of temperature

The temperature dependence of transformation is well known. This is often shown by means of a TTT diagram. Figure 2.15 is the diagram of Sandvik Nanoflex™in an unstable condition, i.e. austenitised at 1323 K for 15 minutes and quenched
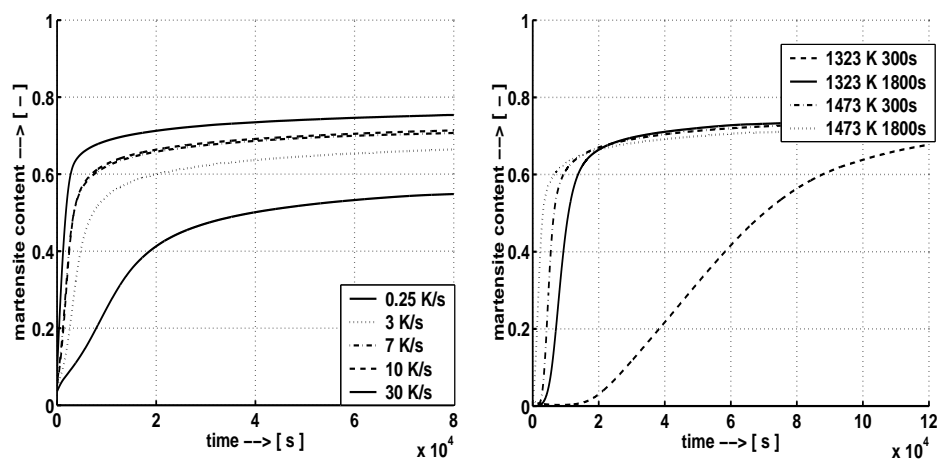
Figure 2.14: The influence of austenitising conditions on the stress-assisted transfor-
mation. Left: the influence of the cooling rate at 1473 K and 300 s.).
Right: the influence of time and temperature at a cooling rate of 10 K/s.

with 6 bar in re-circulating inert gas. This diagram was generated on the basis of
inductive transformation measurements at different temperatures, see Figure 2.15.

Influence of stress state

The stress dependence of transformation was measured inductively. The results are
shown in Figure 2.16 on the right. These data are based on inductive measurements
performed on tensile specimens that had been transformed under an external load
at 233 K for 24 hours.

2.4.5   Combined transformations

If plastic deformation of Sandvik Nanoflex™is required, it can be austenitised in
such a way that it does not start to transform spontaneously. This does not mean
that no transformation occurs. Depending on the hydrostatic stress, transforma-
tion will occur at some stage. For transformation to occur in a stable material, the
hydrostatic stress will have to be positive. When the hydrostatic stress is negative,
no transformation occurs. Figure 2.16 shows on the left-hand site how important
stress is for this type of transformation. The material was pre-deformed by pla-
stic deformation until it contained 50 % martensite. Then the transformation was
measured under various stresses.
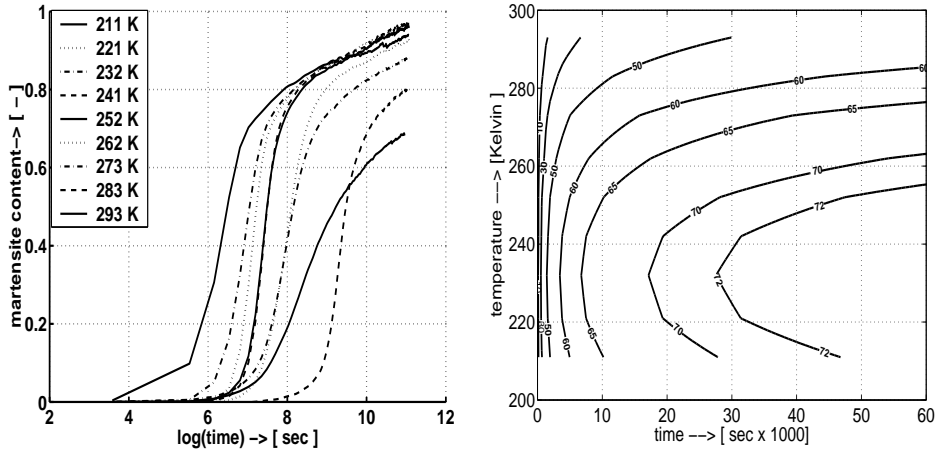
Figure 2.15: A TTT diagram (right) of unstable material (pre-treatment 2) based on inductive measurements (Left).

2.4.6 Work hardening

Due to strain-induced transformation, the hardening of Sandvik Nanoflex™is a complex process:

- On the one hand there is work hardening related to the generation of a dislocation structure, a process that takes place in all metals, at least below the recrystallisation temperature.

- On the other hand Sandvik Nanoflex™also shows transformation-related hardening because:

  1. Martensite has a higher initial flow stress than austenite;
  2. The dislocation density is partly inherited by the martensite;
  3. Dislocations are generated on the transformation boundary during the transformation.

This means that the total work hardening of the composite depends on the plastic strain rate (deformation-related work hardening) and the transformation rate (transformation-related hardening).

Figure 2.11 shows the flow stresses at different temperatures as a result of deformation and transformation. It is clear that not only the transformation rate is high at low temperatures, but also the hardening. The TRIP effect is also clearly visible. This is due to the influence of transformation hardening, as transformation is temperature dependent. Figure 2.17 shows the results of upsetting test on martensite and austenite. It seems that the work hardening of martensite is very low which is related to the low Carbon content of Sandvik Nanoflex™.

(a) Stable   (b) Unstable
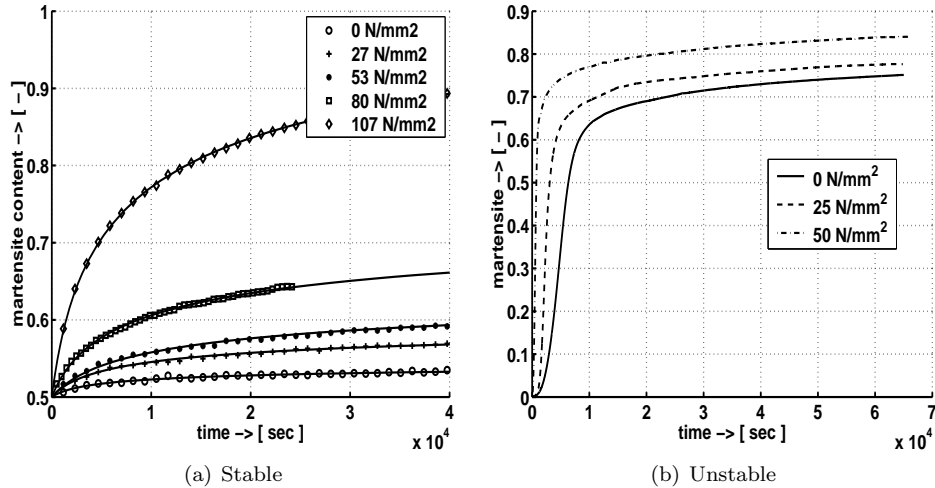
Figure 2.16: Left: the influence of hydrostatic stress on stress-assisted transformation after plastic deformation up to a strain-induced martensite content of 50% of stable material. Right: the influence of hydrostatic stress on stress-assisted transformation on unstable material (pre-treatment 2).

Influence of plastic strain rate and temperature on austenite

To gain insight into the influence of strain rate and temperature, a number of tests were carried out to establish the effect of both strain rate and temperature on the hardening and flow stress of austenite. To prevent transformation in the material, low temperatures were avoided. The results of the tests are shown in Figure (2.18)

Influence of plastic strain rate and temperature on martensite

The same tests as on austenite were also performed on martensite. After austenitisation to make the material unstable, it was transformed by means of isothermal stress-assisted transformation. This caused the martensite content to rise to 80%. Then the strain rate tests and the temperature tests were carried out. During the temperature tests, a peculiar phenomenon occurs at elevated temperature i.e. the martensite starts to age, which results in higher flow stresses. At temperatures above ± 800 K this phenomenon vanishes as some of the martensite also transforms back to austenite, assuming an equilibrium (T_0) between martensite and austenite of about 680 K. For the results, see Figure 2.19.
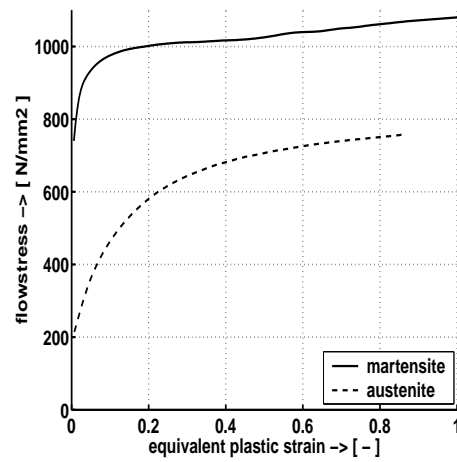
Figure 2.17: The results from upsetting tests on martensite and austenite.
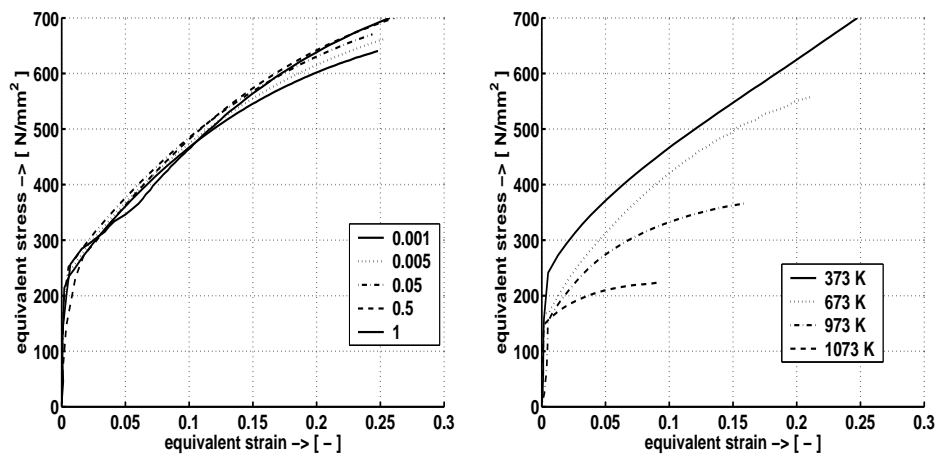
Figure 2.18: The flow stress of austenite. Left: the influence of plastic strain rate at a temperature of 443 K. Right: influence of the temperature on the flow stress of austenite at a strain rate of 0.002/sec.
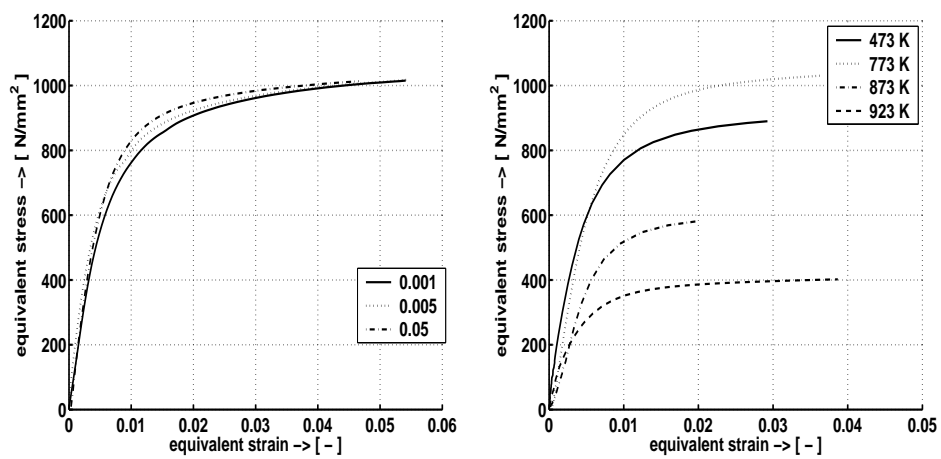
Figure 2.19: The flow stress of martensite. Left: the influence of plastic strain rate at
            room temperature (293 K). Right: influence of the temperature on the
            flow stress of martensite at a strain rate of 0.002/sec.

2.5 Physical-based model description

2.5.1 Introduction

In this section the data from the preceding section will be fitted into two models. The description starts with existing models for both strain-induced and stress-assisted transformation. Two models are fitted to the data. Then, the physical background of these models is briefly discussed. The physical model for stress-assisted martensite is mainly based on the work of Raghavan *et. al.* [23]. The model for strain-induced transformation is based on the models developed by Olson *et al.* [14]. As well as a model for the transformation, a model for the hardening of the material should be introduced. Because of the complexity of this problem, it was decided to use the approach of Estrin [17, 28, 29], which describes the dislocation density - at least the part of the structure change during plastic deformation that causes hardening - as an internal state variable. This approach was used in order to describe the complexity of hardening, including the path dependence and the inheritance of dislocations. Subsequently, the data was fitted to a new model.

After the discussion of the existing models, a new model will be introduced.

2.5.2 Stress-assisted macroscopic isothermal transformation model of Raghavan *et al.*

The most frequently used model for stress-assisted transformation is based on the work of Patel and Cohen. This work is taken as a starting point. Raghavan suggested that the number of new nucleation sites is proportional to the formed martensite content. As the transformation rate depends on the number of nucleation sites, this assumption implies an autocatalytic effect, as:

$$\dot{\varphi} = f(\varphi) \tag{2.12}$$

According to Raghavan [23], three factors influence the number of nucleations:

- the number of initial sites in the austenite

- the number of new sites that develop through transformation

- the number of sites that become passive in the austenite phase

Raghavan [30] suggest the following simple equation to describe this:

$$n_\varphi = n_i + p\varphi - N_v \tag{2.13}$$

where φ is the martensite content, p is the autocatalytic factor, n_φ is the number of sites at a martensite content of φ and N_v is the number of martensite plates.

As the austenite content available for transformation decreases during transformation, Patel and Cohen [7] later added the term $1 - \varphi$. If φ approaches 1, the number of sites automatically becomes 0, see also Figure 2.20. Tests have shown that in Sandvik Nanoflex™a martensite content of 100% is never reached. Therefore the saturation value is not 1 but f_s. For the sake of convenience, this value
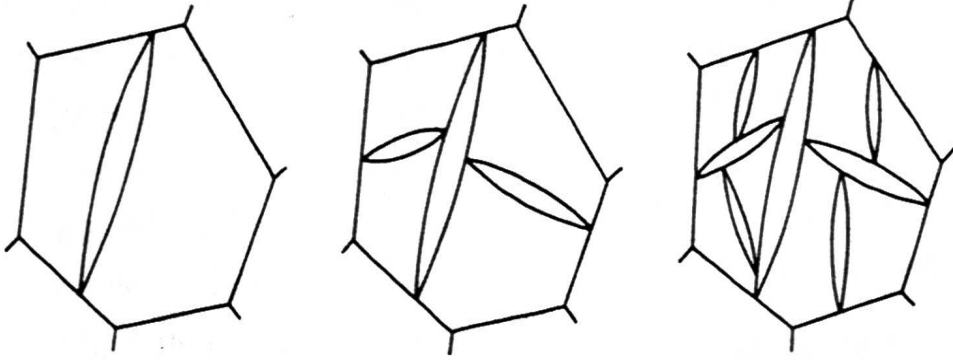
Figure 2.20: Progressive partitioning of the austenite grain by martensite plates.

is referred to as the saturation value of transformation. This value depends on the stability of the material and therefore on its chemical composition and austenitising conditions and it also depends on the hydrostatic stress on the material. This results in the following equation (2.13):

$$n_\varphi = (n_i + p\varphi - N_v)(f_s - \varphi) \tag{2.14}$$

Patel and Cohen showed that the following applies to the nucleation rate:

$$\dot{N}_{0.0002}^{fit} = [n_i + \varphi(p - \frac{1}{\bar{v}})\nu e^{-\frac{\Delta W_a}{RT}}] \tag{2.15}$$

where $\bar{v}$ is the average volume of the martensite plates, v is the vibration frequency and ΔW_a is the activation energy for the nucleation process.

In general, the following applies to the transformation rate $\dot{\varphi}$:

$$\dot{\varphi} = \dot{N}v \tag{2.16}$$

where $\dot{N}$ is the nucleation rate and v the instantaneous size of the martensite plates.

Patel and Cohen [23] showed that the instantaneous plate volume is related to the average plate volume by means of:

$$v = \bar{v} + \frac{d\bar{v}}{dln(N_v)} \tag{2.17}$$

Combination of (2.15), (2.16) and (2.17) results after some calculation in:

$$\dot{\varphi} = [n_i + p\varphi - \frac{\varphi}{\bar{v}}](f_s - \varphi)[\bar{v} + \frac{d\bar{v}}{dln(N_v)}]\nu e^{(\frac{-\Delta W_a}{RT})} \tag{2.18}$$

Fischer [24] extended this classical nucleation theory by including the effects of elastic strain energy in the formation of isothermal martensite. Later, Magee

[31] and Patel and Cohen [25] stressed the importance of the autocatalytic effect, which they incorporated in their kinetic formulation that led to an expression of the overall transformation rate. Their formula has served as a basis for the analysis of the isothermal transformation data. The model adopted for fitting the experimental transformation curves is then given as:

$$\dot{\varphi} = [n_i + p\varphi - \frac{\varphi}{\bar{v}}](f_s - \varphi)(1 - \varphi)^{m_1 + m_2\varphi}\bar{v}(1 - d(1 - \varphi))\nu e^{(\frac{-\Delta W_a}{RT})} \qquad (2.19)$$

where $\bar{v}$ is the mean volume of the martensite plates, p is the autocatalytic factor, $(f_s - \varphi)$ includes the sweeping out of the untransformed austenite phase. The saturation parameter f_s was introduced to describe the sweeping effect more accurately, as it is related to the amount of retained (stabilised) austenite and depends on the hydrostatic pressure built up in the austenite during the transformation. n_i is the initial number of sites in the austenite phase. The change of the plate size $\bar{v}$ also has an influence at a later stage of the transformation. The values of the relevant parameters taken from the fit are given in Table 2.4.
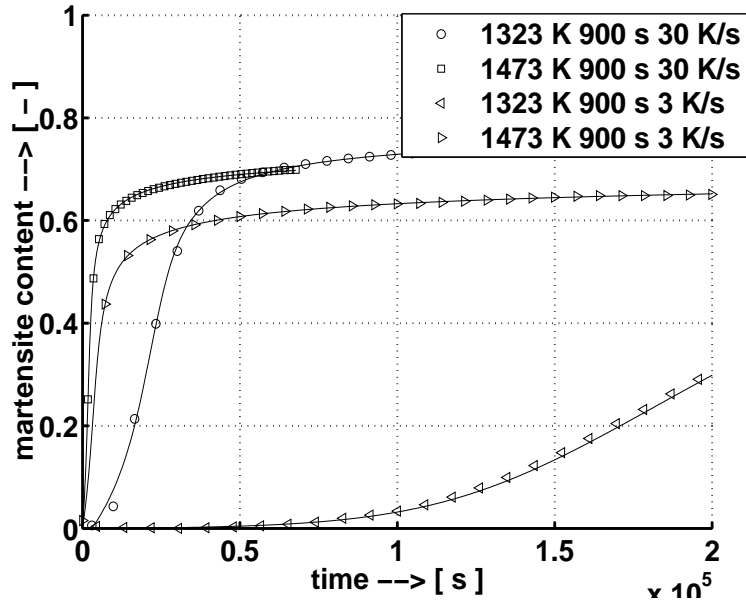
Figure 2.21: The model fitted to the data, the lines are from the model, the symbols are the measured data.

In principle this model is easy to implement in a FEM code. Still, a number of points require attention:

- Due to the large number of parameters with a similar effect, there is no unambiguous solution for the fitting process. To prevent this problem, a number

Table 2.4: Parameters of fitted model(2.19), $\bar{v}$=1e-10 cm^3, R=8.32 J/mol.K, T=233
K, ν=1.05e07 1/s, p=1e10 $/cm^3$, d=-0.3.

data of model (1)	n_i [*1e07/ cm^3]	ΔW [1*e04 kJ/mol]	f_s [-]	m_1 [-]	m_2 [-]
1323 K 15min 30 K/s	0.0001	2.16	0.78	-9.41	10.0
1473 K 15min 30 K/s	4.8203	3.92	0.74	-9.54	13.4
1323 K 15min 3 K/s	0.0151	4.26	0.62	2.46	-3.31
1473 K 15min 3 K/s	3.0653	3.96	0.70	-9.74	15.58

of fixed parameters must be selected to obtain a good convergence process
during fitting.

To avoid these problems a more general formulation was chosen for the imple-
mentation: easy to fit, including the stress state and as simple as possible, this
formulation is based on Šestàk [32]:

$$\dot{\varphi} = C(T, \sigma^{\mathrm{H}}, \varepsilon^p, Z)[(D + \varphi)^{n_a}(f_s(T, \sigma^{\mathrm{H}}, Z) - \varphi)^{n_b}] \qquad (2.20)$$

where C is a function that describes the dependence of transformation on stress,
temperature and material structure. T is the temperature, Z a parameter which
represents the chemical composition and autenitising conditions, n_a and n_b are fit
constants, D is related to the initial transformation rate and f_s is the saturation
value of the transformation.

2.5.3 Macroscopic strain-induced model of Olson *et al.*

The model for martensite volume fraction φ is based on a model for the kinetics of strain-induced nucleation developed by Olson and Cohen [6]. Assuming that shear-band intersection is the dominant mechanism of strain-induced nucleation, an expression (2.21) for the volume fraction of martensite versus plastic strain is derived by considering the course of shear band formation. We define P as the probability of a shear band intersection acting as a nucleation site. The resulting transformation curve has a sigmoidal shape and, in general, approaches saturation below 100%. The transformation curve is thus defined by two temperature dependent parameters, α and β, and a fixed exponent n. The form of the derived expression reveals that the saturation level is determined by the β parameter, while the rate of approach to saturation is controlled by both α and β.

$$\varphi^{\alpha'} = 1 - e^{-\beta[1-e^{-\alpha\epsilon}]^n} \tag{2.21}$$

where:

$$\beta = \frac{\bar{v}^{\alpha'} \pi^2 d^2}{16(\bar{v}^{sb})^n} P \tag{2.22}$$

The parameter α (which defines the course of shear band formation with strain) is temperature sensitive through its dependence on stacking-fault energy. The parameters $\bar{v}^{\alpha'}$, $\bar{v}^{sb}$ are the average volume per martensitic unit and the shear band average volume respectively.

The stress-state sensitivity of the transformation kinetics was not explicitly considered in this original model. Only temperature and plastic strain were considered as the parameters controlling martensite evolution. In 1991 an update was presented [14] for strain-induced martensitic transformation kinetics, into which the stress-state sensitivity of the transformation process was incorporated.

In order to incorporate pressure sensitivity, (2.21) was recast into a rate form, which allows the evolution of the stress state to be incorporated:

$$\dot{\varphi} = (1 - \varphi)\bar{v}_m \dot{N_m} \tag{2.23}$$

where $\bar{v}_m$ is the average volume per martensite unit. The factor $(1 - \varphi)$ represents the decrease in fraction available for transformation. The number of operational nucleation sites, N_m, was taken to be equal to the number of shear-band intersections per unit volume:

$$N_m = PN_i \tag{2.24}$$

Recasting (2.24) in the rate form:

$$\dot{N_m} = P\dot{N_i} + N_i\dot{P}H(\dot{P}) \tag{2.25}$$

In this equation $H(\dot{P})$ represents a Heaviside step function, to incorporate the irreversibility of the transformation. N_i is the number of shear band intersections per unit volume, which is taken to evolve with plastic shear strain in austenite:

$$N_i = \frac{C}{\bar{v_i}}(1 - e^{-\alpha\gamma_a})^r \tag{2.26}$$

where C and r are geometric parameters and $\bar{v}_i$ is the average volume of a shear-band intersection. The parameter α represents the rate of shear band formation, at low strains. It depends upon stacking-fault energy.

P is defined as follows:

$$P = \frac{1}{\sqrt{s_g 2\pi}} \int_{-\infty}^{g} e^{[-\frac{1}{2}(\frac{g'-\bar{g}}{s_g})^2]} dg' \qquad (2.27)$$

where $\bar{g}$ is the dimensionless mean of a given probability distribution function and s_g is its standard deviation. The parameter g is a normalised net thermodynamic driving force for martensitic transformation, defined as:

$$g = g_0 - g_1\theta + g_2\Sigma \qquad (2.28)$$

where g_0, g_1 and g_2 are positive constants. θ is the normalised temperature, which is related to the absolute temperature, T, according to:

$$\theta = \frac{T - M_{s,ut}^{\sigma}}{M_{d,ut} - M_{s,ut}^{\sigma}} \qquad (2.29)$$

where $M_{s,ut}^{\sigma}$ and $M_{d,ut}$ are the absolute M_s^{σ} and M_d temperatures for uniaxial tension. The triaxiality parameter Σ represents a ratio of the volumetric and deviatoric stress invariants:

$$\Sigma = \frac{p}{\sigma^{Y}} \qquad (2.30)$$

where:

$$p = \frac{1}{3}tr(\boldsymbol{\sigma}) \qquad (2.31)$$

$$\sigma^{Y} = \sqrt{\frac{3}{2}\boldsymbol{s} : \boldsymbol{s}} \qquad (2.32)$$

ans $\boldsymbol{s}$ is the stress deviator.

For this study α, β and r are assumed to be temperature dependent and implemented in the model as polynomial functions, see Figure 2.22.

2.5.4 The flow stress model of Olson *et al.*

The macroscopic equivalent strain rate due to slip in the composite is given by a volume average of the contributions of the austenitic and martensitic phases plus TRIP effect and elastic deformation:

$$\dot{\varepsilon} = \dot{\varepsilon}^p + \dot{\varepsilon}^{el} + \dot{\varepsilon}^{trip} + \dot{\varepsilon}^{dil} \qquad (2.33)$$

where:

$$\dot{\varepsilon}^p = \varphi\dot{\varepsilon}_m^p + (1-\varphi)\dot{\varepsilon}_a^p \qquad (2.34)$$

where $\dot{\varepsilon}^{trip}$ is the transformation plasticity strain and $\dot{\varepsilon}^{dil}$ the dilation strain. A similar correlation is imposed to determine the macroscopic equivalent shear stress:

$$\sigma^{Y} = \varphi\sigma_m^{Y} + (1-\varphi)\sigma_a^{Y} \qquad (2.35)$$

In (2.34) $\dot{\varepsilon}_a^p$ is defined as:

$$\dot{\varepsilon}_a^p = \frac{5\bar{\mu}}{3\bar{\mu} + 2\mu_a}\dot{\varepsilon}^p \tag{2.36}$$

and:

$$\dot{\varepsilon}_m^p = \frac{5\bar{\mu}}{3\bar{\mu} + 2\mu_m}\dot{\varepsilon}^p \tag{2.37}$$

where $\bar{\mu}$ is an instantaneous effective viscosity for the composite matrix, μ_a the viscosity of the austenite and μ_m the viscosity of the martensite. The evolution equations for ε_a^p and ε_m^p are based on a self-consistent estimate of the apportionment of plastic strain between the two phases Stringfellow *et al.* [14].

The evolution equation for ε_m^p includes a contribution from the self-consistent partitioning of the plastic slip rate to the two phases, analogous to the evolution equation for ε_a^p, and an additional contribution due to the inherited dislocation structure of the newly-formed martensite: it has been established that a unit of martensite which forms at a given austenite plastic strain level actually inherits the dislocation structure of its parent austenite, Socrate [15]. The value $\bar{\mu}$ is an instantaneous effective viscosity for the composite matrix:

$$\sigma^{\mathrm{Y}} = \bar{\mu}\dot{\varepsilon}^p \tag{2.38}$$

and the value μ_i is an instantaneous effective viscosity for the ith phase:

$$\sigma_i^{\mathrm{Y}} = \mu_i\dot{\varepsilon}_i \tag{2.39}$$

The increase of $\dot{\varepsilon}_m^p$ is given by:

$$\dot{\varepsilon}_m = \dot{\varepsilon}_m^p + \dot{\varepsilon}_m^{inh} \tag{2.40}$$

where:

$$\dot{\varepsilon}_m^{inh} = \left(\frac{\dot{f}}{f}\right)(\varepsilon_a^p - \varepsilon_m^p) \tag{2.41}$$

The stress level in the ith phase is determined by the following rate dependent constitutive relation (Nadai):

$$\sigma_i^{\mathrm{Y}} = s_i^*(\varepsilon_i + \varepsilon_i^*)^{\frac{1}{n_i}}\left(\frac{\dot{\varepsilon}_i^p}{\dot{\varepsilon}_0}\right)^{\frac{1}{M_i}} \tag{2.42}$$

where M_i is the strain rate sensitivity [15]. This model is fitted to the material data of Sandvik Nanoflex™, using the data from Figure 2.11 and 2.17. In the first step the temperature dependences of α, β and r are calculated and fitted, see Figure 2.22. These functions (polynomials) are implemented in the model. This final model is compared with the tensile test at different temperatures as shown in Figure 2.23.

This model provides a proper insight into what happens during strain-induced transformation. Nevertheless, a number of critical comments can be made:
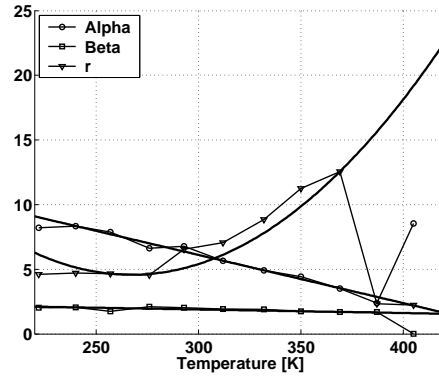
Figure 2.22: Polynominal fit on α, β and r.
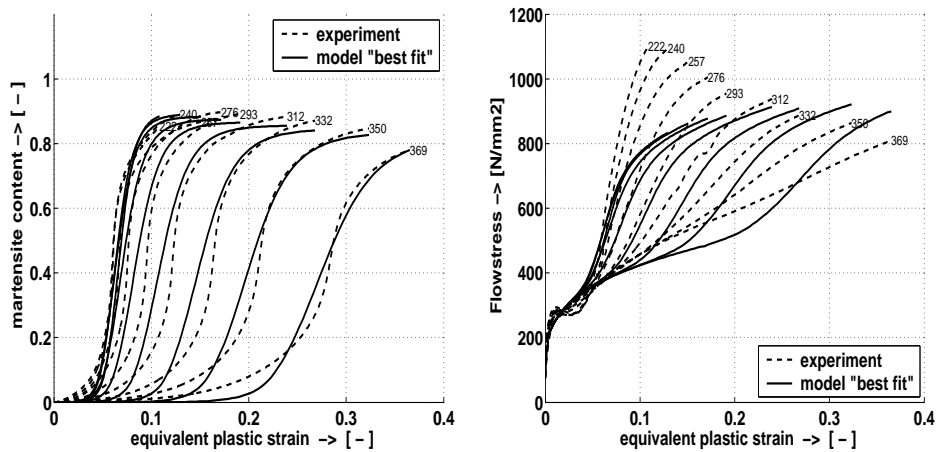
Figure 2.23: The fitted model according to Olson and Stringfellow and the measured data. Left: the strain-induced martensite. Right: the flow stress.

- The most important comment is that for each increment in the calculation a convergence process is required to reach a solution. This leads to longer computation times. Calculating complex forming processes involving several steps will require unacceptably long times;

- The temperature dependence has not been fully implemented in this model, but is implicitly included in various parameters;

- The complex interaction between transformation and plastic deformation is not implemented correctly.

2.5.5 Macroscopic dislocation-based model of Estrin

In view of the complexity of the material, the path dependence and the inheritance of dislocations during transformation, it was decided to select Estrin's approach [16, 28, 29, 33, 34], especially as described in [17], for modelling work hardening. Perhaps it is better to speak of the structure defects that affect the work hardening than to speak of dislocation density. The advantage of this process is that the work hardening can be influenced from different angles by adjusting the dislocation densities. The rate form makes the model path dependent, which is necessary for this material.

This means:

- mobile dislocations;

- im-mobile dislocations;

- possible evolution of the Taylor factor.

The evolution of the two-dimensional dislocation-based model proposed by Estrin [17] can be described by two evolution equations:

$$\frac{\partial \rho_m}{\partial \varepsilon^p} = M(-K_1 - K_2\sqrt{\rho_f} - K_3\rho_m + K_4\frac{\rho_f}{\rho_m}) \tag{2.43}$$

$$\frac{\partial \rho_f}{\partial \varepsilon^p} = M(K_1 + K_2\sqrt{\rho_f} - K_5\rho_f + K_3\rho_m) \tag{2.44}$$

where ρ_m is the mobile dislocation density, ρ_f is the immobile dislocation density, M is the Taylor factor, ε_p is the plastic deformation and $K_1..K_5$ represents the material parameters. The origins of the terms used in this model are all discussed in [35]. It is seen that the negative terms in (2.43), which represent the loss of mobile dislocation density due to various dislocation reactions, reappear as positive terms in (2.44). Parameter K_3 corresponds to the immobilization of the mobile dislocations due to binary reactions between them. Parameter K_3 represents the efficiency of this type of reaction. Another new parameter K_4 appears in the term corresponding to the generation of mobile dislocations by the forest sources. All these parameters are treated as constants. The value K_5 is not a constant but depends on the temperature and on the plastic strain rate:

$$K_5 = K(T)\left(\frac{\dot{\varepsilon^p}}{\dot{\varepsilon_0}}\right)^{\frac{1}{n}} \tag{2.45}$$

M, representing the Taylor factor, was chosen to be constant ($M = 1$), this means that the texture and texture evolution are neglected. The parameter σ^{Y}, representing the flow stress, was written as a kinetic equation:

$$\dot{\varepsilon^p} = \dot{\varepsilon_0}\left(\frac{\sigma^{\mathrm{Y}}}{\sigma_0}\right)^{\frac{1}{m}}\rho_m\rho_f^{\frac{-m}{2}} \tag{2.46}$$
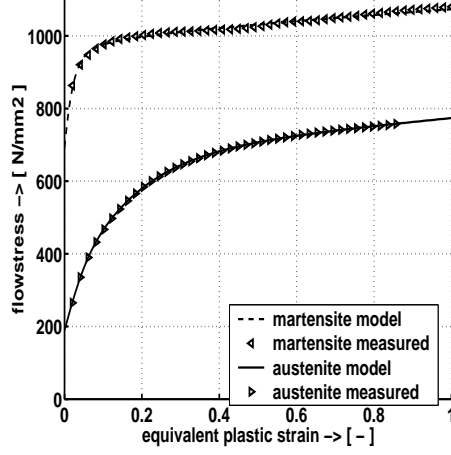
Figure 2.24: The Estrin model fitted for both martensite and austenite.

Here $\dot{\varepsilon}_0$ the reference plastic strain rate, and σ_0 is the temperature dependent reference flow stress, defined as:

$$\sigma_0 = M\alpha Gb\sqrt{\rho_{fo}} \tag{2.47}$$

Now the following equations are introduced:

$$X = \frac{\rho_m}{\rho_{mo}} \qquad Y = \frac{\rho_f}{\rho_{fo}} \tag{2.48}$$

where ρ_{mo} and ρ_{fo} are the initial dislocation densities. Two new evolution equations are introduced for the dislocations densities based on (2.43) and (2.44):

$$\frac{dX}{d\varepsilon^p} = q(C_1 - C_2\sqrt{Y} - C_3 + C_4\frac{Y}{X}) \tag{2.49}$$

$$\frac{dY}{d\varepsilon^p} = (-C_1 + C_2\sqrt{Y} - C_5 + C_3 X) \tag{2.50}$$

The parameters in these equations are related to the ones in (2.43) and (2.44) as follows:

$$
\begin{aligned}
C_1 &= \frac{MK_1}{\rho_{fo}} \qquad C_2 = \frac{M}{\sqrt{\rho_{fo}}} \frac{K_2}{} \qquad C_3 = MK_3 \\
C_4 &= \frac{MK_4\rho_{mo}}{\rho_{fo}} \qquad C_5 = \frac{MK_4}{\rho_{mo}} \qquad q = \frac{\rho_{f0}}{\rho_{mo}}
\end{aligned}
\tag{2.51}
$$

Although the martensite phase and the austenite phase individually can be easily fitted to this model it has a number of disadvantages that will be briefly discussed:

- Due to the large number of unknowns - 8 for each phase - there are many local minima in the fitting window. This does not cause any problems in case of interpolation, but for extrapolation it is not clear within which limits the model still gives a good solution.

- Use of a two coupled differential equation may lead to a situation in which the function gets out of control, i.e. the dislocation densities in a certain area increase dramatically.

- The dislocation inheritance can cause control problems in relation to the differential equations.

The conclusion from the above is that the model in this form is hard to implement in a FEM code for metal forming processes. Use in a FEM code calls for a model that provides good solutions within the entire calculation window. In this case there are problems, as transformation causes the dislocation density of the austenite to be inherited by the martensite. It is difficult to predict how accurate the solution will be under various conditions. Despite these disadvantages, the setup of this model is useful enough to warrant further exploration.

The original model of Estrin is simplified in such way that the framework of the model remains but it is much more easy to fit, making it possible to solve the system for a complex composite such as Sandvik Nanoflex™. This is achieved by choosing one simplified dislocation density for each phase:

$$
\begin{aligned}
\dot{Y} &= [C_1(C_2 - Y)^{C_3} + C_4(\dot{\varepsilon}^{\mathrm{p}}, T)]\dot{\varepsilon}^{\mathrm{p}} \qquad \text{if } Y < C_2 \\
\dot{Y} &= [C_4(\dot{\varepsilon}^{\mathrm{p}}, T)]\dot{\varepsilon}^{\mathrm{p}} \qquad \text{if } Y > C_2
\end{aligned}
\tag{2.52}
$$

This dislocation density can be inherited from austenite by the martensite.

2.6   The two-phase macroscopic model

Introduction.

For the creation of the model we have to consider the following issues:

- The models developed have to be implemented in a FEM package. The target group for this package consists of engineers who work in a research or innovation environment and who have no detailed knowledge of material behaviour. For this reason the model should be simple and transparent to ensure that the knowledge can be used during the development of metal forming processes;

- The model must be correct for the total calculation window necessary for performing calculations on metal forming processes;

- The model must be as simple as possible for an easy fit on the composite Sandvik Nanoflex™;

- The model must be in a rate formulation to implement the path dependency of the transformation and work hardening;

- The inheritance of the dislocation structure or work hardening from austenite to martensite must be implemented, to reach this goal the dislocation structure is implemented as internal state variables;

- Both the strain-induced and stress-assisted transformations must be included. These can be active or passive or both be active in the same time;

- Dilatation strain and transformation plasticity have to be implemented to describe the dimensional changes during the transformation;

- Because of the complex deformation path that can occur during plastic deformation the transformation model must be fully stress state and temperature dependent;

- Because plastic deformation heat influences the transformation behaviour, the model must be fully thermo-mechanically coupled;

- The framework must be in the same way modular to facilitate the implementation of improvements.

Based on the information of the model of strain-induced martensite after, a general differential equation was chosen [6, 14]. This model was fitted to the measured data.

Because the work hardening of the material is complex and path dependent in relation to martensite and plastic strain, it was decided to use a modified Estrin [17] model with two internal state variables to describe the dislocation densities. A rate formulation was chosen to incorporate the path dependence.

2.6.1 General transformation model

A general differential equation for the transformation behaviour was constructed:

$$\dot{\varphi} = C(D + \varphi)^{n_a}(f_s - \varphi)^{n_b} \tag{2.53}$$

where C is related to the mean transformation rate, D is related to the nucleation or initial transformation rate, f_s is the saturation value of the transformation and n_a and n_b are fit constants that determine the shape of the curve. The first part of the equation $(D + \varphi)^{n_a}$ describes how the transformation rate increases because the formed martensite has a bigger volume, which causes positive stresses around this region. These stresses accelerate the transformation.

When most of the material has transformed, the transformation rate decreases. The local hydrostatic stress becomes negative in the retained austenite. Depending on the kinetics, the transformation will stop. This is described by the last term of equation (2.53) : $(f_s - \varphi)^{n_b}$.

The martensite transformation is split into two parts:

- One below the yield stress of the composite, the stress-assisted transformation;

- One at above the yield stress of the composite, the strain-induced transformation.

The total martensite content is the summation of both types of transformation:

$$\dot{\varphi} = \dot{\varphi}_{strain} + \dot{\varphi}_{stress} \tag{2.54}$$

The kinetics of the strain-induced martensite transformation depends only on the amount of plastic energy generated during the deformation. The plastic energy is the driving force of the transformation and therefore the saturation value f_s is chosen as a constant with a high level (95-100%). The kinetics of the stress-assisted transformation is based on the chemical composition and austenitising conditions of the material. There is no external energy. Therefore, the saturation value f_s is chosen not to be a constant.

2.6.2 Strain-induced transformation

Equation (2.53) was adapted to apply to the strain-induced transformation:

$$\dot{\varphi}_{strain} = C_{strain}(T, \sigma^{\mathrm{H}}, Z)[(D_1 + \varphi)^{n_1}(f_{strain} - \varphi)^{n_2}]\dot{\varepsilon}^{\mathrm{P}} \tag{2.55}$$

where φ is the martensite content and C_{strain} is a function that describes the temperature, hydrostatic stress and material structure dependence of the transformation. Z is a parameter that depends on the annealing conditions before metal forming, the chemical composition and crystal orientation, see Figure 2.25 and Figure 2.27 right. C_{strain} is related to the thermodynamics of the transformation. The following function is assumed based on curve fitting:

$$C_{strain} = Q_1(1 + Q_2 \tanh(Q_3 \sigma^{\mathrm{H}}))(e^{\frac{(T - T_0)^2}{Q_4}} - Q_5) \tag{2.56}$$

Here Q_1 is a constant describing the mean transformation rate; Q_2, Q_3 describe the influence of the stress state and Q_4, Q_5 describe the influence of the temperature on the transformation and T_0 is the temperature of the nose of the TTT-diagram. The influence of the chemical composition and the crystal orientation are neglected, The values of Q, n_2 and T_0 can be found in Table 2.5.
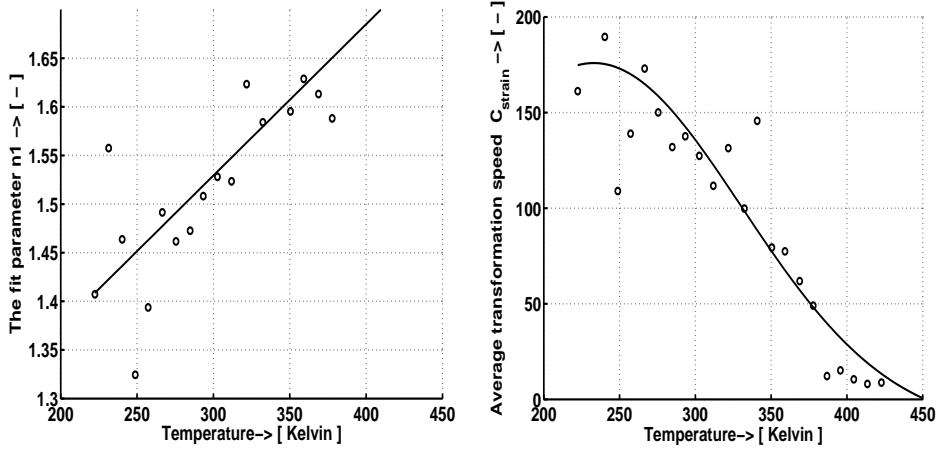
Figure 2.25: Right: the temperature dependence of the strain-induced transformation C_{strain}. Left: the fit parameter n_1. See for the other fitted parameters table(2.5).

Table 2.5: Value of the fitted parameters for the flow stress and the strain-induced transformation

Q_1	184	Q_2	0.50
Q_4	14629	Q_5	0.056412
$\sigma_{0\gamma}$	175.8 $[N/mm^2]$	$\sigma_{0\alpha}$	694.2 $[N/mm^2]$
m_α	1087	m_γ	140
n_1	$1.108 + 1.3624E - 3.T$	n_2	2
C_1	12.477	C_2	22.822
C_4	$-1.0267 + 1.3282\dot{\varepsilon} + 0.020436T$	C_5	62.268
C_7	1.7934	C_8	$0.54154 - 0.46797\dot{\varepsilon} - 4.7171E - 4.T$
C_{10}	1.8961	ψ_γ	1.9061E-4
Q_3	0.005	f	0.95
φ_0	$0.7981 + 1.278E - 4.T$	q	$0.24 + 3.1079E - 4.T$
C_3	0.61054	D_1	$9.7259E - 3$
C_6	2.7907	C_9	$0.8062 \exp(-\frac{(T-196)^2}{7457.3})$
ψ_α	9.78E-4	T_0	223 K

2.6.3   Stress-assisted transformation

The description of the stress-assisted transformation is based on equation (2.53) [23], but in a more general form:

$$\dot{\varphi}_{stress} = C_{stress}(T, \sigma^{\mathrm{H}}, \varepsilon^{\mathrm{p}}, Z)[(D_2 + \varphi)^{n_3}(f_{stress}(T, \sigma^{\mathrm{H}}, Z) - \varphi)^{n_4}] \qquad (2.57)$$

where C_{stress} is a function that describes the dependence of transformation on stress, temperature and material structure.

For both annealing conditions the following model was used to describe the transformation. The interaction between the state variables that influence the transformation have not been investigated. Therefore, the dependency of C_{stress} and f_{stress} can be split up into a temperature dependence, a hydrostatic pressure dependence and a plastic strain dependence. D_2 is a constant.

$$C_{stress}(T, \sigma_h, \varepsilon_p) = C^1_{stress}(T) \; C^2_{stress}(\sigma_h) \; C^3_{stress}(\varepsilon^P) \tag{2.58}$$

$$f_{stress}(T, \sigma_h, \varepsilon^P) = f^1_{stress}(T) \; f^2_{stress}(\sigma_h) \; f^3_{stress}(\varepsilon^P) \tag{2.59}$$

The following relations for C_{stress}, D_2 and f_{stress} are proposed, where $R_1 \ldots R_{17}$ are constants, based on fitting.

$$C^1_{stress}(T) = R_1 \exp^{\frac{-(T-232)^2}{R_2}} \tag{2.60}$$

$$C^2_{stress}(\sigma_h) = R_3 + \left[\frac{1}{2} + \frac{1}{2}\tanh\left(R_4(\sigma_h - R_5)\right)\right](1 - R_3) \tag{2.61}$$

$$C^3_{stress}(\varepsilon^P) = R_6 + \left[\frac{1}{2} + \frac{1}{2}\tanh\left(R_7(\varepsilon^P - R_8)\right)\right](1 - R_6) \tag{2.62}$$

$$D_2 = R_9 \tag{2.63}$$

$$f^1_{stress}(T) = R_{10} + \exp^{\frac{-(T-232)^2}{R_{11}}}(1 - R_{10}) \tag{2.64}$$

$$f^2_{stress}(\sigma_h) = R_{12} + \left[\frac{1}{2} + \frac{1}{2}\tanh\left(R_{13}(\sigma_h - R_{14})\right)\right](1 - R_{12}) \tag{2.65}$$

$$f^3_{stress}(\varepsilon^P) = R_{15} + \left[\frac{1}{2} + \frac{1}{2}\tanh\left(R_{16}(\varepsilon^P - R_{17})\right)\right](1 - R_{15}) \tag{2.66}$$

The fit resulted in the parameters presented in Table 2.6 and Table 2.7, the results of the model are shown in Figure (2.26).

Table 2.6: Value of the fitted parameters for stable material

R_1	1.2E-1	R_2	2.8E3	R_3	0	R_4	2.4E-3 [MPa]
R_5	4.2E-3	R_6	19.6	R_7	4.4	R_8	3.0E-2
R_9	1.3E-1	R_{10}	-2.0	R_{11}	8.9E4	R_{12}	6.2E-1
R_{13}	1.6E-2	R_{14}	0	R_{15}	0	R_{16}	20
R_{17}	2.5E-2	n_3	2.9	n_4	6.0		

This model provides a good prediction of the saturation value of the martensite content, especially for the unstable material.
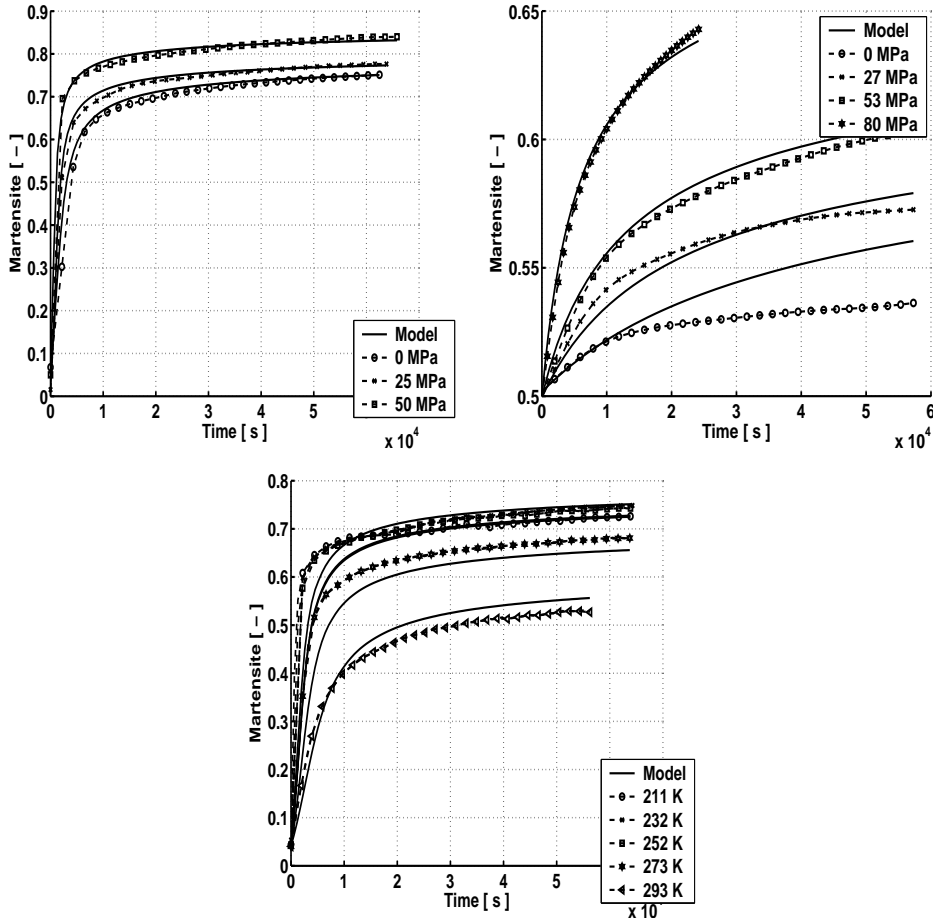
Figure 2.26: The stress-assisted transformation. Top Left: the influence of the applied stress on the stress-assisted transformation of unstable material. Top right: the influence of the hydrostatic stress on the stress-assisted transformation, of stable material (pre-treatment 1) after deforming the specimen until the strain-induced martensite reaches 0.5. Bottom: temperature dependence of the transformation of unstable material (pre-treatment 2).

2.6.4   Path dependent dislocation based on work hardening.

For this study it was assumed that the work hardening depends on plastic strain, martensite content, temperature, and plastic strain rate. The model used was based on the physical-based models of Estrin [17], describing dislocation densities as internal state variables. The work hardening mechanism is not only based on change in dislocation density but also on other structural defects such as subgrains

Table 2.7: Value of the fitted parameters for instable material

R_1	1.2E-1	R_2	2.8E3	R_3	-4.6E-4	R_4	2.46E-3 [MPa]
R_5	4.2E-3	R_6	2.6	R_7	4.4	R_8	3.0E-2
R_9	1.5E-1	R_{10}	-2.0	R_{11}	8.9E4	R_{12}	7.5E-1
R_{13}	1.6E-2	R_{14}	65	R_{15}	1.2	R_{16}	20
R_{17}	2.5E-2	n_3	2.9	n_4	6.0		
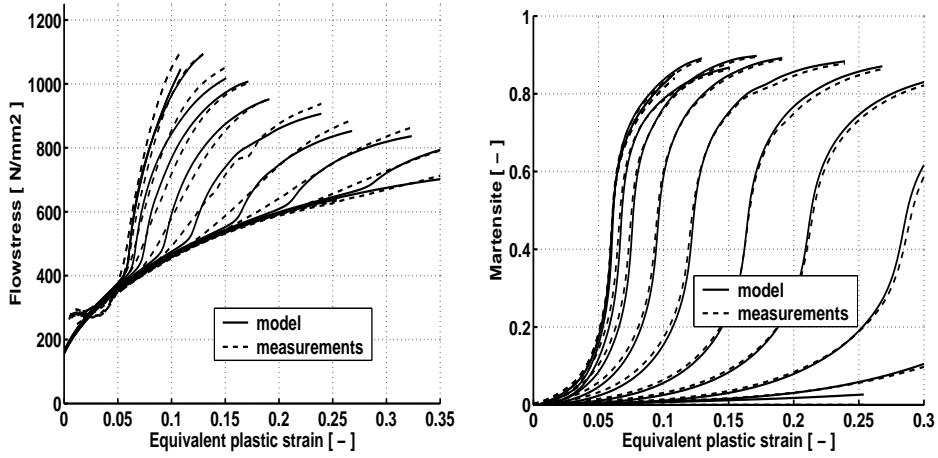
Figure 2.27: The fitted model and measuring data. Left: the flow stress. Right: the strain-induced martensite.

etc. Therefore, parameter Y is not the dislocation density alone but the resistance of dislocation movement caused by structural defects in relation to plastic deformation. In this study only one dislocation density was used for each phase. The original model was modified to make it as simple as possible and reduce the number of unknowns. For the flow stress of austenite we assumed:

$$\sigma_\gamma^{\mathrm{Y}} = \sigma_{0_\gamma} \sqrt{Y_\gamma} (1 + \frac{\dot{\varepsilon}^{\mathrm{P}}}{\psi_\gamma})^{\frac{1}{m_\gamma}} \qquad (2.67)$$

And for the flow stress of martensite:

$$\sigma_\alpha^{\mathrm{Y}} = \sigma_{0_\alpha} \sqrt{Y_\alpha} (1 + \frac{\dot{\varepsilon}^{\mathrm{P}}}{\psi_\alpha})^{\frac{1}{m_\alpha}} \qquad (2.68)$$

Value 1 was implemented to avoid a high derivative $d\dot{\varepsilon}/dt$ at low strain rates, for example at the beginning of plastic deformation. In the equation σ_0 is the basic stress that depends on strain rate and temperature, φ represents the martensite content, Y the general dislocation density for one phase, $\dot{\varepsilon}^{\mathrm{P}}$ is the equivalent plastic strain rate, $\psi_{\alpha,\gamma}$ the reference strain rate and $m_{\alpha,\gamma}$ a constant depending on strain

rate and temperature. For the combination of both phases the equation becomes:

$$\sigma^{\mathrm{Y}} = \sigma_\gamma^{\mathrm{Y}} - \frac{1}{2}(1 + \tanh(\frac{\varphi - \varphi_0}{q}))(\sigma_\alpha^{\mathrm{Y}} - \sigma_\gamma^{\mathrm{Y}}) \qquad (2.69)$$

The constants φ_0, q were introduced to describe the non-linear relation between the flow stresses as a mixture rule. At low martensite contents the influence of martensite will be lower than at high levels of martensite fraction. The evolution of the dislocation density in the austenite is described as follows:

$$\begin{aligned}
\dot{Y}_\gamma &= [C_1(C_2 - Y_\gamma)^{C_3} + C_4(\dot{\varepsilon}^{\mathrm{P}}, T)]\dot{\varepsilon}^{\mathrm{P}} \\
\dot{Y}_\gamma &= [C_4(\dot{\varepsilon}^{\mathrm{P}}, T)]\dot{\varepsilon}^{\mathrm{P}} \quad \text{if } Y_\gamma > C_2
\end{aligned} \qquad (2.70)$$

where C_1, C_2, C_3 are material constants and C_4 depends on temperature and strain rate. The constants are not directly related to physical phenomena but are chosen to fit the model. In a similar way the following applies to the dislocation density in the martensite phase:

$$\begin{aligned}
\dot{Y}_{\alpha 1} &= [C_5(C_6 - Y_\alpha)^{C_7} + C_8(\dot{\varepsilon}^{\mathrm{P}}, T)]\dot{\varepsilon}^{\mathrm{P}} \\
\dot{Y}_{\alpha 1} &= [C_8(\dot{\varepsilon}^{\mathrm{P}}, T)]\dot{\varepsilon}^{\mathrm{P}} \quad \text{if } Y_\alpha > C_7
\end{aligned} \qquad (2.71)$$

Where C_5, C_6, C_7 are material constants and C_8 depends on temperature and strain rate.

During transformation three different phenomena occur:

- recovery of the dislocation density takes place due to generation of virgin martensite;
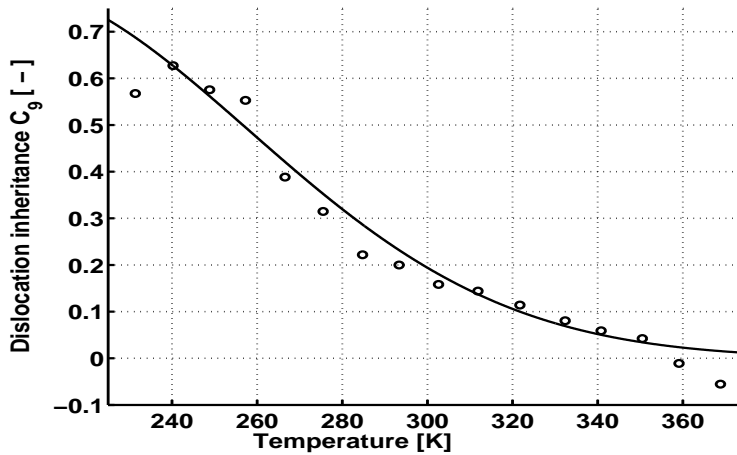

Figure 2.28: The dislocation inheritance parameter C_9.

- the dislocation density in the austenite is not annihilated during the transformation but is partly transferred to the martensite;

- New dislocations are formed at the transformation boundary.

The second effect depends on the temperature.

Suppose we start with a volume V with a specific amount of martensite φ and a dislocation density of Y_α. After a deformation step the martensite content has increased by $d\varphi$ and the dislocation density has increased by dY_φ. This means:

$$(\varphi + d\varphi)(Y_\alpha + dY_\alpha) = \varphi Y_\alpha + C_9(T)d\varphi Y_\gamma + d\varphi C_{10} \qquad (2.72)$$

where φY_α is the initial dislocation density, C_9 is the parameter which describes the inheritance of dislocations from austenite to martensite and C_{10} represents the generation of dislocations on the transformation boundary. It is assumed that at this temperature, C_9 will reach its maximum. From (2.72) it follows:

$$C_9(T)d\varphi Y_\gamma + C_{10}d\varphi = d\varphi Y_\alpha + \varphi dY_\alpha \qquad (2.73)$$

or:

$$\dot{Y}_\alpha = \frac{\dot{\varphi}}{\varphi}(C_9(T)Y_\gamma + C_{10} - Y_\alpha) \qquad (2.74)$$

Here $\frac{\dot{\varphi}}{\varphi}C_9(T)$ is the dislocation inheritance of the dislocation density, $\frac{\dot{\varphi}}{\varphi}C_{10}$ represents the generation of new dislocations on the transformation boundary and $-\frac{\dot{\varphi}}{\varphi}Y_\alpha)$ is the recovery due to new, virgin martensite.

It is assumed that the generation of dislocation density on the boundary is much higher with lath martensite, resulting from the strain-induced transformation, than with plate martensite, resulting from the stress-assisted transformation. This means that the generation of dislocations on the boundaries is related only to the φ_{strain}, and the inheritance and recovery effects are related to the total martensite content. We have to split (2.74) into two parts, one related to the total transformation rate and one related to the strain-induced transformation rate:

$$\dot{Y}_{\alpha2} = \frac{-\dot{\varphi}}{\varphi}(C_9(T)Y_\gamma + Y_\alpha) \qquad (2.75)$$

For the generation of dislocations on the transformation boundary the following equation is introduced:

$$\dot{Y}_{\alpha3} = \frac{\dot{\varphi}_{strain}}{\varphi}C_{10} \qquad (2.76)$$

where C_9 is a constant that depends on the temperature. The values of C_9 and C_{10} were calculated by curve fitting, see Figure 2.28 for the temperature dependence of C_9. From (2.71), (2.75) and (2.76) the following equation is defined for the dislocation density in the martensite:

$$\dot{Y}_\alpha = \dot{Y}_{\alpha1} + \dot{Y}_{\alpha2} + \dot{Y}_{\alpha3} \qquad (2.77)$$

For a comparison between measured and calculated stress strain curves, see Figure 2.27, left. This model gives better results than the original model of Olson concerning the flow stress of the composite, see Figure 2.23.

Table 2.8: The fitting scheme of the strain-induced transformation and the flow stress of the composite.

nr	What to fit	constants
1	σ_γ	$C_1, C_2, C_3, C_4, \sigma_{0_\gamma}, \psi_\gamma, m_\gamma$
2	σ_α	$C_5, C_6, C_7, C_8, \sigma_{0_\alpha}, \psi_\alpha, m_\alpha$
3	φ	$C_{strain}, D_1, n_1, n_2, f, Q_1, Q_2, Q_4, Q_5$
4	$\sigma_\gamma, \sigma_\alpha, \varphi$	$\varphi_0, q, C_{12}, C_{13}, C_1, C_5$
5	all	all

2.6.5   The fitting procedure

The total model for the formation of strain-induced martensite and work hardening based on transformation and 'classical' work hardening consists of 27 unknowns. Fitting a model like this requires a fitting procedure. The procedure for fitting the model was chosen as follows:

1. First, fit the work hardening of austenite, using strain rate and temperature information from the tensile tests and the work hardening behaviour at high strains from the upsetting tests;

2. Second, do the same with the data from the martensite, using the influence of strain, temperature and strain rate of the flow stress of martensite;

3. Fit the temperature and stress state dependence of the strain-induced transformation. The relation of the stress state is partly based on the feedback of the FEM calculation and is not fitted directly from the tensile tests at different temperatures;

4. Fit the combination of the first 3 items, using only the interaction parameters as unknowns. Most others are treated as constants based on the the first 3 items;

5. If necessary, the total model can be adjusted by varying all the parameters at the same time. This is only possible for small adjustments.

See for the fitting scheme Table 2.8. In this way all the constants can be fitted.
The fit resulted in the parameters presented in Table 2.5.

2.6.6   Relation between hardness and flow stress

For the samples of Table 2.3 the hardness was measured in the non-aged and aged condition. As only the martensite phase is precipitation hardable, there must be a very strong relationship between the martensite content and the change in hardness caused by the ageing process. From the literature it is well known that there should be a relationship between the hardness and the flow stress. See for the result Figure 2.29.
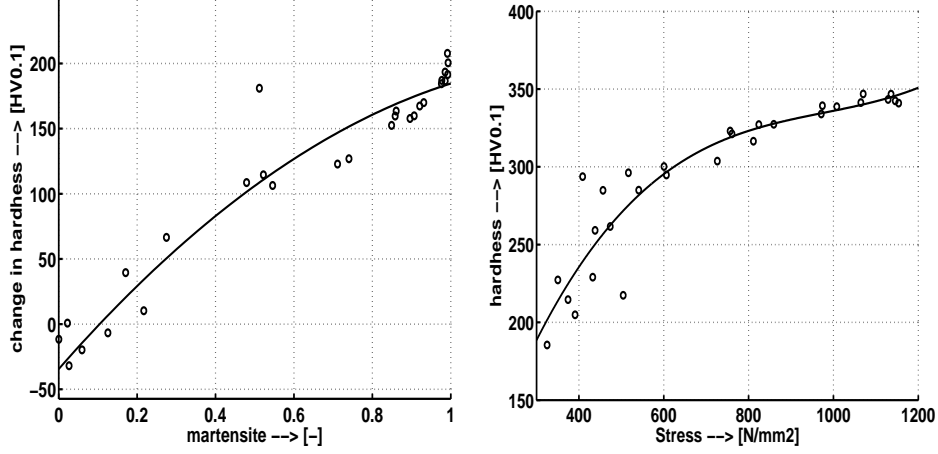
Figure 2.29: Right: the relation between hardness and flow stress. Left: the relation between change in hardness and martensite content.

2.6.7 Transformation dilation and transformation plasticity

The change in density during the transformation is given by:

$$\dot{\rho} = (\rho_\alpha - \rho_\gamma)\dot{\varphi} \tag{2.78}$$

where ρ_α is the density of martensite, ρ_γ is the density of austenite and φ is the martensite content. This change in density causes an extra strain in the material:

$$\dot{\varepsilon}^{dil} = \frac{-\dot{\rho}}{3\rho} \tag{2.79}$$

where $\dot{\varepsilon}_{dil}$ represents the dilation strain rate.

For the transformation plasticity the following equation is proposed based on [15]. The transformation plasticity of [15] is only valid for strain-induced martensite. To extend this model to strain-induced and stress-assisted martensite formation the influence of the stress is implemented:

$$\dot{\varepsilon}^{\mathrm{trip}} = \dot{\varphi}A(\varphi)\sigma\sqrt{\frac{2}{3}} \tag{2.80}$$

Here $A(\varphi)$ is given by:

$$A(\varphi) = \frac{0.05(3 + \tanh(10(0.5 - \varphi)))}{\sigma^{\mathrm{Y}}} \tag{2.81}$$

This equation is a smooth version of the original stepwise function of Socrates [15].

2.7 The three-phase macroscopic model for the flow stress and strain-induced transformation

2.7.1 Introduction
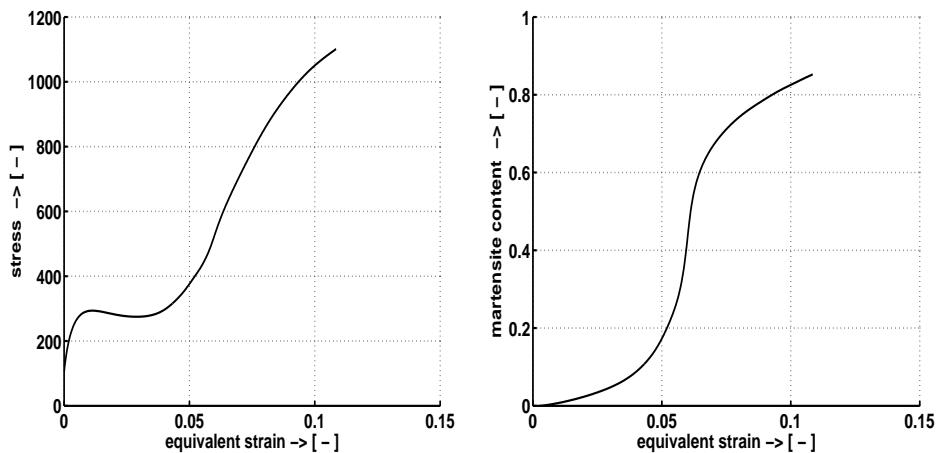
Figure 2.30: The result of the tensile test at low strain rates (0.001/sec) at 222 K.

In the two phase model the drop of the flow stress at low plastic strains can not be fitted correctly. For this phenomena there are two possible explanations:

- The transformation plasticity, during the plastic deformation, is implemented as a part of the work hardening. A more direct implementation of the transformation plasticity gives more possibilities and a better fit. For this we need a better model for this transformation plasticity and the dependence of the other state variables.

- In other metastable stainless steels there is a third phase present [36, 37]: epsilon martensite. This extra intermediate phase accompanies his own transformation plasticity, this can be the explanation of the drop in flow stress.

It is assumed that at lower temperatures the transformation from austenite to martensite takes an extra transformation step, epsilon martensite or hexagonal martensite. Figure 2.30 shown the results of a tensile test at a low temperature (222 K). It shows very clearly that the extreme work hardening is related to the transformation to cubic martensite. At low strains there is a softening phenomenon which is not related to the transformation to cubic martensite. It is assumed that this phenomenon is related to the transformation to hexagonal martensite which is paramagnetic and will not effect the magnetic sensor. Because this third phase allows some recovery during the plastic deformation, a model was constructed that also included the hcp (hexagonal close packed) martensite.
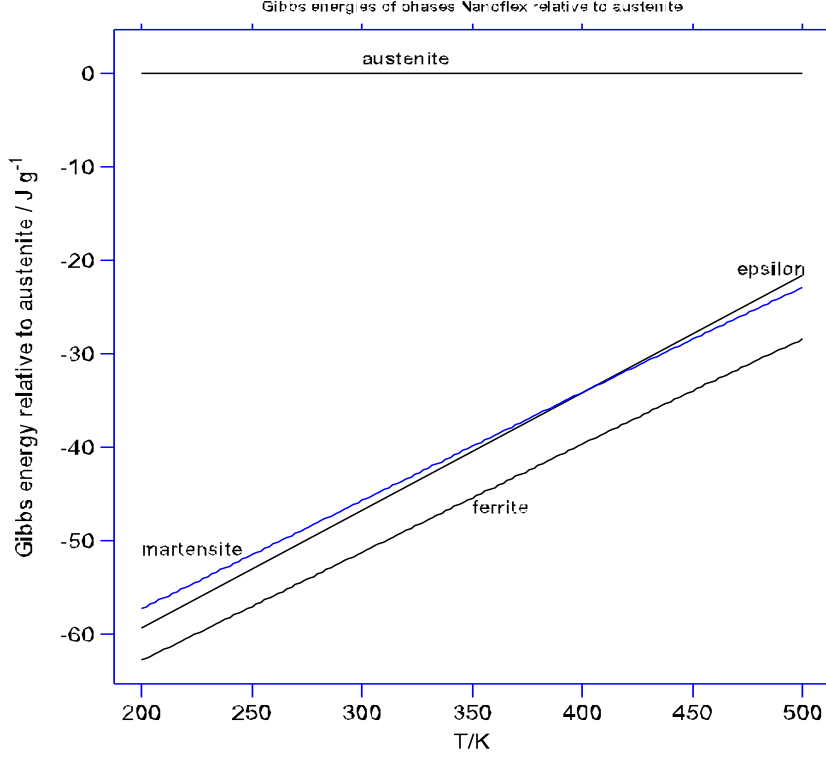
Figure 2.31: The free energies of the different phases of Sandvik Nanoflex™ based on MTDATA.

2.7.2 Strain-induced transformation

From the literature and the calculations with the thermodynamic package MT-DATA it is known that the hcp martensite transformation occurs mostly at lower temperatures in alloys with a low stacking fault energy. At those temperatures the hcp martensite is much more unstable then the martensite. Hence the transformation from austenite to hcp martensite will be a precursor of the transformation to martensite. The implementation was based on the proposed model of chapter 2 (2.55) but, the model is extended to make the transformation from austenite to hcp martensite a precursor of the transformation to cubic martensite:

$$\dot{\psi}_{strain} = C_{strain}(T, \sigma^{\mathrm{H}}, Z)[(D_1 + \psi_{strain})^{n_1(T)}$$
$$(f_{strain} \cdot A_1 e^{\frac{-(T-A_2)^2}{A_3}} - \psi_{strain})^{n_2}]\dot{\varepsilon}^{\mathrm{P}} \qquad (2.82)$$

where ψ is the hcp martensite content, A_1, A_2, A_3, A_4 are fit constants to describe the relative stability of hcp martensite, T is the temperature in Kelvin and C_{strain} is a function that describes the temperature, hydrostatic stress and material

structure dependence of the transformation. Z is a parameter that depends on the annealing conditions before metal forming, the chemical composition and treated as a constant. C_{strain} is related to the thermodynamics of the transformation. Of
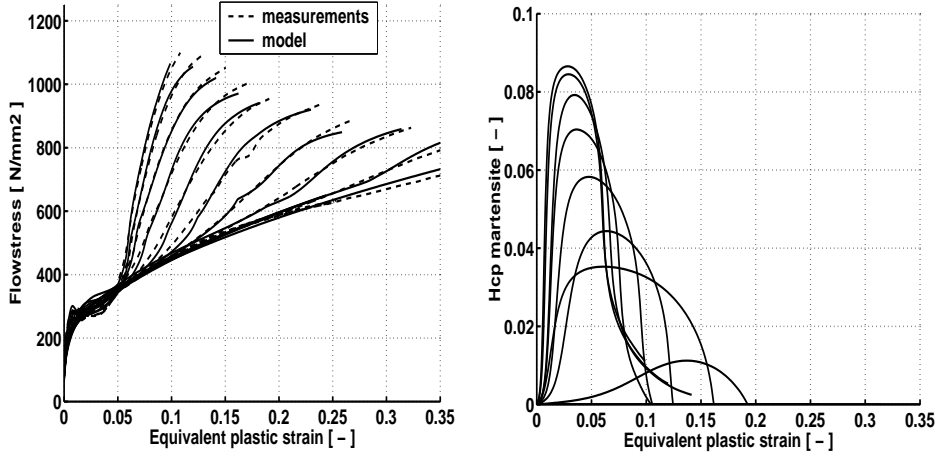
Figure 2.32: The fitted model with 3 phases and measuring data. Left: the flow stress. Right: the strain-induced hcp martensite (ϵ).

course it would be more elegant to let the martensite transform out of the content on hcp martensite, but for curve fitting reasons (2.82) was based on inductive measurements. Because of the fact that the cubic martensite transforms from the hcp martensite, the hcp martensite will vanish during the process. For the calculation of the flow stress we need to know the momentum of hcp and cubic martensite. For the free hcp martensite we obtain from (2.82):

$$\dot{\psi}_{free} = \dot{\psi} - \dot{\varphi} \tag{2.83}$$

The kinetics of the strain-induced martensite transformation depends on the amount of plastic energy generated during deformation. Therefore the saturation value is constant and has a high level (95-100%). This is assumed for both phases (cubic and hexagonal martensite)

2.7.3 Path-dependent dislocation based on work hardening.

For this study it is assumed that the work hardening depends on plastic strain, martensite content, temperature, and the influence of strain rate. For the flow stress of austenite we use (2.67) and for cubic martensite (2.68) was used. For the flow stress of eps martensite:

$$\sigma_\psi^Y = \sigma_{0_\psi} \sqrt{Y_\psi} (1 + \frac{\dot{\varepsilon}^P}{\varepsilon_{0_\psi}})^{\frac{1}{m_\psi}} \tag{2.84}$$
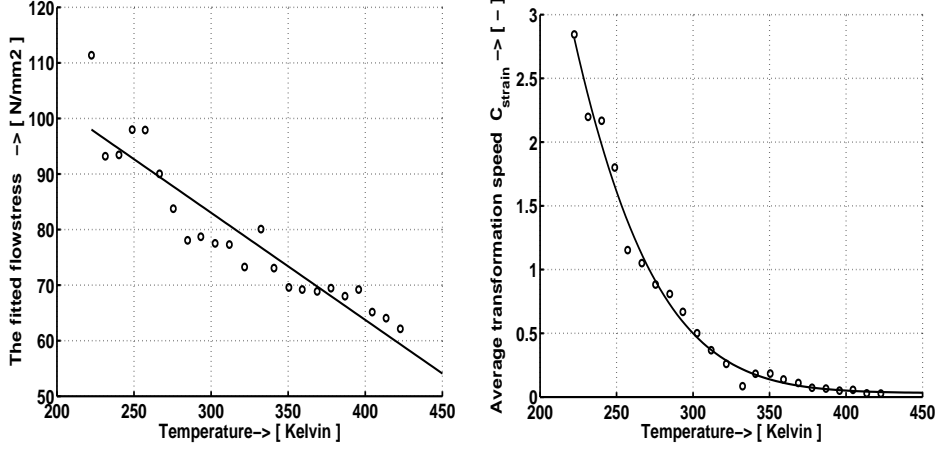
Figure 2.33: Left: The temperature dependence of the flow stress of austenite: $\sigma_\gamma^{\mathrm{Y}}$.
Right: the temperature dependence of the strain-induced transformation C_{strain}.

In the equation σ_{0_ϵ} is the basic stress that depends on strain rate and temperature, φ represents the martensite content, Y the general dislocation density for one phase, $\dot{\varepsilon}^p$ is the equivalent plastic strain rate, ε_{0_ϵ} the reference strain rate and m_ϵ a constant depending on strain rate and temperature. For the combination of the three phases the equation becomes:

$$
\begin{aligned}
\sigma^{\mathrm{Y}} =& \sigma_\gamma^{\mathrm{Y}} \\
&+ \frac{1}{2}(1 + \tanh(\frac{\psi - \psi_0(T)}{q_1(T)}))(\sigma_\psi^{\mathrm{Y}} - \sigma_\gamma^{\mathrm{Y}}) \\
&+ \frac{1}{2}(1 + \tanh(\frac{\varphi - \varphi_0(T)}{q_2(T)}))(\sigma_\alpha^{\mathrm{Y}} - \sigma_\gamma^{\mathrm{Y}})
\end{aligned}
\tag{2.85}
$$

In the equation σ^{Y} is the equivalent flow stress, ψ represents the hcp martensite, φ represents the cubic martensite content. The values ψ_0, φ_0, q_1 and q_2 are fit constants describing the mixture rules for the phases. The evolution of the dislocation density in the austenite is described in (2.70).

In a similar way the following applies to the dislocation density in the hcp martensite phase:

$$
\begin{aligned}
\dot{Y}_\psi =& [C_{11}(C_{12} - Y_\psi)^{C_{13}} + C_{14}(\dot{\varepsilon}^{\mathrm{P}}, T)]\dot{\varepsilon}^{\mathrm{P}} \\
\dot{Y}_\psi =& [C_{14}(\dot{\varepsilon}^{\mathrm{P}}, T)]\dot{\varepsilon}^{\mathrm{P}} \quad \text{if } Y_\psi > C_{12}
\end{aligned}
\tag{2.86}
$$

where C_{11}, C_{12}, C_{13} are material constants and $C14$ depends on temperature and strain rate. And for the cubic martensite (2.71) is used.

During transformation two different phenomena occur:

- recovery takes place due to generation of virgin martensite;

- the defect density, like dislocation density, in the austenite will not annihilate during the transformation but is partly transferred to the hcp or cubic martensite.

To describe the recovery effect and the dislocation inheritance form austenite to hcp martensite the following is assumed:

$$\dot{Y}_\psi = \dot{Y}_\psi - \frac{\dot{\psi}}{\psi + \psi_0}[Y_\psi + C_{15}(T)Y_\gamma] \tag{2.87}$$

Here C_{15} is the inheritance parameter for gamma to hcp martensite. For the dislocation transfer and recovery from hcp martensite to cubic martensite the following equation is introduced:

$$\dot{Y}_\varphi = \dot{Y}_\varphi - \frac{\dot{\varphi}}{\varphi + \varphi_0}[Y_\varphi + C_{16}(T)Y_\varphi] \tag{2.88}$$

Where C_{16} is a constant that describes the inheritance of the dislocation from hcp martensite to cubic martensite, depending on the temperature. The value er is added to avoid numerical problems if ψ or φ become zero. The values of $C_1...C_{14}$ were determined by curve fitting, see Figure 2.32, left.

2.7.4 Results of the fit.

This model was fitted to the measured data. For a comparison between measured and calculated stress strain curves, see Figure 2.32. It is clear that the model is much better for small strains. In the right-hand figure the calculated hcp martensite is shown. This is not exact because the recovery effect caused by the transformation plasticity is implicit in the measured flow stress, but is not implemented in this fit. It is clearly shown that this transformation is temperature dependent, as described in the literature. In Figure 2.33 the inheritance parameter is illustrated in the right-hand graph, it shows the same pattern as in the two-phase model. In the left-hand graph the temperature dependence of the calculated flow stress of the composite is given.

Chapter 3

FEM implementation

3.1 Abstract

Sandvik Nanoflex™combines good corrosion resistance with high strength. Sandvik Nanoflex™has good deformability in austenitic conditions. It belongs to the group of metastable austenites, which means that during deformation a strain-induced transformation to martensite takes place. After deformation, transformation continues as a result of internal stresses. Depending on the previous heat treatment, this stress-assisted transformation is more or less autocatalytic. Both transformations are stress-state and temperature dependent. A constitutive model for this steel, based on the macroscopic material behaviour measured by inductive measurements is presented. Both the stress-assisted and the strain-induced transformations into martensite have been incorporated in this model. Path dependent work hardening has also been taken into account. Also, the implementation in an internal Philips FEM code called CRYSTAL for carrying out simulations is described. The implementation is based on lookup tables in combination with feed-forward neural networks and a material definition file. This approach has been chosen in order to allow the use of different complex material models with one executable, to realize a flexible and robust solver. In the simulations the tools are treated as rigid bodies. Friction has been taken into account because it influences the stress state during metal forming and, indirectly, the transformation behaviour. The material properties after a calculation step are mapped to the next step to incorporate the cumulative effects such as transformation and work hardening during the different operations. The implemented model was validated by different one-step metal-forming processes. Finally a multi-stage metal-forming process was simulated. The process consisted of different forming steps with intervals between them to simulate the waiting time between different metal-forming steps. The results of the transformation behaviour are presented together with the measured shape of the product during and after metal forming and the measured local hardness of the product.

3.2   Introduction

Metastable austenites can undergo two types of transformation: stress-assisted and strain-induced transformation. Because both types of transformation depend on temperature and hydrostatic stress, it is almost impossible to use analytical models to describe them during metal forming. Because of the influence of temperature on the transformation, the calculations need to be thermo-mechanically coupled. The calculations also have to incorporate the effects of friction because it influences the stress state. The material used for these calculations was a corrosion-resistant steel, referred to as Sandvik Nanoflex™[3].

Implementing complex material behaviour as shown by Sandvik Nanoflex™is not straightforward. Such material behaviour is not standardly available in commercial non-linear solvers such as MSC.Marc and Abaqus. As the model developed will be used for process window studies, maximum robustness was required. For this reason, it was decided to build the material model into an internal Philips solver. The calculations described have therefore been made with a dedicated internal Philips FEM code. This code was specifically developed to describe multi-stage metal forming processes involving complex material behaviour. In addition, it was decided not to perform the implementation in the usual way by means of user subroutines, but to use a flexible implementation based on lookup tables and/or neural networks. One of the advantages of this approach is that it allows the material models to be adapted without affecting the robustness of the solver. This approach also simplifies version control. The solver developed is specifically dedicated to multi-stage metal forming processes, including possible heat treatments.

3.3 General constitutive behaviour of metastable stainless steel

3.3.1 Model description

The major problem with implementing a model for a metastable stainless steel is that there are many internal state variables such as:

- different phases;

- structural defects which influence the work hardening of the different phases, such as dislocation density;

- different densities;

- elastic properties of every phase;

- etc.

In one way or another all these state variables interact. The literature does not fully explain the importance of all these state variables and how they interact. For this reason a very flexible implementation was preferred, which describes all the internal state variables as p_i.

For example the macroscopic flow stress of Sandvik Nanoflex™can be defined as:

$$\sigma^{\mathrm{Y}} = \sigma^{\mathrm{Y}}(p_i) \tag{3.1}$$

where σ^{Y} is the macroscopic flow stress of the composite and p_i stands for the other internal state variables such as:

- flow stress of every phase;

- fraction of the phases.

Over time or during plastic strain Sandvik Nanoflex™transforms from austenite to martensite, which is implemented as:

$$\varphi = \varphi(p_i) \tag{3.2}$$

During this transformation the density changes as martensite has a lower density than austenite. This means that during transformation, the volume will expand. This has a major influence on the hydrostatic stress in the material. Therefore, the change in density was also implemented:

$$\rho = \rho(p_i) \tag{3.3}$$

During transformation not only the density changes but there is also an extra plastic deformation known as transformation plasticity. This can be defined as:

$$\varepsilon^{trip} = \varepsilon^{trip}(p_i) \tag{3.4}$$

where ε^{trip} is the transformation plasticity.

3.4 The lookup and neural network-based implementation of material models

Complex material models are generally implemented by user subroutines in standard commercial solvers. In this case the target was to create an environment in which the following would be possible:

- for metal forming engineers who are not FEM specalists to calculate complex multi-stage metal forming processes, including complex material behaviour;

- To control versions, which means that one executable has to be used;

- To further optimise the material models parallel to standard simulations, without losing any of the robustness of the solver;

- For the solver to have maximum robustness, making it suitable for process window studies;

- To implement new material models quickly, irrespective of their complexity and without any negative effect on the robustness of the solver;

- To use different material models in multi-stage calculations and to switch from one model to the next in order to include possible changes in material models if additional processes are used.

In view of the above requirements the following approach was used:

- One executable;

- Implementing material behaviour on the basis of the material definition file in combination with lookup tables and/or neural networks;

- Using a clearcut file structure to ensure that mesh and material data transfer is easy and takes place in a structured way.

This material model and the implementation are presented in the following sections.

Most material models in the field of metal forming, including those for metastable stainless steels, can be defined as follows:

$$\sigma^{\mathrm{Y}} = f(\varepsilon^{\mathrm{p}}, \dot{\varepsilon}^{\mathrm{p}}, \varphi, T) \tag{3.5}$$

The derivative of the yield stress in relation to time can be written as follows, assuming $\dot{\varepsilon}^{\mathrm{p}} \geq 0$:

$$\dot{\sigma}^{\mathrm{Y}} = \frac{\partial \sigma^{\mathrm{Y}}}{\partial \varepsilon^{\mathrm{p}}} \dot{\varepsilon}^{\mathrm{p}} + \frac{\partial \sigma^{\mathrm{Y}}}{\partial \dot{\varepsilon}^{\mathrm{p}}} \ddot{\varepsilon}^{p} + \frac{\partial \sigma^{\mathrm{Y}}}{\partial \varphi} \dot{\varphi} + \frac{\partial \sigma^{\mathrm{Y}}}{\partial T} \dot{T} \tag{3.6}$$

In this formula, the partial derivatives are material properties and the time derivatives concern the internal state variables that are provided by the calculation.

Now the partial derivatives can be replaced by lookup tables. From (3.6) it follows that:

$$\dot{\sigma}^{\mathrm{Y}} = \mathrm{Lup01}(\varepsilon^{\mathrm{p}}, \dot{\varepsilon}^{\mathrm{p}}, T, \varphi)\dot{\varepsilon}^{\mathrm{p}} + \mathrm{Lup02}(\varepsilon^{\mathrm{p}}, \dot{\varepsilon}^{\mathrm{p}}, T, \varphi)\dot{\varphi} +$$
$$\mathrm{Lup03}(\varepsilon^{\mathrm{p}}, \dot{\varepsilon}^{\mathrm{p}}, T, \varphi)\dot{T} + \mathrm{Lup04}(\varepsilon^{\mathrm{p}}, \dot{\varepsilon}^{\mathrm{p}}, T, \varphi)\ddot{\varepsilon}^{p} \tag{3.7}$$

3.4.1 The lookup based implementation

Complex materials such as Sandvik Nanoflex™require more internal state variables, such as the martensite content. The time derivative of a randomly selected state variable can be defined as p_i. Using the Einstein convention, (3.7) can be written as:

$$\dot{p}_i = \mathrm{Lup}_{ij}(p_j)\,\dot{p}_j, \qquad i \neq j \tag{3.8}$$

The rate formula was been selected to ensure correct implementation of possible path-dependent processes. If path-dependent processes do not have to be taken into account, the closed form can be implemented:

$$p_i = \mathrm{Lup}_{ij}(p_j) \tag{3.9}$$

3.4.2 The neural network-based implementation

A feed-forward neural network can generally be defined as:

$$output_i = Neural_{Network}(input_j) = Nur(input_j) \tag{3.10}$$

This is a general definition, irrespective of the architecture of the network, such as number of neurons, number of layers and number of networks used. For a general introduction to feed-forward neural networks, see appendix A. If the lookup tables are replaced by neural networks, it follows from (3.8) and (3.10) that:

$$\dot{p}_i = Nur_{ij}(p_j)\,\dot{p}_j, \qquad i \neq j \tag{3.11}$$

Lookup tables can therefore be simply exchanged by neural networks or a combination of the two can be used. In general it is the best strategy to use as much lookup tables as possible, because lookup tables consume less calculation time than neural networks. This is only the case for low < 4 dimensions of the lookup table. For a dimension ≥ 4 it is preferable to use a neural network in order to avoid taking up too much computer memory.

3.4.3 Structure

A FEM package consists of three parts: the pre-processor, the solver and the post-processor. In the pre-processing phase all the necessary files are created to define the model. This implies defining the tool geometries, setting the initial values of the state variables and defining the material model. The necessary files are created with Matlab and other pre-processing programs. In the solver phase the actual
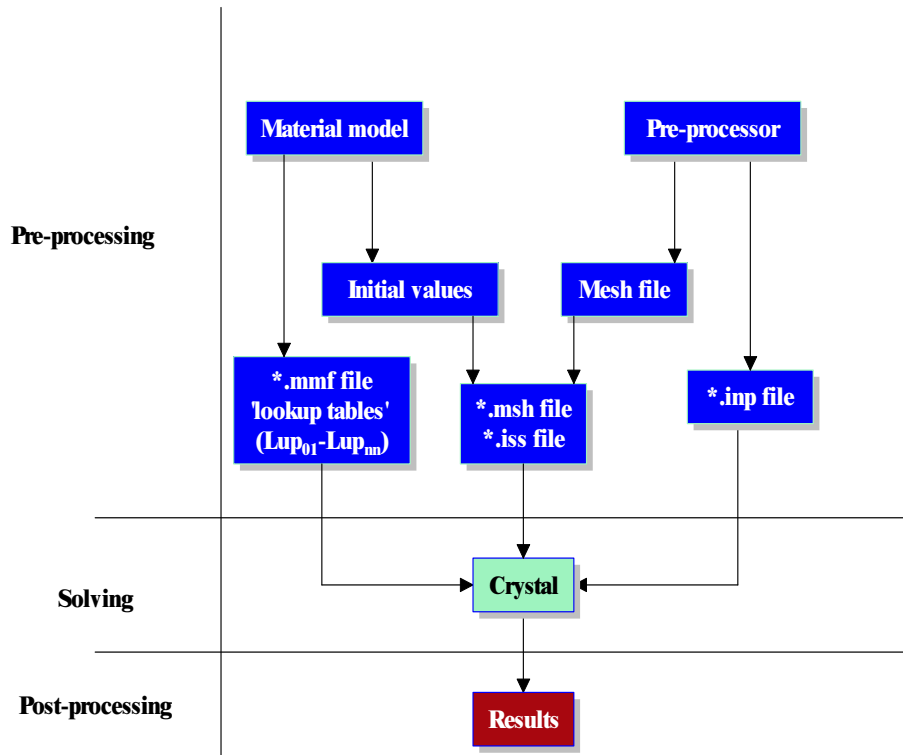
Figure 3.1: File structure for lookup table material model.

solution for the model is calculated. The FEM package reads the input deck that has been created in the pre-processing phase. After the calculations, the results are interpreted in the post-processor. In Figure 3.1 the files created during the pre-processing phase can be found. CRYSTAL uses the *.inp file, from the pre-processor as the main input. In the *.mmf file the material model is defined. The material model consists of dependent and independent state variables. CRYSTAL also reads the location of the lookup tables from the *.mmf file. The *.iss file is a text file containing the initial values for each integration point. Lup01 − Lupnn are the actual lookup tables from which CRYSTAL obtains its new state variables values. The *.msh file defines the meshed product.

3.5   A macroscopic model for Sandvik Nanoflex™

3.5.1   Introduction

The transformations depend on temperature and stress state. The transformation can be split up into two parts, see Figure 3.2:

- Transformation above the flow stress, meaning that it is strain-induced because it is accompanied by plastic deformation;

- Transformation below the flow stress, meaning that the transformation is not accompanied by plastic deformation but that it strongly depends on the stress applied.

Based on the information about the model of strain-induced martensite as put forward in [6, 14], a general differential equation was chosen. This model was fitted to the measured data.
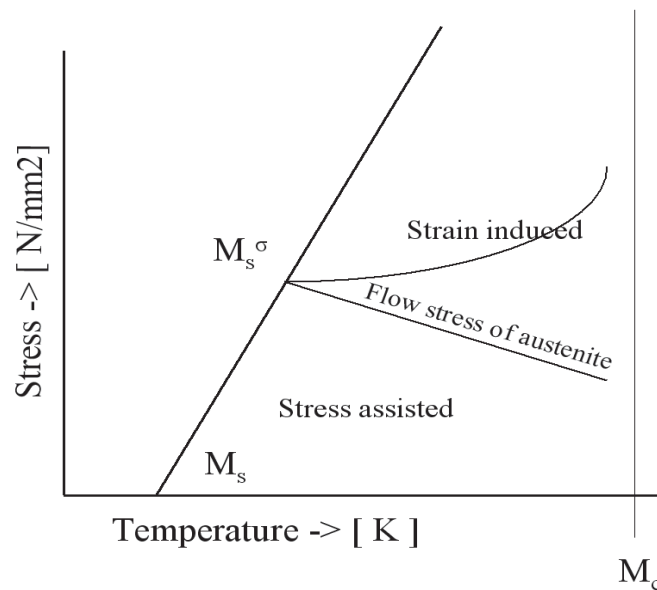
Figure 3.2: Schematic representation of critical stress for martensitic transformation as a function of temperature.

Because the work hardening of the material is complex and path dependent in relation to martensite content and plastic strain, it was decided to use a modified Estrin [17] model with two internal state variables to describe structural defects that influence the work hardening such as the dislocation densities. A rate formulation was chosen to incorporate the path dependence.

3.5.2 Strain-induced transformation

The following equation was adapted to describe the strain-induced transformation:

$$\dot{\varphi}_{strain} = C_{strain}(T, \sigma_h, Z)[(D_1 + \varphi)^{n_1}(f - \varphi)^{n_2}]\dot{\varepsilon}^{\mathrm{p}} \tag{3.12}$$

For implementation, (3.12) was split into two functions. First:

$$\dot{C}_{strain} = \mathrm{Lup61}(T, \sigma_h, Z)\dot{T} + \mathrm{Lup62}(T, \sigma^{\mathrm{H}}, Z)\dot{\sigma}^{\mathrm{H}} \tag{3.13}$$

The Z term was not implemented because it is assumed that Z does not change during metal forming. Second:

$$\dot{\varphi}_{strain} = \mathrm{Lup71}(C_{strain}, \varphi, T)\dot{C}_{strain} + \mathrm{Lup72}(C_{strain}, \varphi, T)\dot{T} \tag{3.14}$$

where φ is the martensite content and C_{strain} is a function that describes the temperature, hydrostatic stress and material structure dependence of the transformation. Z is a parameter that depends on the annealing conditions before metal forming, the chemical composition and crystal orientation. C_{strain} is related to the thermodynamics of the transformation.

3.5.3 Stress-assisted transformation

The description of the stress-assisted transformation is based on [23], but in a more general form:

$$\dot{\varphi}_{stress} = C_{stress}(T, \sigma^{\mathrm{H}}, \varepsilon^p, Z)[(D_2(Z) + \varphi)^{n_3}(f_{stress}(T, \sigma^{\mathrm{H}}, \varepsilon^{\mathrm{P}}, Z) - \varphi)^{n_4}] \tag{3.15}$$

where C_{stress} is a function that describes the dependence of the transformation on stress, temperature and material structure. D depends on the annealing condition and f_{stress} depends on the temperature, hydrostatic stress, plastic deformation and the annealing condition. For both annealing conditions the following model was used to describe the transformation. The interaction between the state variables that influence the transformation were not investigated. Therefore, the dependence of C_{stress} and f_{stress} can be split up into a temperature dependence, a hydrostatic pressure dependency and an plastic strain dependence. D_2 is a constant.

For implementation, (3.15) is split into three functions:

$$\dot{C}_{stress} = \mathrm{Lup81}(T, \sigma^{\mathrm{H}}, \varepsilon^{\mathrm{P}}, Z)\dot{T} + \mathrm{Lup82}(T, \sigma^{\mathrm{H}}, \varepsilon^{\mathrm{P}}, Z)\dot{\sigma}^{\mathrm{H}} + \mathrm{Lup83}(T, \sigma^{\mathrm{H}}, \varepsilon^{\mathrm{P}}, Z)\dot{\varepsilon}^{\mathrm{P}} \tag{3.16}$$

where Z is a constant for homogeneous transformations, so it has no influence on the change of C_{stress} during a calculation, and:

$$\dot{f}_{stress} = \mathrm{Lup91}(T, \sigma^{\mathrm{H}}, \varepsilon^{\mathrm{P}}, Z)\dot{T} + \mathrm{Lup92}(T, \sigma^{\mathrm{H}}, \varepsilon^{\mathrm{P}}, Z)\dot{\sigma}^{\mathrm{H}} + \mathrm{Lup93}(T, \sigma^{\mathrm{H}}, \varepsilon^{\mathrm{P}}, Z)\dot{\varepsilon}^{\mathrm{P}} \tag{3.17}$$

And finally:

$$\dot{\varphi}_{stress} = \mathrm{Lup101}(C_{stress}, f_{stress}, \varphi) \tag{3.18}$$

By splitting (3.12) and (3.15), the values C_{strain}, C_{stress} and f_{stress} are treated as state variables and will be stored locally at the integration points. For calculations with inhomogeneous transformation, the initial values of these state variables can be varied.
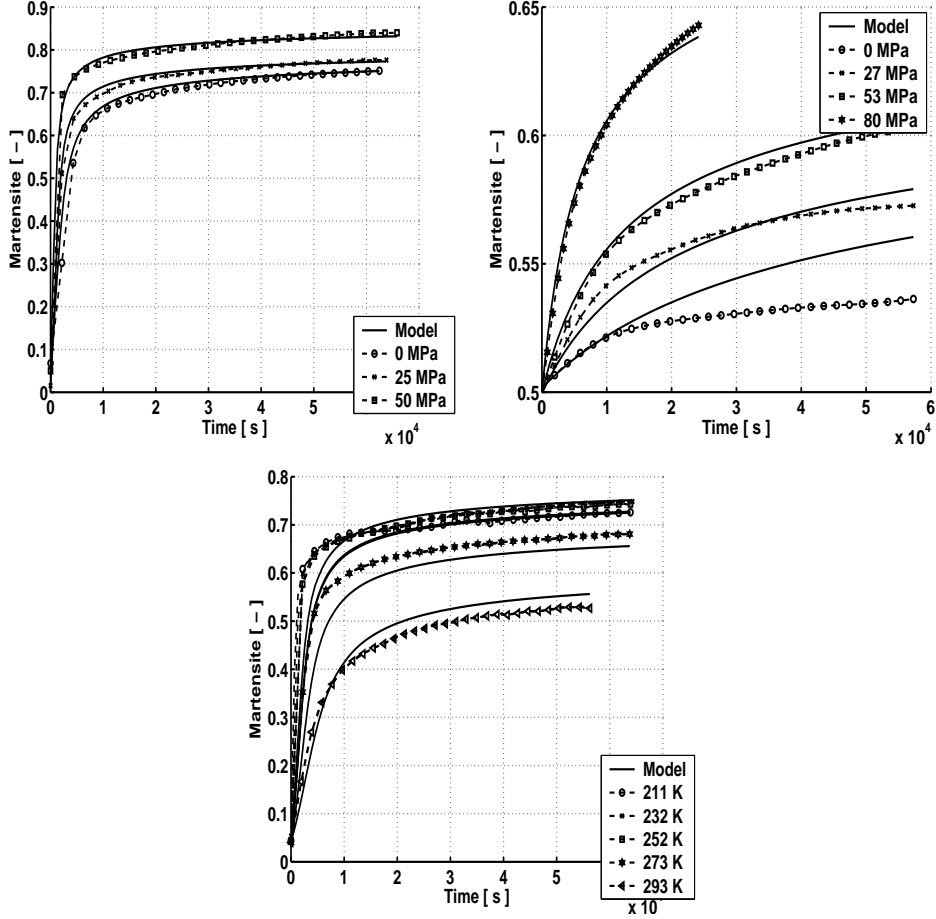
Figure 3.3: The stress-assisted transformation. Top Left: the influence of the applied
stress on the stress-assisted transformation of unstable material. Top right:
the influence of the hydrostatic stress on the stress-assisted transformation,
of stable material, after deforming the specimen until the strain-induced
martensite reaches 50%. Bottom: temperature dependence of the trans-
formation of unstable material.

3.5.4   Total martensite content.

For reasons of consistency of the LUP table method we define the following for the
total martensite content as a limiter function:

$$\dot{\varphi} = \text{Lup111}(\varphi)\dot{\varphi}_{strain} + \text{Lup112}(\varphi)\dot{\varphi}_{stress} \qquad (3.19)$$

3.5.5 Path dependent dislocation density based on work hardening.

Figure 3.4: The fitted model and measuring data. Right: the strain-induced martensite. Left: the flow stress.

For the flow stress of austenite the following is assumed:

$$\sigma_\gamma^Y = \sigma_{0_\gamma} \sqrt{Y_\gamma} (1 + \frac{\dot{\varepsilon}^P}{\psi_\gamma})^{\frac{1}{m_\gamma}} \tag{3.20}$$
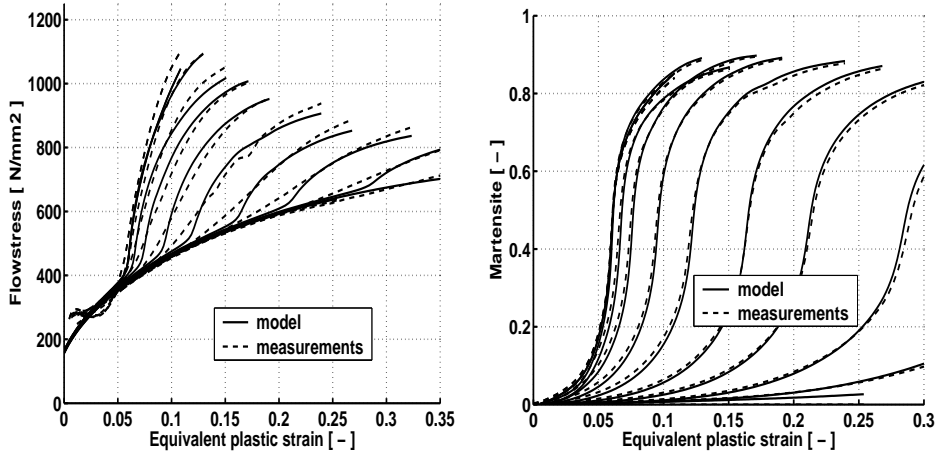
In this study only one dislocation density was used for every phase. For implementation, this was changed into:

$$\dot{\sigma^Y}_\gamma = \mathrm{Lup}21(Y_\gamma, T, \dot{\varepsilon}^P)\dot{Y}_\gamma + \mathrm{Lup}22(Y_\gamma, T, \dot{\varepsilon}^P)\dot{T} + \mathrm{Lup}23(Y_\gamma, T, \dot{\varepsilon}^P)\ddot{\varepsilon}^P \tag{3.21}$$

And for the flow stress of martensite:

$$\sigma_\alpha^Y = \sigma_{0_\alpha} \sqrt{Y_\alpha} (1 + \frac{\dot{\varepsilon}^P}{\psi_\alpha})^{\frac{1}{m_\alpha}} \tag{3.22}$$

For implementation, this was changed into:

$$\dot{\sigma^Y}_\alpha = \mathrm{Lup}51(Y_\alpha, T, \dot{\varepsilon}^P)\dot{Y}_\varphi + \mathrm{Lup}52(Y_\alpha, T, \dot{\varepsilon}^P)\dot{T} + \mathrm{Lup}53(Y_\alpha, T, \dot{\varepsilon}^P)\ddot{\varepsilon}^P \tag{3.23}$$

Value 1 in (2.67) and (2.68) is implemented to avoid a high derivative $\dot{\varepsilon}$ at low strain rates, for example at the beginning of plastic deformation. The values σ_{0_γ}, σ_{0_α}, m_γ, and m_α are temperature dependent. For the combination of both phases the equation becomes:

$$\sigma^Y = \sigma_\gamma^Y + \frac{1}{2}(1 + \tanh(\frac{\varphi - \varphi_0}{q}))(\sigma_\alpha^Y - \sigma_\gamma^Y) \tag{3.24}$$

Or, in LUP description in closed form:

$$\sigma^{\mathrm{Y}} = \mathrm{Lup121}(\sigma_\alpha^{\mathrm{Y}}, \sigma_\gamma^{\mathrm{Y}}, \varphi) \tag{3.25}$$

In the equation, σ_0 is the basic stress that depends on strain rate and temperature, φ represents the martensite content, Y the general dislocation density for one phase, $\dot{\varepsilon}_p$ is the equivalent plastic strain rate, ψ the reference strain rate and m a constant depending on strain rate and temperature. q_1 and q_2 are introduced to describe the non-linear relation between the flow stresses as a mixture rule. The evolution of the dislocation density in the austenite is described as follows:

$$\begin{aligned}
\dot{Y}_\gamma &= [C_1(C_2 - Y_\gamma)^{C_3} + C_4(\dot{\varepsilon}^{\mathrm{P}}, T)]\dot{\varepsilon}^{\mathrm{P}} \quad \text{if } Y_\gamma < C_2 \\
\dot{Y}_\gamma &= [C_4(\dot{\varepsilon}^{\mathrm{P}}, T)]\dot{\varepsilon}^{\mathrm{P}} \quad \text{if } Y_\gamma > C_2
\end{aligned} \tag{3.26}$$

For the LUP model this function is split in two:

$$\dot{C}_\gamma = \mathrm{Lup01}(\dot{\varepsilon}^{\mathrm{P}}, T)\ddot{\varepsilon}^{\mathrm{P}} + \mathrm{Lup02}(\dot{\varepsilon}^{\mathrm{P}}, T)\dot{T} \tag{3.27}$$

and:

$$\dot{Y}_\gamma = \mathrm{Lup11}(Y_\gamma, C_\gamma)\dot{\varepsilon}^{\mathrm{P}} \tag{3.28}$$

where C_1, C_2 and C_3 are material constants and C_4 depends on temperature and strain rate. The constants are not directly related to physical phenomena but are chosen to fit the model. In a similar way the following applies to the dislocation density in the martensite phase:

$$\begin{aligned}
\dot{Y}_{\alpha 1} &= [C_5(C_6 - Y_\alpha)^{C_7} + C_8(\dot{\varepsilon}^{\mathrm{P}}, T)]\dot{\varepsilon}^{\mathrm{P}} \quad \text{if } Y_\alpha < C_6 \\
\dot{Y}_{\alpha 1} &= [C_8(\dot{\varepsilon}^{\mathrm{P}}, T)]\dot{\varepsilon}^{\mathrm{P}} \quad \text{if } Y_\alpha > C_6
\end{aligned} \tag{3.29}$$

$$\dot{C}_\alpha = \mathrm{Lup31}(\dot{\varepsilon}^{\mathrm{P}}, T)\ddot{\varepsilon}^{\mathrm{P}} + \mathrm{Lup32}(\dot{\varepsilon}^{\mathrm{P}}, T)\dot{T} \tag{3.30}$$

where C_5, C_6 and C_7 are material constants and C_8 depends on the temperature and the strain rate. To describe the recovery effect, the following is proposed:

$$\dot{Y}_{\alpha 2} = \frac{\dot{\varphi}}{(\varphi)}(C_9(T)Y_\gamma - Y_\alpha) \tag{3.31}$$

The following equation was introduced to describe the dislocation transfer during transformation:

$$\dot{Y}_{\alpha 3} = \frac{\dot{\varphi}_{strain}}{(\varphi_{strain})}C_{10} \tag{3.32}$$

Where C_9 depends on the temperature. The values of C_9 and C_{10} were calculated by curve fitting. From (3.29), (3.31) and (3.32). The following equation was defined for the dislocation density in martensite:

$$\dot{Y}_\alpha = \dot{Y}_{\alpha 1} + \dot{Y}_{\alpha 2} + \dot{Y}_{\alpha 3} \tag{3.33}$$

For a comparison between measured and calculated stress strain curves, see Figure 3.4, right. For the LUP model the following equation was obtained:

$$\dot{Y}_\alpha = \mathrm{Lup41}(Y_\alpha, C_\alpha)\dot{\varepsilon}^{\mathrm{P}} + \mathrm{Lup42}(Y_\alpha, \varphi, T)\dot{\varphi} + \mathrm{Lup43}(Y_\gamma)\dot{\varphi}_{strain} \tag{3.34}$$

relation between hardness and flow stress

For this conversion the following is known:

$$Hv = f_1(\sigma^{\mathrm{Y}}) \tag{3.35}$$

Or as a LUP:

$$\dot{Hv} = \mathrm{Lup}31(\sigma^{\mathrm{Y}})\dot{\sigma^{\mathrm{Y}}} \tag{3.36}$$
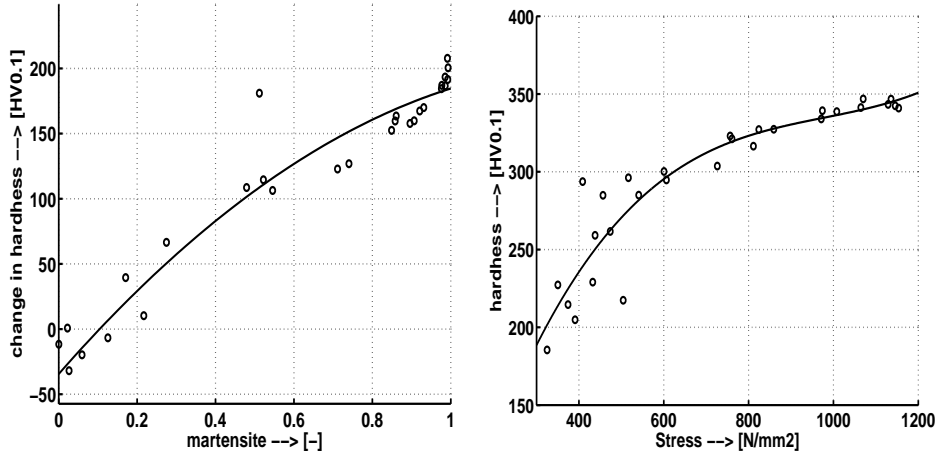
Figure 3.5: Left: the relation between change in hardness and martensite content. Right: the relation between hardness Vickers and the flow stress.

3.5.6 Ageing behaviour

One of the advantages of Sandvik Nanoflex™is the possibility of ageing the martensite phase. This ageing process increases the hardness. Because only the martensite phase is hardenable, the hardness increase depends on the martensite content, see Figure 3.5. The following is assumed:

$$Hv_{afterageing} = f_2(\sigma^{\mathrm{Y}}, \varphi) \tag{3.37}$$

Or in rate form as a lookup table:

$$\dot{Hv}_{afterageing} = LUP31(\sigma^{\mathrm{Y}})\dot{\sigma^{\mathrm{Y}}} + LUP41(\sigma^{\mathrm{Y}}, \varphi)\dot{\varphi} \tag{3.38}$$

3.5.7 Transformation dilation and plasticity

The change in density during transformation is given by:

$$\dot{\rho} = (\rho_\alpha - \rho_\gamma)\dot{\varphi} \tag{3.39}$$

where ρ_α is the density of martensite, ρ_γ is the density of austenite and φ is the martensite content. This change in density causes an extra irreversible strain in the material:

$$\dot{\varepsilon}^{dil} = \frac{-\dot{\rho}}{3\rho} \tag{3.40}$$

where $\dot{\boldsymbol{\varepsilon}}^{dil}$ represents the dilation strain rate.

The implementation has the following form:

$$\dot{\boldsymbol{\varepsilon}}^{dil} = \frac{-\text{Lup131}(\varphi)\dot{\varphi}}{3\rho}\mathbf{I} \tag{3.41}$$

For the transformation plasticity the following equation was proposed:

$$\dot{\boldsymbol{\varepsilon}}^{\text{trip}} = \dot{\varphi}A(\varphi)\boldsymbol{\sigma}\sqrt{\frac{2}{3}} \tag{3.42}$$

Here $A(\varphi)$ is:

$$A(\varphi) = \frac{A_0(3 + \tanh(Q_a(0.5 - \varphi)))}{\sigma^{\text{Y}}} \tag{3.43}$$

For implementation, (3.42) is rewritten as:

$$\dot{\boldsymbol{\varepsilon}}^{\text{trip}} = \boldsymbol{\sigma}\sqrt{\frac{2}{3}}\text{Lup171}(\varphi, \sigma^{\text{Y}})\dot{\varphi} \tag{3.44}$$

3.6 FEM implementation of the material model

The elasto-plastic constitutive model is based on a hypo-elastic relation between the objective Jaumann rate of the Cauchy stress tensor $\overset{\circ}{\boldsymbol{\sigma}}$ and the elastic strain rate tensor $\mathbf{D}^{\mathrm{e}}$; combining this relation with the additive decomposition of the total strain rate tensor into an elastic part and a plastic part ($\mathbf{D} = \mathbf{D}^{\mathrm{e}} + \mathbf{D}^{\mathrm{p}}$) gives

$$\overset{\circ}{\boldsymbol{\sigma}} = {}^{4}\mathbf{C} : (\mathbf{D} - \mathbf{D}^{\mathrm{p}}) \tag{3.45}$$

in which the isotropic elastic fourth order stiffness tensor is given by:

$$^{4}\mathbf{C} = \frac{\nu E}{(1+\nu)(1-2\nu)}\Big(\mathbf{II} + \frac{1-2\nu}{\nu}{}^{4}\mathbf{I}\Big) \tag{3.46}$$

where E and ν are Young's modulus and Poisson's ratio, respectively.

The plastic strain rate tensor is determined by assuming an associative flow rule, in which the direction of plastic flow is defined by the normal on the yield surface:

$$\mathbf{D}^{\mathrm{p}} = \dot{\lambda}\frac{\partial F}{\partial \boldsymbol{\sigma}} = \dot{\lambda}\mathbf{n} \tag{3.47}$$

in which $\dot{\lambda}$ is the plastic multiplier, which determines the fraction of the plastic strain rate tensor, and $\mathbf{n}$ is the normal on the yield surface F:

$$F(\boldsymbol{\sigma}, \varepsilon^{\mathrm{p}}) = \sigma_{\mathrm{eq}}(\boldsymbol{\sigma}) - \sigma^{\mathrm{Y}}(\varepsilon^{\mathrm{p}}) = \sqrt{\frac{3}{2}\mathbf{s} : \mathbf{s}} - \sigma^{\mathrm{Y}}(\varepsilon^{\mathrm{p}}) \tag{3.48}$$

where the deviatoric stress $s_{ij} = \sigma_{ij} - \frac{1}{3}\sigma_{ii}\delta_{ij}$ and σ^{Y} is the hardening law as function of the effective plastic strain ε^{p} defined as:

$$\varepsilon^{\mathrm{p}} = \int_{0}^{t}\dot{\varepsilon}^{\mathrm{p}}(\tau)\mathrm{d}\tau \quad \text{with} \quad \dot{\varepsilon}^{\mathrm{p}} = \sqrt{\frac{2}{3}\mathbf{D}^{\mathrm{p}} : \mathbf{D}^{\mathrm{p}}} \tag{3.49}$$

Notice that in 3.48, the equivalent Von Mises stress has been chosen as the equivalent stress σ_{eq}.

In order to integrate the plastic rate constitutive equations, the so-called implicit radial return method was used [38]. It is, in fact, a particular form of the backward Euler method, in the sense that the return mapping algorithm is performed in the deviatoric space.

3.6.1 The stress update during plastic deformation

In CRYSTAL, strain increments are calculated from the displacement increments using a midpoint rule. Therefore, the constitutive equation 3.45 can be integrated by a conventional small strain return mapping. The final stress state is than referred to a local (rotated) basis and has subsequently to be mapped to the global basis [39].

The radial return method is based on an operator-split methodology, in which first the entire increment is assumed to be elastic, and second, if necessary, an iterative elasto-plastic corrector step is initiated. The deviatoric elastic trial stress is defined as:

$$\mathbf{s}_{n+1}^{\text{trial}} = \mathbf{s}_n + 2\mu\triangle\mathbf{e}_{n+1} \tag{3.50}$$

where $\mathbf{e}_{n+1}$ is the deviatoric strain tensor, and μ the shear modulus. The radial return stress update equation is given by:

$$\mathbf{s}_{n+1} = \mathbf{s}_{n+1}^{\text{trial}} - 2\mu\triangle\lambda_{n+1}\mathbf{n}_{n+1} \tag{3.51}$$

from which it follows that:

$$\mathbf{n}_{n+1} = \frac{3\mathbf{s}_{n+1}}{2\sigma_{\text{eq}}} = \frac{3\mathbf{s}_{n+1}^{\text{trial}}}{2\sigma_{\text{eq}}^{\text{trial}}} \tag{3.52}$$

and hence:

$$\mathbf{s}_{n+1} = \left(1 - \frac{3\mu\triangle\lambda}{\sigma_{\text{eq}}^{\text{trial}}}\right)\mathbf{s}_{n+1}^{\text{trial}} \equiv \alpha\,\mathbf{s}_{n+1}^{\text{trial}} \tag{3.53}$$

Taking the dot product of 3.51 with $\mathbf{n}_{n+1}$, the following scalar equation is obtained:

$$\sigma_{\text{eq}} = \sigma_{\text{eq}}^{\text{trial}} - 3\mu\triangle\lambda \tag{3.54}$$

The yield criterion F must be obeyed at all times, which results in a scalar nonlinear equation in $\triangle\lambda$

$$\sigma_{\text{eq}}^{\text{trial}} - 3\mu\triangle\lambda_{n+1} - \sigma^{\text{Y}}(\kappa_{n+1}) = 0 \tag{3.55}$$

As this equation contains variables defined in the unknown state $n+1$, this equation must be solved iteratively. For this purpose, a residual is defined:

$$g(\triangle\lambda) = \sigma_{\text{eq}}^{\text{trial}} - 3\mu\triangle\lambda_{n+1} - \sigma^{\text{Y}}(\kappa_{n+1}) = 0 \tag{3.56}$$

Linearising these equations ($g^{i+1} = g^i + \delta g$) yields an iterative expression for the incremental plastic multiplier:

$$\delta\lambda = \frac{g^i}{3\mu + \sigma^{\text{Y}}(\kappa_{n+1})'} \tag{3.57}$$

where $\sigma^{\text{Y}}(\kappa_{n+1})' = \partial\sigma^{\text{Y}}/\partial\kappa$. When a value for $\delta\lambda$ is obtained, the incremental value $\triangle\lambda$ can be updated, and hence the deviatoric stresses can be calculated using 3.51. The hydrostatic part of the stress tensor, denoted by $\boldsymbol{\sigma}_{n+1}^{\text{h}}$, is constant and can be determined from the hydrostatic part of the trial stress. The expression for the Cauchy stress tensor at the end of the increment is now:

$$\boldsymbol{\sigma}_{n+1} = \kappa\text{tr}(\boldsymbol{\varepsilon}_{n+1})\mathbf{I} + \mathbf{s}_{n+1}^{\text{trial}} - 2\mu\triangle\lambda_{n+1}\mathbf{n}_{n+1} \tag{3.58}$$

3.6.2 Stress update including transformation plasticity

Transformation plasticity is taken into account by modifying the deviatoric part of the constitutive equations according to [15]:

$$\dot{\mathbf{s}} = 2\mu(\dot{\mathbf{e}} - \dot{\mathbf{e}}^{\mathrm{p}} - \dot{\mathbf{e}}^{\mathrm{trip}}) \qquad (3.59)$$

Here, $\dot{\mathbf{e}}^{\mathrm{trip}}$ is the (deviatoric) transformation plasticity strain rate tensor, defined as:

$$\dot{\mathbf{e}}^{\mathrm{trip}} = \dot{\varphi}A\mathbf{n} = \dot{\varphi}(A^*\sigma_{\mathrm{eq}})\frac{3}{2}\frac{\mathbf{s}}{\sigma_{\mathrm{eq}}} = \frac{3}{2}\dot{\varphi}A^*\mathbf{s} \qquad (3.60)$$

in which $A^* = A/\sigma_{\mathrm{eq}}$ and a linear dependence has been assumed between A and σ_{eq}. For the elastic part (including TRIP effects, i.e. $\dot{\mathbf{e}}^{\mathrm{p}} = \mathbf{0}$), the constitutive equations 3.59 can be written as a set of differential equations according to:

$$\dot{\underset{\sim}{s}} = \underset{\sim}{C} - B\underset{\sim}{s} \rightarrow \dot{\underset{\sim}{s}} + B\underset{\sim}{s} = \underset{\sim}{C} \qquad (3.61)$$

in which $\underset{\sim}{C} = 2\mu\dot{\underset{\sim}{e}}$ and $B = 3\mu\dot{\varphi}A^*$. The solution can be written as:

$$\underset{\sim}{s} = \underset{\sim}{\lambda}e^{-Bt} + \underset{\sim}{C}/B \qquad (3.62)$$

At $t = 0$, we have $\underset{\sim}{s}(t = 0) = \underset{\sim}{s}_0 = \underset{\sim}{\lambda} + \underset{\sim}{C}/B$ from which it follows that $\underset{\sim}{\lambda} = \underset{\sim}{s}_0 - \underset{\sim}{C}/B$. We thus obtain the final solution for the deviatoric stresses:

$$\underset{\sim}{s} = (\underset{\sim}{s}_0 - \underset{\sim}{C}/B)e^{-Bt} + \underset{\sim}{C}/B \qquad (3.63)$$

In the elastic case, the stresses can be calculated according to 3.63. In the case of plastic deformation, the TRIP strains are incorporated by assuming that the work hardening function K is not a function of the equivalent plastic strain only, but of the summation of the equivalent plastic strain and the equivalent TRIP strain: $K(\varepsilon^{\mathrm{p}} + \varepsilon^{\mathrm{trip}})$. This means that only the sum of plastic and TRIP strains are calculated in the case of plastic deformation.

3.6.3 Integration of the LUP material model

The LUP material model is expressed by means of differential equations and, employing the Einstein summation convention, it can be denoted as:

$$\dot{p}_i = \mathrm{Lup}_{ij}(p_k)\,\dot{p}_j \qquad i \neq j \qquad (3.64)$$

The rate form has been selected to ensure correct implementation of possible path-dependent processes. As can be seen from 3.64, the rate of p_i (i.e. the depending state variable) equals the sum of the rate of the defining state variable p_j multiplied by table values Lup_{ij}, which in turn are determined by the values of the dimensional state variables from which the lookup tables are constructed.

Integration of the Lup-equations 3.64 was achieved by applying the trapezoidal rule, for which the begin and end incremental values are needed. These two values

are determined by a simple predictor-corrector scheme:

$$\Delta p_i^p = \mathrm{Lup}_{ij}(p_k^0)\Delta p_j \tag{3.65}$$

$$\rightarrow \quad \Delta p_i^c = \mathrm{Lup}_{ij}(p_k^0 + \triangle p_k^p)\Delta p_j \tag{3.66}$$

$$\rightarrow \quad \Delta p_i = \frac{\Delta p_i^p + \Delta p_i^c}{2}, \tag{3.67}$$

in which p_j^0 is the begin increment value, Δp_i^p is the predictor value of Δp_i and Δp_i^c is the corrector value of Δp_i. The final step 3.67 corresponds to the trapezoidal rule.

The application of the predictor-corrector scheme relies on the fact that the predictor value is a good approximation for the final value. However, the character of the differential equation for the hydrostatic stress (which is in fact a dependent variable in the model) that is caused by the transformation from austenite to martensite, as defined by the lookup tables, appeared to be very stiff: the transformation to martensite causes dilational strains. Consequently, these strains result in hydrostatic stresses, which will have an adverse effect on the martensite transformation rate. This even resulted in values with opposite signs for the predictor $\triangle p_j^p$ and the final value of the hydrostatic stress increment $\triangle p_i$. This can be explained by the fact that a positive value of the hydrostatic stress predictor $\triangle p_j^p$ results in a density decrease which in turn gives rise to a decrease of the hydrostatic stress value. In the scheme, the corrector step 3.66 was reformulated as:

$$\Delta p_i^c = \mathrm{Lup}_{ij}(p_k^0 + \triangle p_k)\Delta p_j \tag{3.68}$$

This strong non-linearity was solved in a robust way by an inner iterative Newton-Raphson loop combined with a Brent algorithm. In fact, this inner iterative loop was performed after each radial return iteration as the quantities in the LUP-model are dependent on the quantities that are determined in the radial return mapping (i.e. stresses, (equivalent) plastic strains and the resulting transformation).

3.7 Validation and verification of the FEM implementation of the material model

3.7.1 Fitting with the inverse method on one element tensile tests

Finding the best model parameters consists of different concurrent processes. This makes it difficult to implement the material model in a feed-forward way. For this reason an inverse method was used. The procedure involved a three step process. The first step was a simulated tensile test on a single element FE-model. The second step was to examine what the influence is of the lookup table size. The third step was to develop a contour fitting algorithm to fit the profiles of a martensite volume fraction on a cross-section of a product.

Inverse method fitting on a single element FEM calculation

The aim of this study was to optimize the parameters of the material model and to counteract for the finite element implementation. The parameters were fitted on tensile test data, using a single element FEM-model. With the FEM solver used it was possible to extract every state variable on each integration point. This data was used to calculate the so called RMS (Root Mean Square) values see Figure 3.6 for the flow stress and the martensite volume fraction.
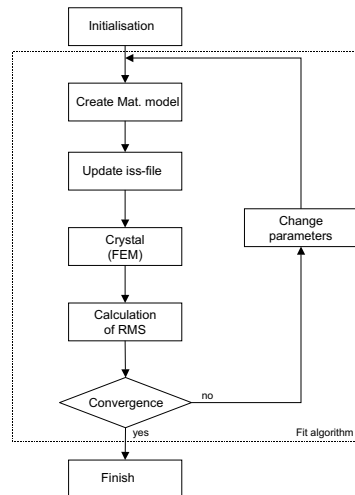

Figure 3.6: Flow scheme of the numerical fit procedure

The fit resulted in the parameters presented in Table 3.1. The set of parameters from this table were used to plot the stress curves, see Figure 3.7(b) and the martensite volume fraction, see Figure 3.7(a). The $\overline{RMS}_{stress}$ error for this fit was 14.552 N/mm^2, and the $\overline{RMS}_f$ error was 0.01972.

Table 3.1: Value of the fitted parameters, compare this with table 2.8 on page 50. See also the equations (2.55), (2.56), (2.67) and (2.68).

Q_1	178	f_{strain}	0.95773	C_1	16.571
Q_3	0.005	σ_{0_γ}	131 N/mm^2	Q_2	0.50
Q_4	14496	σ_{0_α}	586 N/mm^2	m_γ	152
Q_5	0.043569	m_α	1102		

(a) Fit of the martensite volume fraction
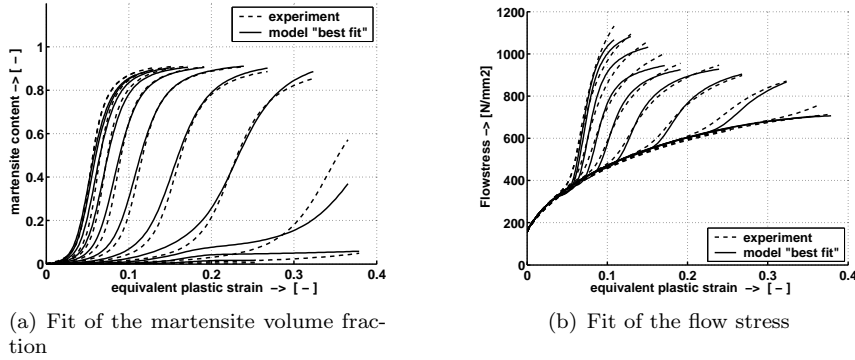

(b) Fit of the flow stress

Figure 3.7: Results of the fit using the inverse method

Lookup table size

To investigate the influence of the Lup size, a single element tensile test FEM calculation at 293 K is performed with different lookup table sizes, between 2 and 65. To visualize the influence the relative RMS error (flow stress and martensite fraction), the value of $(\overline{RMS})$ was calculated for each test, see Figure 3.8(a). To gain insight into the CPU time as a function of the Lup size the solution time is recorded for the single element tensile test. This data is presented in Figure 3.8(b). A remark must be made about the latter figure. The time in Figure 3.8(b) is not purely the solution time but also the time needed for reading the material model.

3.7.2   Stress-assisted transformation

To validate the stress-assisted transformation two different tests were carried out. These tests where done by experiments and by simulating with CRYSTAL:

- First a tensile test bar is plastically deformed until it reaches a strain-induced martensite content of 50%. After this the tensile specimen remains in the testing machine for 24 hours with an externally applied stress. See for the comparison between the calculation and measurement Figure 3.9. The test material was annealed for 0.5 min at 1323 K and quenched with 1 bar recirculating inert gas.

- To validate the temperature dependence of the unstable material (annealing

(a) The influence of Lup size on the relative RMS

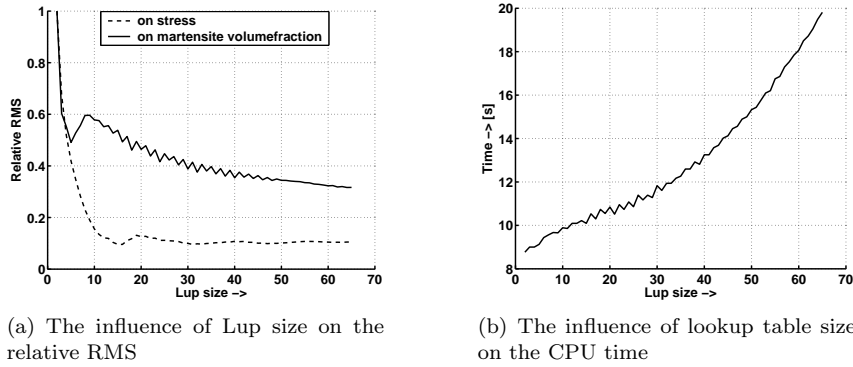(b) The influence of lookup table size on the CPU time

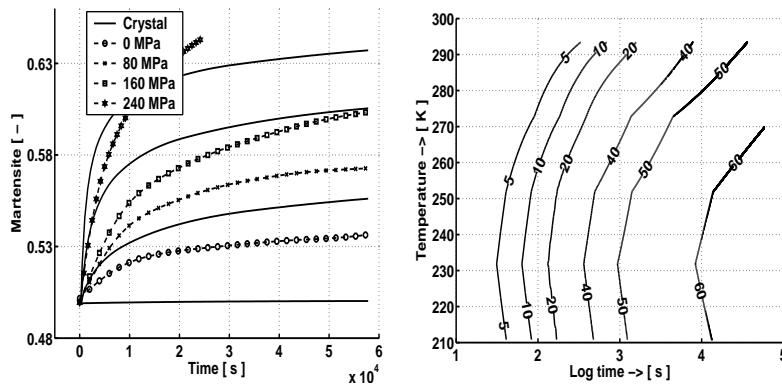Figure 3.8: The influence of Lup size

Figure 3.9: Left: the stress-assisted transformation after plastic deformation. Right: A calculated TTT diagram.

for 15 min at 1323 K and quenched with 6 bar re-circulating inert gas) a TTT diagram was calculated, see for the results Figure 3.9.

3.7.3 Tensile tests

Inhomogeneous transformation and necking

In principle it is possible to predict the moment of necking during a tensile test based on the work hardening. A problem that normally occurs in these kind of calculations is that the mesh and material behaviour is too homogeneous which will delay the necking moment. In reality the material will not deform homogenously. To implement this inhomogeneous material behaviour the C_{strain} is varied at the integration points to simulate the crystal distribution. The stochastic phenomenon

of dislocation generation was implemented by adding a normal distribution in the dislocation rate in the austenite and martensite. For (3.21) we obtain:

$$\dot{Y}_\alpha = \text{Lup41}(Y_\alpha, C_\alpha)N(1, s)\dot{\varepsilon}^{\text{p}} \tag{3.69}$$

And for (3.21):

$$\dot{Y}_\gamma = \text{Lup01}(Y_\gamma, C_\gamma)N(1, s)\dot{\varepsilon}^{\text{p}} \tag{3.70}$$

where $N(1, s)$ is the normal distribution with a mean of 1 and a standard deviation of s. Figure 3.11 on page 80 shows the results of this calculation. The problem that remains it that this solution will be mesh dependent; a possible solution for the mesh dependence is the use of a mask that is related to the grain distribution.

Influence of the strain rate on the strain-induced transformation

Because the transformation is very sensitive to the temperature, the plastic strain rate seems to have a big influence on the stress-strain curve. This is caused by the temperature distribution in the tensile test specimen. This phenomenon is shown is Figure 3.10. The change in flow stress is caused by two effects:

- Temperature dependence of the strain-induced transformation;

- Higher temperature dependence of the flow stress of martensite in comparison to the flow stress of austenite.

3.7.4 The Erichsen test

The Erichsen or Olsen test is a method of measuring the ductility and drawing properties of strip or sheet metal which involves determination of the width and depth of impression. The test, simulating a deep drawing operation is made by a standard steel ball under pressure, continuing until the cup formed from the metal sample fractures, see Figure (3.12(a)). The model is axi-symmetric with 6 elements across the plate thickness. The four tests, at different penetration depths, were simulated with the FEM solver. After the ball had moved it was retrieved as well as the blank holder. The geometry after the test was also visualized by plotting the measured outside contour (dashed line) over the calculated contour, see Figure 3.13 on page 82 for the martensite volume fraction and Figure 3.14 on page 83 for the hardness in Vickers (Hv0.2). Both the hardness and the martensite content showed a good comparison between the measured values and the calculated ones.

3.7.5 One-stage deep drawing

The model was not only validated with an Erichsen test but also with a one-stage axi-symmetric deep drawing test, using 6 element over the thickness. See for the setup of the test Figure 3.12(b) and for the validation Figure 3.15 on page 84. This validation was only performed on the martensite and this showed a good comparison between the measured values and the calculated ones.
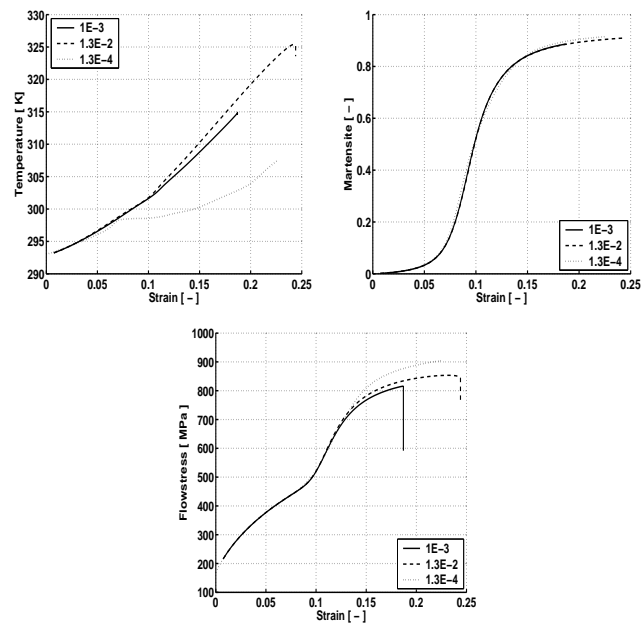
Figure 3.10: Influence of the plastic strain rate during tensile testing. Left top: the temperature. Right top: the strain-induced transformation. Bottom: The flow stress.
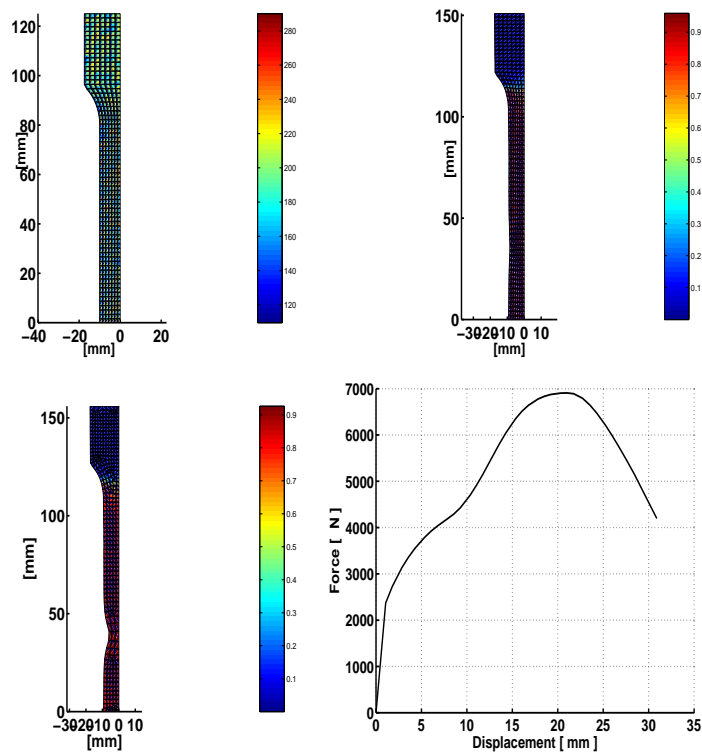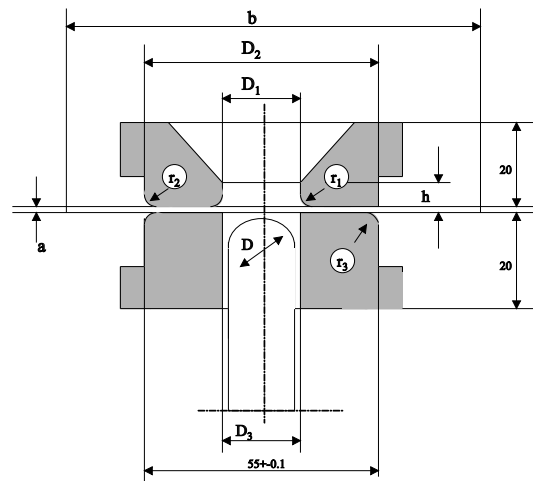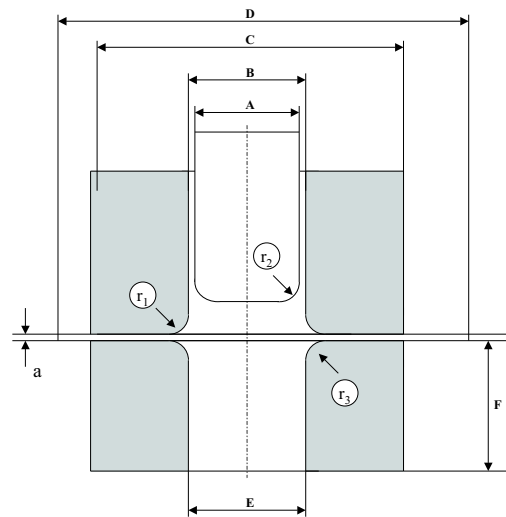
Figure 3.11: Tensile test with in homogenous material behaviour. Left top: the initial mesh with the initial values of C_{strain}. Right top: The mesh at the beginning of necking. Left bottom: The mesh during necking. Right bottom: the force-displacement curve.

(a) Erichsen test.

(b) Deep drawing test.

Figure 3.12: Schematic views

(a) depth: 1.33 mm

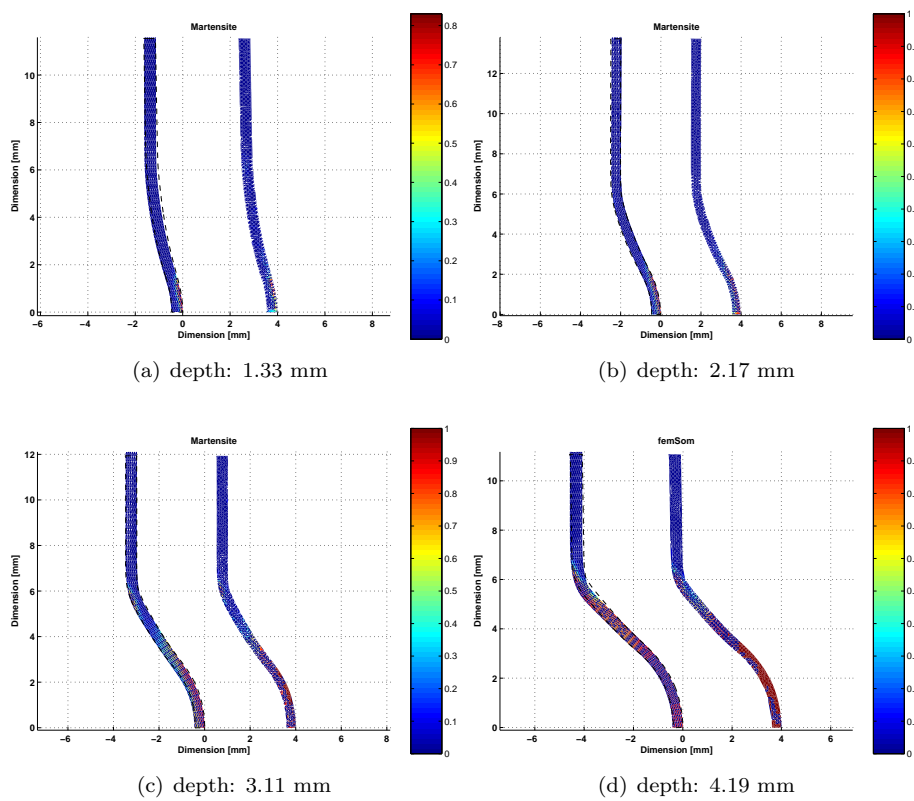(b) depth: 2.17 mm

(c) depth: 3.11 mm

(d) depth: 4.19 mm

Figure 3.13: Erichsen tests; comparison of the measured data and the FEM simulations (on martensite content). On the righthand the measured contour, on the left-hand site the calculated contour with the dashed outside geometry of the measured product.

(a) depth: 1.33 mm

(b) depth: 2.17 mm

(c) depth: 3.11 mm

(d) depth: 4.19 mm

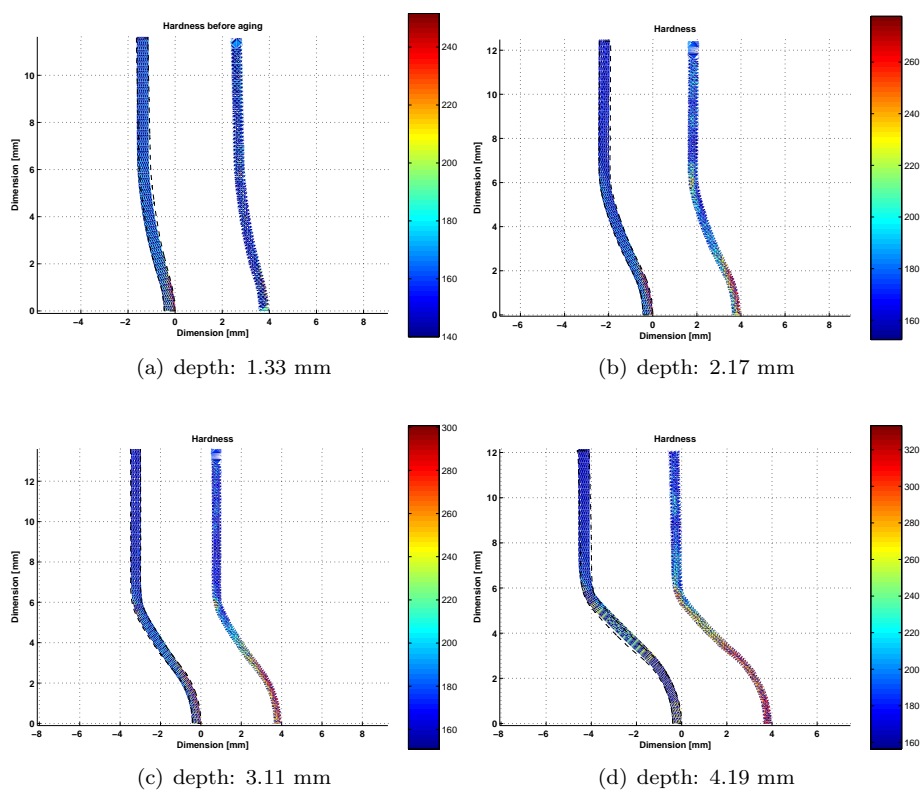Figure 3.14: Erichsen tests: comparison of the measured data and the FEM simulations (on hardness Vickers). On the right-hand site the measured contour, on the left-hand site the calculated contour with the dashed outside geometry of the measured product.

(a) Depth: 3.4 mm

(b) Depth: 5.2 mm

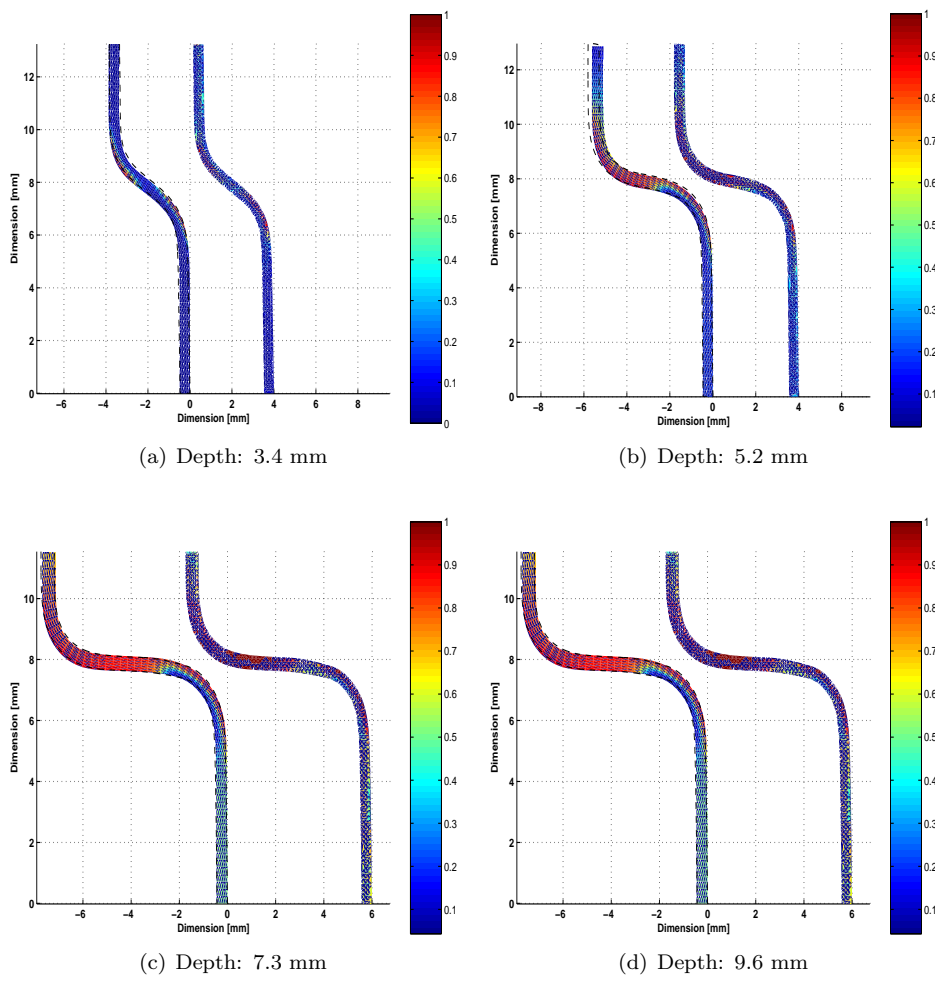(c) Depth: 7.3 mm

(d) Depth: 9.6 mm

Figure 3.15: The results (martensite) of the deep drawing process.

3.8 Single-stage deep drawing test, including austenitisation and stress-assisted transformation

3.8.1 The process

Besides simulating a multi-stage process, it was also interesting to analyze the effects of heat treatment on dimensional accuracy. This is done by means of a single-stage deep-drawing process, followed by spontaneous isothermal transformation. The austenitising treatment selected causes the material to become unstable to the extent that it starts to transform spontaneously after austenitisation. This test was not only simulated by means of the FEM program, but was also actually performed and the dimensional stability during isothermal transformation was measured to establish whether the simulations corresponded to the actual sample. Should deviations be found, it would becomes immediately be clear what the difference was between simulations and reality enabling a targeted search for the phenomena causing these differences. Ultimately this would lead to the development of an improved model.

3.8.2 Austenitisation

During austenitisation three major phenomena occur:

- Dilatation, i.e. during austenitisation the martensite present in the material is transformed back into austenite. This is accompanied by dilation strain, which is a volume-alteration strain. Dilatation is a local phenomenon, which only occurs at sites where the material is martensitic. Austenitic parts stay austenitic and do not deform. The result is that plastic deformation may occur due to inhomogeneous dilation.

- Transformation plasticity, i.e. extra plastic strain in the direction of the strain tensor due to transformation. The same applies as in the case of dilation. Transformation plasticity is not homogeneous and depends on the local martensite/austenite content. In this case too, extra plastic strain may occur due to inhomogeneous plasticity.

- Lowering of the flow stress. After deep drawing of the cup, flow stress increases due to work hardening and transformation. Back-transformation and dissolution of the dislocation structure reduces flow stress to the original austenite level, causing elimination of the residual stresses left behind in the material after the forming process. These stresses do not disappear completely, however. The flow stress of austenite is still 100 N/mm^2 at 1273 K. The remaining stresses strongly influence the transformation rate after austenitisation.

To reset the relevant state variables to their original, initial values, the following function was used:

$$\dot{p}_i = \text{Lup}(p_i)\dot{T} \qquad (3.71)$$

And for LUP:

$$\text{Lup}_{p_i} = A1 \frac{p_i - p_{min}}{p_{max} - p_{min}}(1 - \tanh(\frac{T_j - T_c}{A2})) \qquad (3.72)$$

where p_i is the state variable, p_{max} and p_{min} are the maximum and minimum values of p_i, T is the temperature in Kelvin, T_c the temperature in the center of the back-transformation and $A1$ and $A2$ are constants describing the temperature dependence of back-transformation. In this way the following state variables are reset:

- for the flow stress of austenite: Y_γ, $\sigma_\gamma^{\mathrm{Y}}$;

- for the flow stress of martensite: Y_α, $\sigma_\alpha^{\mathrm{Y}}$;

- for strain-induced martensite: C_{strain}, φ_{strain};

- for stress-assisted martensite: C_{sat}, f_{stress}, φ_{stress};

- for the total martensite content: φ;

- for hardness and flow stress: σ^{Y}, Hv_{before}, Hv_{after};

- and finally for density: ρ.

In this manner austenitisation can be calculated to such an extent that it becomes possible to predict form changes as well as back-transformation and state variables. In Figure 3.19 the change in martensite and flow stress during austenitising is visualized.

3.8.3 Stress-assisted transformation

After austenitisation, the product is so unstable that it will transform without outside intervention. This transformation will starts at nucleation points in the product. The exact nature of these nuclei is not entirely known. The only thing that is clear is that, provided the hydrostatic component is positive, residual stresses clearly increase the transformation rate and stimulate nucleation. During the simulations two aspects cause nucleation:

- local residual hydrostatic stress;

- numerical inhomogeneity in C_{stress}, f_{stress} and φ_{stress}.

As nucleation does not match reality, the transformation rate will not correspond to the actual rate. However, this does not affect the calculated variables such as dilation, plastic strain, stresses and transformation plasticity. See for some results of this simulations Figure 3.20 on page 90

3.8.4 Measurements

It is evident that stress-assisted transformation of a product will not be axi-symmetric but will be an inhomogeneous 3D transformation. Nucleation depends on imperfections such as voids in the grid. Depending on the number of nuclei, a highly inhomogeneous transformation may evolve.

To obtain clarity on this inhomogeneity and the relationship between the inhomogeneity and the actual deformation, a measurement setup was created to measure these phenomena. As temperature is expected to be an important parameter, the measurement setup was placed in a climatic chamber, see Figure 3.17. A hydraulic spindle placed on the climatic chamber caused axial and radial movement of a deep-drawn cup placed on a spindle. Before the cup was mounted in the climatic chamber, it is austenitised (15 min at 1323 K and quenched using 6 bar re-circulating inert gas). In the climatic chamber the cup is continuously measured with an inductive sensor to establish the martensite content and with a mechanical-inductive distance sensor (tesa modules) to measure its dimensions. The measured data were then processed in such a way that the dimensions of the cup could be reconstructed, including the martensite content measured. The martensite content is made visible by the color of the cup, see Figure 3.16 on page 88 and Figure 3.18 on page 89.

3.8.5   Results and discussion

The measured data show two results:

- The mean dilation and transformation plasticity and are both fairly predictable.

- The greatest effect is the change in out-of-roundness during austenitisation and transformation. This effect must be attributed to plastic deformation occurring during inhomogeneous transformation and to the texture and the resulting direction-dependent dilation and transformation plasticity.

Although the model is able to calculate the various steps, the results are inadequate because the greatest inaccuracies are caused by 3D effects, in this study more than 200 microns. These effects have not been included in the model, as the model is only axi-symmetric.
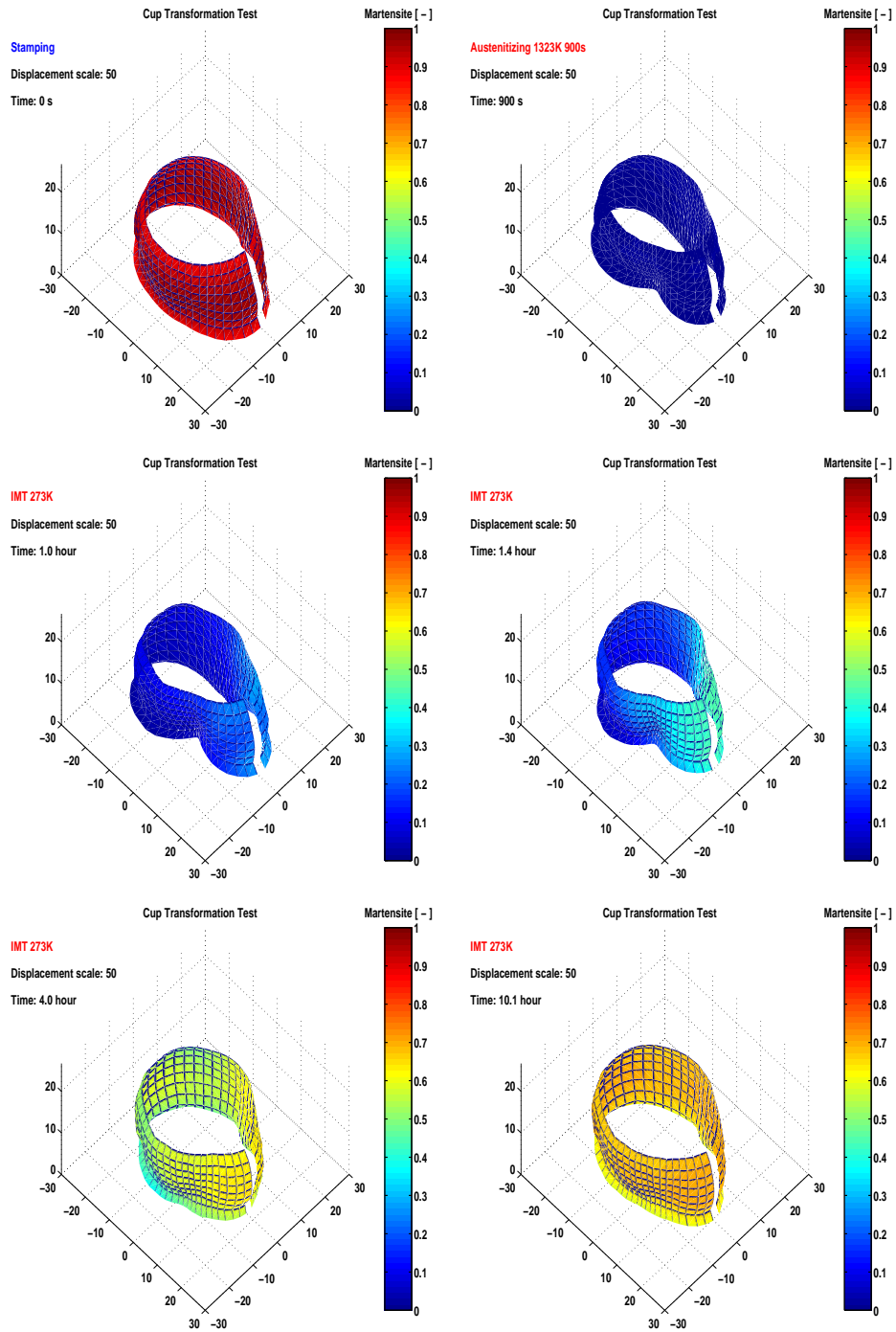
Figure 3.16: The dimensional stability during austenitisation and subsequent isother-
         mal transformation (dimensions in mm) .
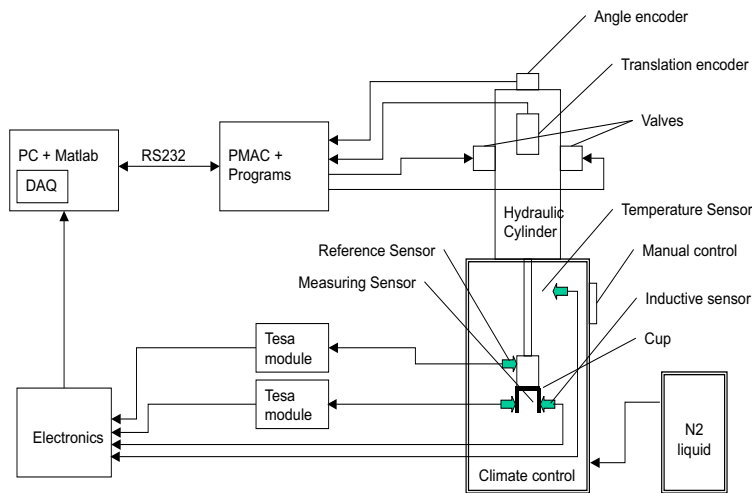
Cup Transformation Test

Figure 3.17: Schematic representation of the test equipment.

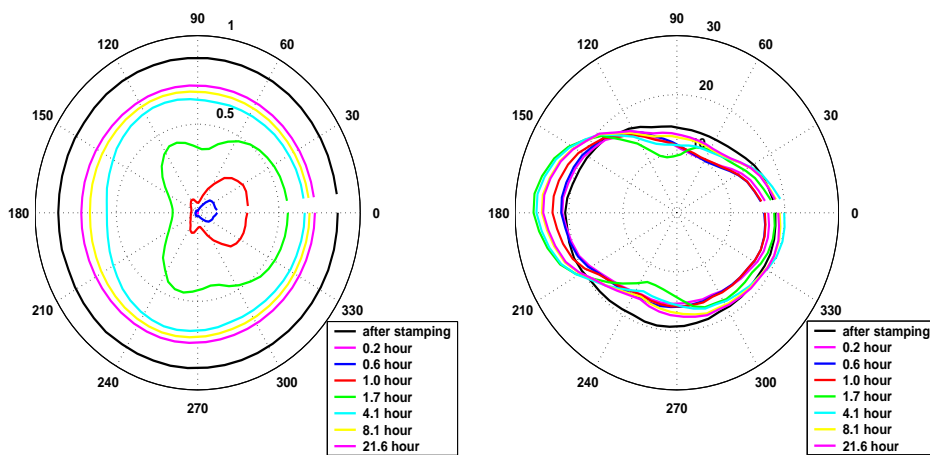Figure 3.18: Above: the change in martensite during the IMT. Right: the change in dimensions during the IMT.
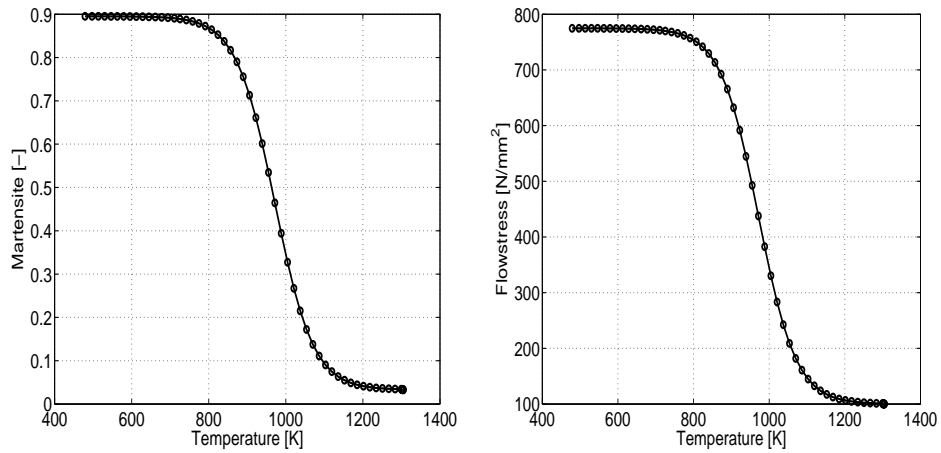
Figure 3.19: Left: the change in martensite. Right: the change in flow stress during austenitising.
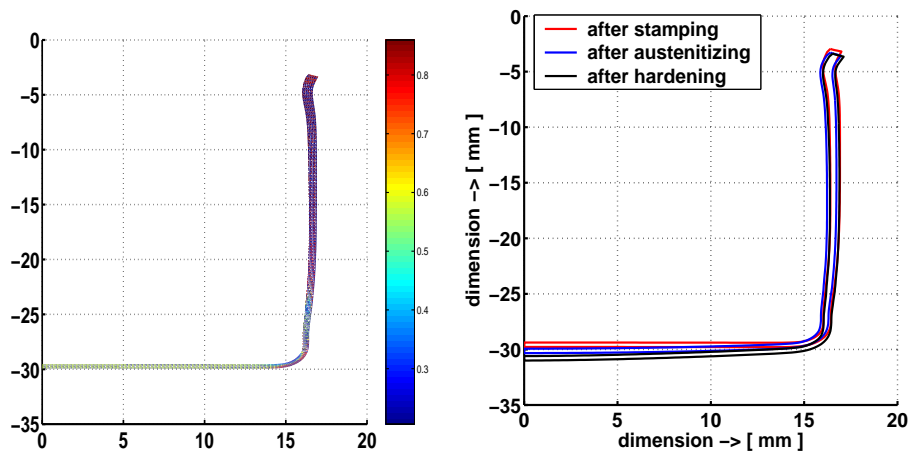

Figure 3.20: Left: dimensions of a deep-drawn cup and the strain-induced martensite content. Right: dimensions of the deep-drawn cup and the cup after austenitising and IMT, based on the FEM calculations.

Figure 3.21: The example process, top left: step 1; top right: step 2; Bottom left: step 3. Dimensions in mm. Bottom right: photographic image of the product. All cross-sections are made at the end of the process.

3.9 Three-stage metal forming process

3.9.1 Introduction

The main purpose for developing the material model for Sandvik Nanoflex™was the calculation of multi-stage metal forming processes. These kinds of processes are normally realized in practice for stamping mass production metal parts, using progressive tooling. To validate the model and its robustness a multi-stage - 3 stamping steps - process was defined. The calculations were performed along with experiments.

The total production process consisted of different steps:

- a stamping step: a simple deep drawing operation;

- a waiting step which simulated the transport of the product from stamping step 1 to 2;

- a stamping step: a second deep drawing step;

- a wait: simulating transport from stage 2 to stage 3;

- a stamping step: biaxial stretching in the reverse direction;

- a wait: This is the time from stamping to austenitising;

- austenitising for 15 min on 1323 K quenching with 6 bar re-circulating inert gas;

- a isothermal transformation step at 223 K for 24 hours;

- a precipitation step 30 min at 773 K.

During the stamping process the product becomes partly martensitic, during waiting this transformation continues: the temperature changes and stress-assisted martensite is formed, and as a reaction on the transformation the residual stresses will decrease. After austenitising the product is fully austenitic and during isothermal transformation it will become martensitic again to a level of about 70% martensite. During this transformation, transformation plasticity and dilation strain will occur, resulting in dimensional changes of the product shape.

3.9.2   Implementation in the FEM code

All functions mentioned above were implemented in a dedicated metal-forming code (internal Philips code) defining 3 different models:

- one for stamping and waiting of stable material;

- one for austenitising;

- one for stamping and waiting of unstable material.

All calculations include thermo-mechanical coupled effects and the effects of friction. The tools were described as rigid bodies. The material properties, after a calculation step, were mapped onto the next step to incorporate the cumulative effect of the transformation and work hardening during the different steps.

3.9.3   Product and stamping process

The example is a axi-symmetric product of relatively small size (about 20 mm in diameter), stamped in 3 different metal forming operations, see Figure 3.21 on page 91.

(a) Step 1: stamping

(b) Step 3: stamping

(c) Step 5: stamping

(d) Step 6: waiting
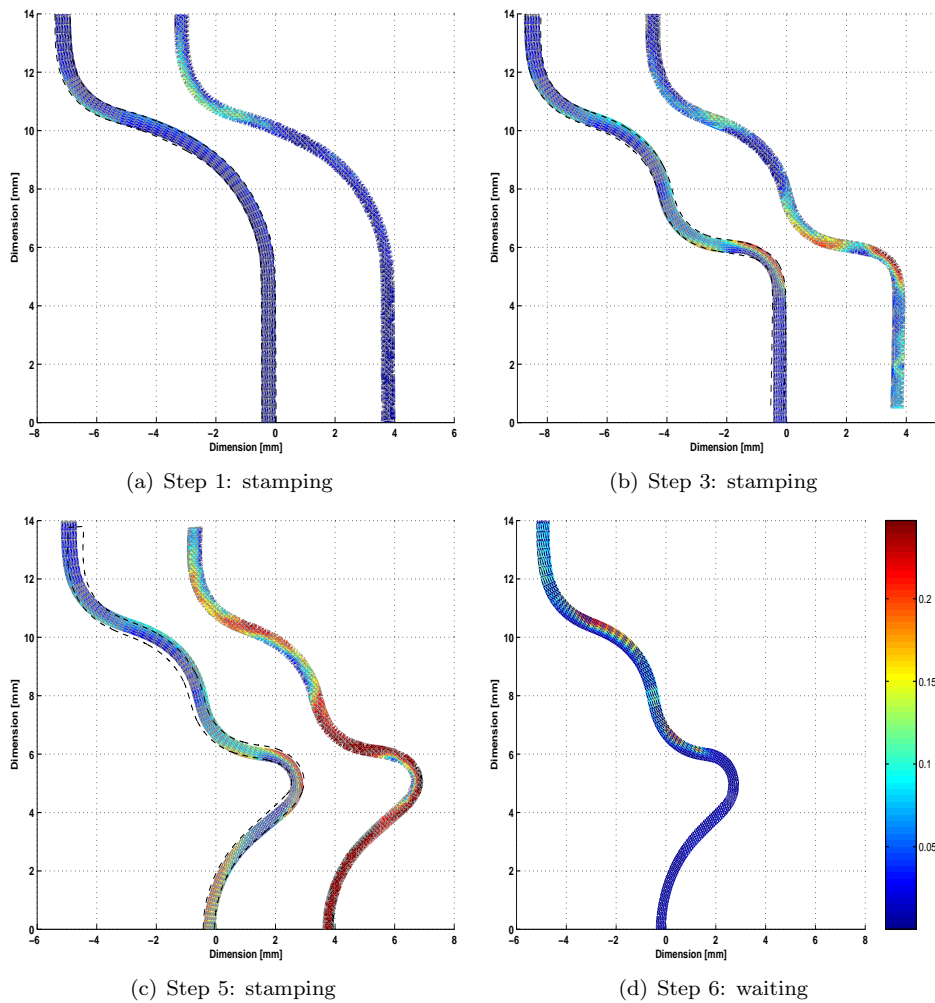
Figure 3.22: The example process. Top left: step 1; Top right: step 2; Bottom left: step 3; Bottom right: step 3; the stress assisted transformation after waiting for 24 hours. Dimensions in mm. In the figures, the contours on the right are the calculated products, the ones on the left are the measurements. Martensite is represented as red and austenite is blue.

3.9.4   FEM simulations and verification

Figure 3.22 on page 93 shows the results of the calculations after the different metal-forming steps and after the waiting steps. In addition, the process was validated after steps 2, 4 and 6 using an automatic measuring method with image processing [40]. In this method the first step is to measure the product contour. The second measurement of the martensite content is by means of image analyzing.

Chapter 4

Verification tool for 2D multi-stage metal forming processes

4.1 Abstract

During the last few years it has become more and more customary for major industries to use FEM simulations during the product creation process. Most of these metal-forming process simulations are based on elastic plastic behaviour of material and use non-deformable tools. For a correct use of FEM simulations in product development stages it is very important to determine the accuracy of the simulations. For multi-stage processes it can be more effective not to simulate the total process but only a few stages of the process, with the last stages usually being the most important ones. To start simulations half way the total process calls for information on the semi-finished product. This information is generated by means of measured values in order to decrease the total modelling time and to increase accuracy. This paper shows a method developed for handling these problems. The method is based on a fully automatic measuring device, including a LECO hardness tester. The method determines:

- Product contours based on image processing;

- Hardness profiles in contours (these are related to the flow stress);

- Martensite profiles based on image correlation (this is important for analysing metastable austenitic steels).

The results of these measurements were used to verify models, including models based on the transformation behaviour of strain-induced martensite. The results were also used for generation of a quad mesh based on a product contour, creating relevant initial parameters at the integration points of the mesh. This was used as input for further calculations. Besides describing the hardware, the measuring method and the mathematics, this article also shows some examples of the possibilities. The examples presented are based on products made of Sandvik Nanoflex™.

4.2 Introduction

Figure 4.1: LECO image analyser and hardness tester.

FEM simulations usually provide a clear and detailed picture of a metal forming process. The detailed nature of the information also causes problems. If we want to verify such models properly, we need to have a verification method which produces the same data density as the FEM simulations. There are various methods that meet this requirement. However, a problem with most of these methods is that they require a lot of manual input and therefore a lot of time. The method described in this article tries to solve this problem. A combination of automated equipment and automated data processing makes it possible to achieve a high data density at an adequate speed. An additional advantage of this method is that, as the entire procedure is virtually identical to the method used for pre- and post-processing in FEM simulations, the measurements can also be used as a starting point for calculations. The method is in principle restricted to 2D calculations. The first part of this article describes the equipment and the measuring method. The second part of the article describes the mathematics used. In the third part two advantages of this system are described on the basis of examples. The material selected for the examples is steel of the type Sandvik Nanoflex™because this material produces strain-induced martensite, which allows the martensite content to be used for verification. All examples are 2D simulations of multi-stage metal forming processes of high precision parts.

4.3 Measuring method

4.3.1 LECO hardware and software

The measuring setup consists of an image analyser and a hardness tester, both made by LECO. A photo of this setup is shown in Figure 4.1 on page 97. Both appliances are connected to a PC by means of interface cards. For more details, visit www.leco.com

4.3.2 Image analyser

The image analyser in this setup consists of a microscope and an XY table, which is controlled by means of a PC and a software package (LECO Image IA3001) that is supplied with the image analyser. Macros allow the analyses to be performed automatically. These analyses involve the processing of various fields. As soon as the analysis has been completed, the results can be stored in a file. The software of the image analyser can also be used together with the hardness tester.

4.3.3 Hardness tester

The hardness tester consists of an XY table and a turret with an automatically revolving head, containing an indenter and two lenses, positioned over the table. The entire mechanism is controlled by means of a software program (LECO Hard AMH3000) that is supplied standard with the hardness tester. The software is used to set the force (0.098 N to 9.8 N) and the positions at which the hardness is to be measured. The hardness tester operates fully automatically, i.e. when the positions have been uploaded from the 'MeasTools' program, the measurements are automatically carried out and processed by means of image analysing. The results of the measurements are stored in a file.

4.3.4 Software developed, MeasTools

Introduction

Hardness testing and measuring the particle sizes (in our case strain-induced martensite) are two distinct procedures. The first part of the two procedures - contour measurement - is identical in both cases. After that, the two measurement methods proceed in different ways. The two procedures are described separately. Ultimately each procedure will produce a result in the form of a contour containing certain properties, such as hardness or martensite, at discrete points. Data processing is the same for both methods.

Contour measurement procedure

A cross-section is taken from the product of which the hardness or martensite content has to be established and this cross-section is polished. The image analysis software determines the contour on the basis of differences in contrast of the product

and the background. The contour is dissected into a row of X and Y co-ordinates describing the contour of the product in the form of a polygon which is the stored in a file.

Procedure for measuring structure profiles

Image analysis software is used to measure the structures. This method uses contrast differences, for instance due to an etching method. By means of a macro, the structures are described as particles with a specific centre of gravity and size. The number of particles in a contour may run to several tens of thousands. Next, the data established with LECO's image software are stored. After this the data are read into MeasTools, which places them in the contour and converts them into discrete points. In the example used in this article, the cross-section was pre-etched with Lichtenegger and Block, which caused a distinct difference in contrast between the martensite and the austenite. The positions and the centres of gravity of these particles were first determined and then translated into the martensite content.

Procedure for hardness profiles

When the product contour is known, it is displayed on the screen. Then the places at which the hardness must be tested can be determined in this contour. These X and Y co-ordinates are transmitted to the hardness tester, which measures the hardness at these points fully automatically. After the hardness has been measured, the data are stored and read into MeasTools.

Creating profiles based on measured data

When the two measuring procedures described above have been completed, two files are obtained. The first file contains the contour of the product and the second contains the data measured within the contour. These data can relate to anything, but within the context of this article they concern strain-induced martensite or hardness. To realise the profiles, the following steps are taken: filtering, extrapolation to the edges, triangular meshing (Delauny-based) and interpolation. To generate the input files for a FEM simulation, a quad mesh was generated within the contour. Next, the data of the profile were interpolated to the integration points of the quad mesh. (In case of Sandvik Nanoflex™, two profiles were interpolated, namely strain-induced martensite and hardness.)
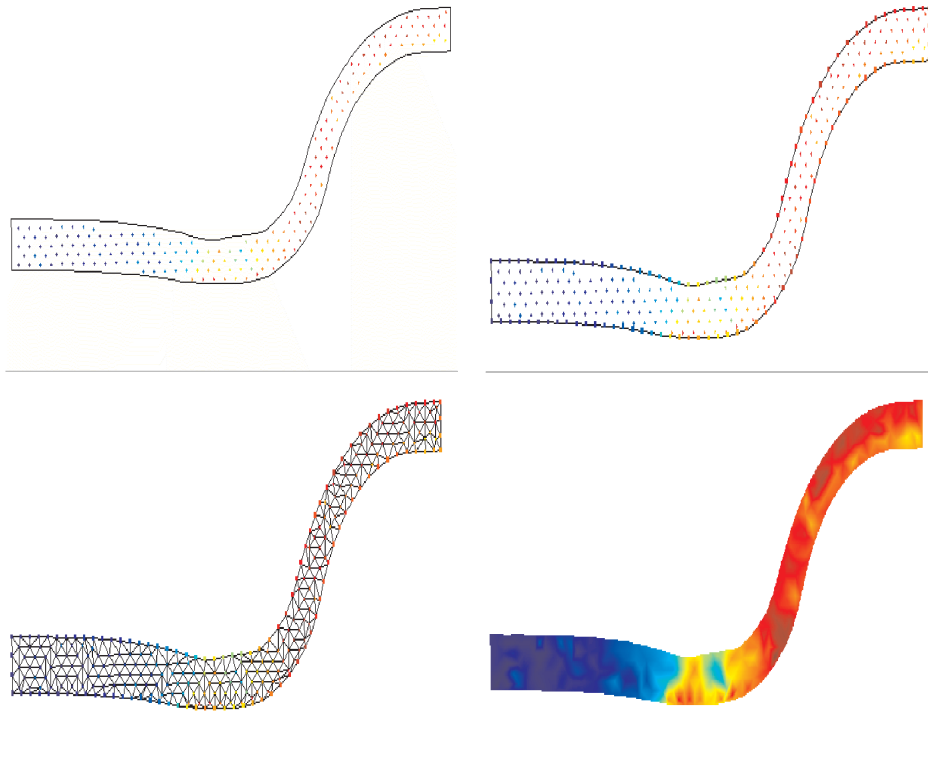
4.4   Mathematical data processing

Figure 4.2: The steps for measuring a hardness profile. Above left: contour and hardness point. Above right : after extrapolation. Below left: after meshing. Below right: after interpolation.

4.4.1   Introduction

In this chapter the numerical part of the software that was developed will be discussed. The measurement was based on a polished cross-section of a product. This cross-section was embedded in plastic. Then the following procedure is followed:

- The outside contour of the product is determined by means of image processing;

- The number of contour points are then reduced;

- The product is then etched (for the martensite profile) or for the hardness profile the points within the product contour where the hardness has to be

measured are sorted by a TSP (Travelling Salesman Problem) algorithm and determined;

- The values measured are translated into discrete points in the product contour. This is already the case for hardness, but not for the martensite content, which requires an extra calculation step to translate the martensite and austenite particles into a martensite content in volume percentage at discrete points;

- Optional the profile can be filtered using a Savitzky-Golay approach;

- The values at discrete points within the product contour are then extrapolated to discrete points on the edge of the product. These marginal points are a subset of the original contour points;

- Then everything is meshed by means of Delauny triangular meshing to create the elements;

- The final step is interpolation from the nodes towards the required positions within the elements.

For an example of the various steps in hardness measurement, see Figure 4.2 on page 100. For an example of a martensite measurement, see Figure 4.3 on page 102.

4.4.2 Mathematics

Contour

The first problem that needs to be solved is the definition of the product contour. By means of image processing, the edge of the product contour was determined and translated into actual co-ordinates $(x_{i..n}, y_{i..n})$; n is equal to the number of contour points. These points are in random order. To obtain the product contour, they must be converted into a polygon. One can start at any given point (x_j, y_j) and then look for the next point by establishing the minimum of ds according to:

$$min(ds_j) \rightarrow i \qquad ds_j = \sqrt{(x_i - x_j)^2 + (y_i - y_j)^2} \qquad i \neq j \qquad (4.1)$$

The point thus established is then marked from the set $(x_{i..n}, y_{i..n})$, n. This is repeated until the distance between the last points is smaller than all points that have been selected. This method can only be used in the case of a closed contour. If there are points far from the determined contour these points are neglected.

Reducing the contour

Next this polygon has to be reduced, to minimize the number of points. This should be done with a minimum loss of contour accuracy. The reduction is carried out in two steps. The first step calculates the average of $2Q$ points in the immediate vicinity:

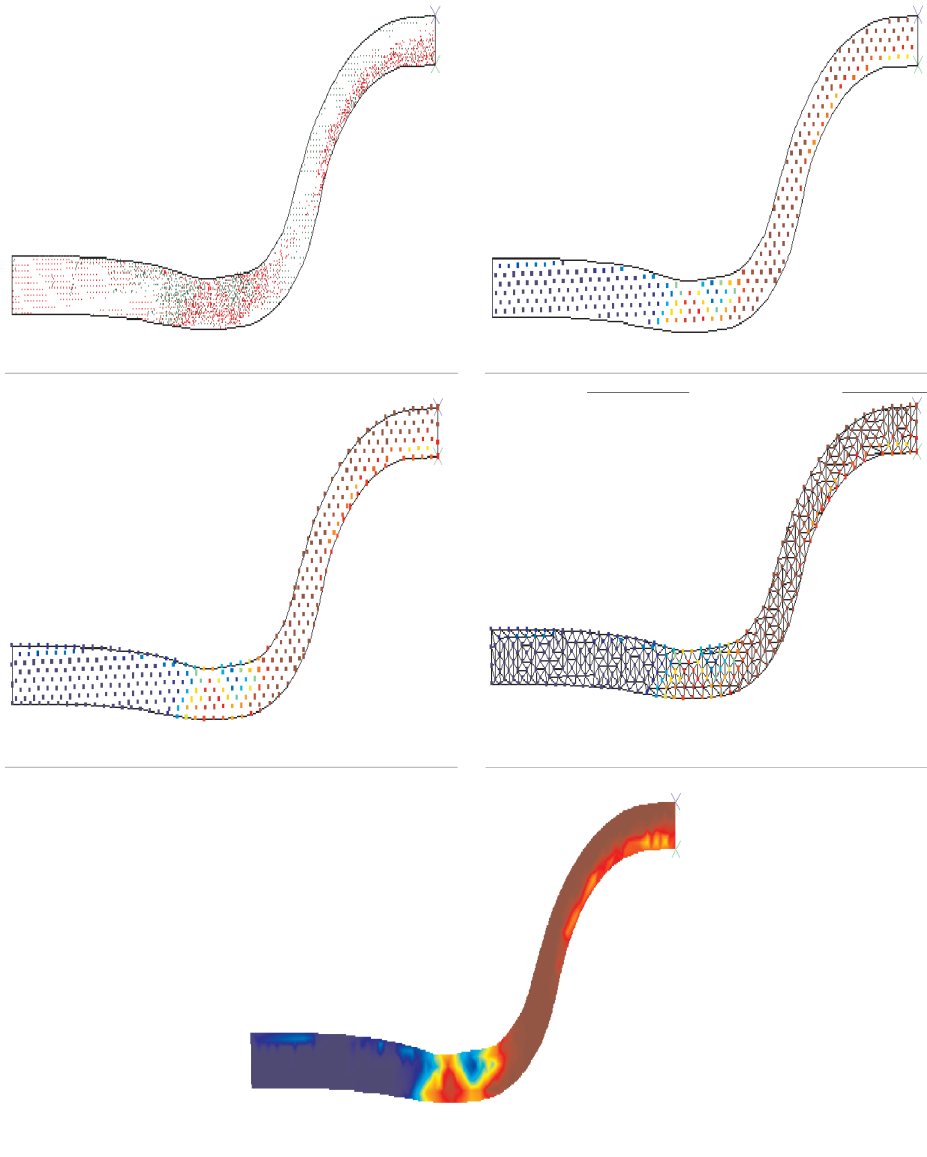$$x_j = \sum_{i=j-Q}^{j+Q} (x_i)/2Q, \qquad y_j = \sum_{i=j-Q}^{j+Q} (y_i)/2Q, \qquad (4.2)$$

Figure 4.3: The steps for measuring a martensite profile. Above left: contour and martensite(green)/austenite(red) particles. Above right: after calculation and mapping to discrete points (martensite=red). Middle left: after extrapolation (martensite=red). Middle right: after meshing (martensite=red). Below: after interpolation (martensite=red).

In this way, the polygon is reduced linearly by means of a moving window. Then a second reduction takes place on the basis of the second derivative:

$$\{i \in \,<j-Q, j+Q>| \; \frac{\Delta(\frac{\Delta y_i}{\Delta x_i})}{\Delta x_i} - E < 0\} \tag{4.3}$$

where E is the limiting value. In this way, points on a straight line are removed.

Travelling salesman problem

If hardness has to be measured within the contour, the problem to deal with is that moving the hardness needle from one position to another is rather time-consuming. These measurements may involve as many as 1000 or 2000 measuring points. The solution to this problem is known as the travelling salesman problem or TSP: finding the shortest and most economical way of visiting a randomly selected number of towns and cities. If n measurements have to be made at positions (x_i, y_i) the distance to be covered is:

$$L = \sum_{i=1}^{n} \sqrt{(x_i - x_{i+1})^2 + (y_i - y_{i+1})^2} \tag{4.4}$$

The closed contour applies: $(x_{n+1}, y_{i+1}) = (x_1, y_1)$. The minimum values can be found by varying the order of the points. This is done on the basis of an algorithm according to [41].

Determination of the martensite values

When determining a martensite profile, another problem is encountered. The cross-section of an aged product made of Sandvik Nanoflex™is etched with Lichtenegger and Block. Then the martensite and austenite particles are measured by means of image processing. This leads to a set of austenite particles with centres of gravity (zx_i, zy_i) and surface areas A_i. The particles have a limited size. If they become larger, they are split. These sets can now be described as follows:

$$(zx\gamma_{i..n}, zy\gamma_{i..n}, A_{i..n}) \qquad and \qquad (zx\alpha_{i..m}, zy\alpha_{i..m}, A_{i..m}) \tag{4.5}$$

where γ represents the austenite particles, α the martensite particles and n, m the number of austenite and martensite particles respectively. In order to mesh, these particles have to be translated into the martensite content in volume percentage at a number of discrete points in the contour. These are defined as $(x_{j..o}, y_{j..o})$, where o stands for the number of discrete points. Based on the set of particles, the martensite content at the discrete points has to be determined. First the distance of the particles relative to the discrete points is defined:

$$\Delta l\gamma_{ij} = \sqrt{(zx\gamma_i - x_j)^2 + (zy\gamma_i - y_j)^2} \quad , \quad \Delta l\alpha_{ij} = \sqrt{(zx\alpha_i - x_j)^2 + (zy\alpha_i - y_j)^2} \tag{4.6}$$

The average particle size at the discrete points is required. This can be calculated as follows:

$$A\gamma_j = \sum_{i=1}^{n}(C\gamma_{ij}A_i)/n \quad , \quad A\alpha_j = \sum_{i=1}^{m}(C\alpha_{ij}A_i)/m \tag{4.7}$$

where C_{ij} is a matrix with weighting factors. These factors have to be selected in such a way that the nearest particles are assigned the greatest weight. To realize this a clock function was selected:

$$C_{ij} = Q_1 \exp(\frac{-\Delta l_{ij}^2}{Q_2}) \tag{4.8}$$

The martensite can now be easily determined on the basis of (4.8), assuming that: $A_\alpha + A\gamma = 1$. This yields:

$$\varphi_j = \frac{A\alpha_j}{A\alpha_j + A\gamma_j} \tag{4.9}$$

Extrapolation

The data of the discrete points are extrapolated to the edges of the product contour. This is done by a general least squares fit [41] of a subset of discrete points around the point to be extrapolated. Singular value decomposition [41] was used to incorporate only those coefficients that really have an effect. A surface in a 3D space is defined as follows:

$$z(x,y) = \sum_{j=1}^{n}(\sum_{i=1}^{n} a_{ij}x^i y^j)) \tag{4.10}$$

Unknowns a_{ij} now have to be determined, using the subset of discrete points with hardness or martensite content values. This is done in the usual manner [41]. The regression problem:

$$[\mathbf{A}]\{\alpha\} = \{y\} \tag{4.11}$$

where $[\mathbf{A}]$ is the matrix with the locations, $\{\alpha\}$ are the unknowns and $\{y\}$ is the vector with responses, i.e. martensite content or hardness values. Multiplication of (4.11) by A^T yields:

$$[\mathbf{A}]^T[\mathbf{A}]\{\alpha\} = [\mathbf{A}]^T\{y\} \tag{4.12}$$

This system can be solved by means of standard techniques, such as LU decomposition and back substitution, Cholesky decomposition, Gauss-Jordan elimination or Singular Value Decomposition.

Delauny triangulation

Meshing can take place after extrapolation to the reduced contour points of the mesh, for which the standard procedure is a Delauny triangular mesh routine. It is also possible to generate a quadrilateral mesh [42]. After meshing, interpolation within the elements can take place by means of a simple linear model through the

nodes. Given the value of a node as $k(x_i, y_i, z_i)$, the value of z_j at a random point in the triangle can be described as:

$$z_j = \begin{pmatrix} x_j & y_j & 1 \end{pmatrix} \begin{pmatrix} x_1 & y_1 & 1 \\ x_2 & y_2 & 1 \\ x_3 & y_3 & 1 \end{pmatrix} \begin{pmatrix} z_1 \\ z_2 \\ z_3 \end{pmatrix} \tag{4.13}$$

where $p(x_j, y_j)$ is the point at which value z_j should be calculated.

Filtering with Savitzky-Golay

The data can be filtered to partly eliminate measuring errors. It was decided to use a Savitzky-Golay filter [41] for this purpose because these filters are less affected by numerical diffusion, i.e. the peaks are not reduced substantially by the filtering process. In principle, this is also possible with polynomials in combination with the least squares method. However, this method is too slow as a filter and that is why a Savitzky-Golay filter was used. The filtering technique of [41] must be extended to include a 3D situation.

The point to be filtered is defined as $p(x_j, y_j)$, with value f_i. The existing points were defined as $p(x_i, y_i, z_i)$. By analogy to (4.6) this yield:

$$\begin{aligned} dl_{ij} &= +\sqrt{(x_i - x_j)^2 + (y_i - y_j)^2} & if \quad x_i < x_j \\ dl_{ij} &= -\sqrt{(x_i - x_j)^2 + (y_i - y_j)^2} & if \quad x_i > x_j \end{aligned} \tag{4.14}$$

The (x, y) domain has been changed into a distance domain dl. This was done for all the points in a moving window with a predefined height and width. The strategy of the filter was now applied according to [41]. Matrix d_L was converted into a vector with incremental elements in which x_j was exactly in the middle. This causes f_i to become $f_i^{\checkmark} \colon f_i \to f_i^{\checkmark}$.

Bearing in mind that a digital filter was applied to a series of equally spaced data values $f_i \equiv f^{\checkmark}(t_i)$, where $t_i \equiv t_0 + i\Delta$ for some constant spacing Δ and $i = \ldots -2, -1, 0, 1, 2 \ldots$, the filter is defined as follows:

$$g_i = \sum_{n=-n_L}^{n_R} c_n f_{i+n}^{\checkmark} \tag{4.15}$$

where n_L is the number of points used 'to the left' of the data points and n_R the number of points 'to the right'. The idea of Savitzky-Golay filtering is to find the coefficients c_n that preserve higher moments. Equivalently, the idea is to approximate the underlying function within the moving window not by a constant (whose estimate is the average), but by a polynomial of higher order, typically quadratic. To derive such coefficients, consider how g_0 might be obtained. To fit a polynomial of degree M in i, namely $a_0 + a_1^i \ldots a_m i^m$ to the values $f^{\checkmark}_{-n_l}, \ldots, f^{\checkmark}_{n_R}$, g_0 will be the value of that polynomial at $i = 0$, namely a_0.

M	n_L	n_R	Sample Savitzky-Golay Coefficients										
2	2	2				-0.086	0.343	0.486	0.343	-0.086			
2	3	1			-0.143	0.171	0.343	0.371	0.257				
2	4	0		0.086	-0.143	-0.086	0.257	0.886					
2	5	5	-0.084	0.021	0.103	0.161	0.196	0.207	0.196	0.161	0.103	0.021	-0.084
4	4	4		0.035	-0.128	0.070	0.315	0.417	0.315	0.070	-0.128	0.035	
4	5	5	0.042	-0.105	-0.023	0.140	0.280	0.333	0.280	0.140	-0.023	-0.105	0.042

The design matrix for this problem was:

$$A_{ij} = i^j \quad i = -n_L, \ldots, n_R, \quad j = 0, \ldots, M \tag{4.16}$$

and the normal equation for the vector a_j's in terms of the vector of f_i's in matrix notation is:

$$(\mathbf{A}^T \cdot \mathbf{A}) \cdot \mathbf{a} = \mathbf{A}^T \cdot \mathbf{f} \quad \text{or} \quad \mathbf{a} = (\mathbf{A}^T \cdot \mathbf{A})^{-1} \cdot (\mathbf{A}^T \cdot \mathbf{f}) \tag{4.17}$$

There are also the specific forms:

$$\left\{ \mathbf{A}^T \cdot \mathbf{A} \right\}_{ij} = \sum_{k=-n_L}^{n_R} A_{ki} A_{kj} = \sum_{k=-n_L}^{n_R} k^{i+j} \tag{4.18}$$

and

$$\left\{ \mathbf{A}^T \cdot \mathbf{f} \right\}_j = \sum_{k=-n_L}^{n_R} A_{kj} f_k = \sum_{k=-n_L}^{n_R} k^j f_k \tag{4.19}$$

Since the coefficient c_n is the component a_0 when $\mathbf{f}$ is replaced by the unit vector $\mathbf{e}_n$, $-n_L \leq n < n_R$, the equation becomes:

$$c_n = \left\{ (\mathbf{A}^T \cdot \mathbf{A})^{-1} \cdot (\mathbf{A}^T \cdot \mathbf{e}_n) \right\}_0 = \sum_{m=0}^{M} \left\{ (\mathbf{A}^T \cdot \mathbf{A})^{-1} \right\}_{0m} n^m \tag{4.20}$$

It should be noted that according to (4.20) only one row of the inverse matrix is needed. This can be solved numerically by means of LU decomposition with only a single back substitution. In fact, the solving method is more or less the same as in standard linear regression.

4.5 Verification of a multi-stage metal forming process

The first example selected concerns a metal part of Sandvik Nanoflex™made in four forming steps according to the Oeillet [43] method. The first step stretches the material in such a way that the extra surface required for the product is realized. The subsequent steps bend the material back so that the final form is created. The ultimate diameter of the product is about 4 mm. Verification took place as follows:

1. A cross-section was made at each step;

2. The shape, i.e. contour, of these cross-sections was measured;

3. The cross-sections were etched to make the martensite content visible;

4. The martensite profiles were determined;

5. Finally, the calculations were verified as regards form and martensite content.

See Figure 4.4 on page 4.4 for the results of the calculations and measurements. The martensite content calculated was plotted in the lower profiles, together with the product contours measured. The martensite content measured was plotted in the upper profiles. The figures clearly show to what extent the calculation deviates from reality. The causes of these deviations are not further elucidated in this article.

4.5.1 Simulation based on measured input

This example demonstrates a measured contour, including initial plastic strain and martensite content, can be used to start FEM simulations from any position. The procedure was as follows:

1. The product contour was measured;

2. The martensite profile was measured;

3. The hardness was measured;

4. Together with the martensite content, hardness was translated into initial strain;

5. A quad mesh was generated in the product contour, mapping the initial dislocation densities and the martensite content at the integration points.

The initial dislocation densities were calculated from a measured relation between Vickers hardness and flow stress. The problem was that no information about the history was available. To solve this it was assumed that the history was the same as in the case of a tensile test. Then the initial values for the dislocation densities

can be solved. Assuming that the result of a FEM calculation on a tensile bar can be defined as follows:

$$Hv = f_{hv}(T_{ini}) \qquad \varphi = f_{\varphi}(T_{ini}) \tag{4.21}$$

where Hv is the Vickers hardness and φ is the martensite content. At an integration point on the mesh the hardness and the martensite were measured and defined as: $P(Hv_i, \varphi_i)$. The dislocation densities were then found numerically by solving the following equation, varying the initial temperature T_{ini}:

$$F(T) = 0 = (Hv_i - f_{hv}(T_{ini}))^2 + (\varphi_i - f_{\varphi}(T_{ini}))^2 \tag{4.22}$$

In this way, the input for simulation of step 3 of example 1 was established, see Figure 4.5 on page 110 left, for the martensite content and hardness profile. This input was used to calculate step 4. The results are shown in Figure 4.5 on page 110, right, in which the lower profile shows the result of the calculation based on the measured input, whereas the upper profile shows the martensite content measured. As is evident from this figure, the results are entirely comparable. A comparison of the figures shows that the calculation based on Figure 4.5 on page 110 gives more accurate results. This is due to the cumulative errors of the constitutive material model. Because Figure 4.5 on page 110 was based on one calculation, this error is less than in Figure 4.4 on page 110, which was based on four calculations.

4.5.2 Influence of elastic tool deformation

In the beginning of the engineering process of a metal part, or product, the tools in a FEM simulation of metal forming are based on rigid bodies, this means that there is no influence of elastic tool deformation. It cannot be done more accurately simply because there is no model for the tool, because the dimensions are still unknown. Tools are already ordered at the end of the engineering process, i.e. in the prototyping phase. Because the dimensions of the tools are already known at this point, the simulations can be corrected by implementing the elastic tool deformation. This can be done in two ways or by a combination of these two ways:

- Rigid bodies on elastic springs, which implements only global elastic tool deformation, the most important part;

- Real elastic tool deformation, which implements the tools as an elastic deformable mesh. This is more accurate, but requires more work and uses a lot of CPU-time.

By measuring a cross-section of a product, or prototype, the influence of the elastic deformation can be made visible. In Figure 4.5.2 an example is given of the calibrated part of a metal part stamped by means of progressive tools as shown in Figure 4.6.
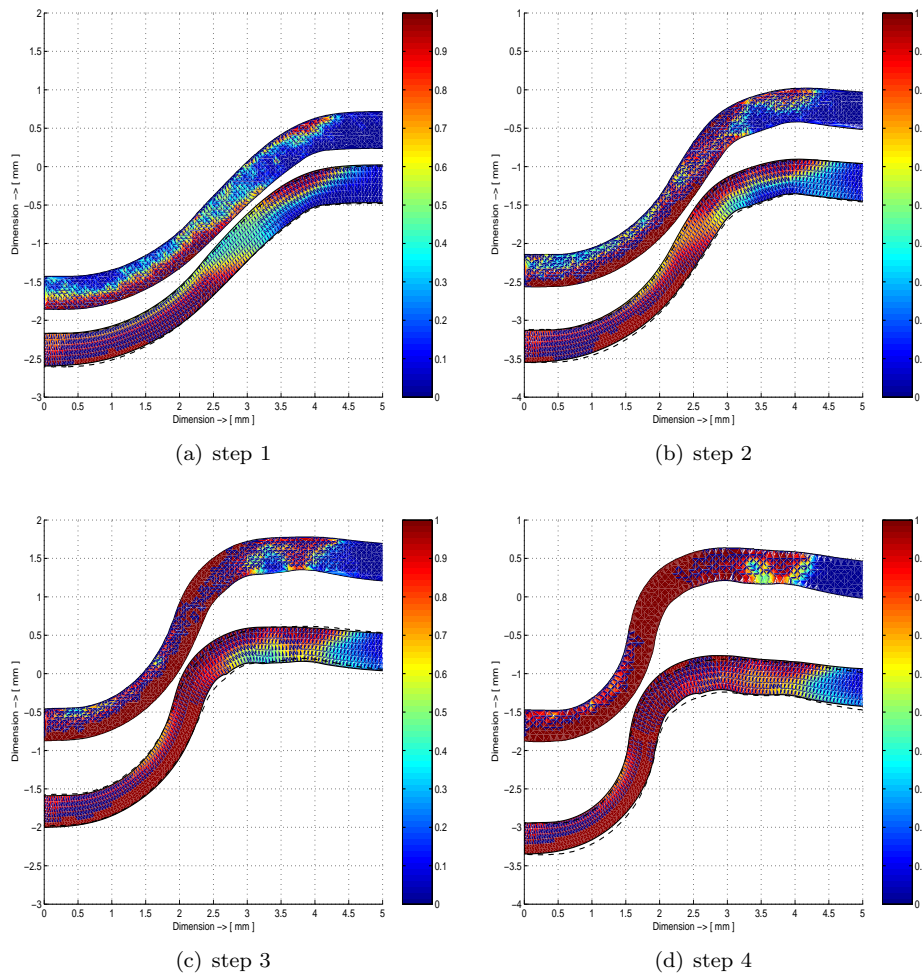
Figure 4.4: 4 steps of Oeillet process - upper profile shows martensite content measured; lower profile shows martensite profiles calculated and the dotted line is the contour measured. 1=martensite, 0=austenite. Above left: step 1; Above right: step 2; Below left: step 3; Below right: step 4.
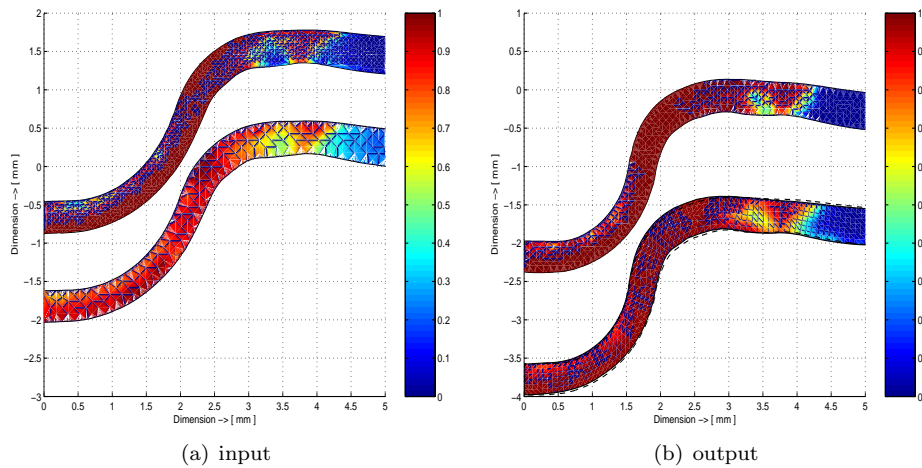
(a) input

(b) output

Figure 4.5: Left: input for fourth step of Oeillet process - upper profile shows the martensite content measured, the lower profile shows the hardness. The data are normalised. Right: The calculated output based on the input from the left Figure. Upper profile shows the martensite content measured, the lower profile is the result of the simulation.
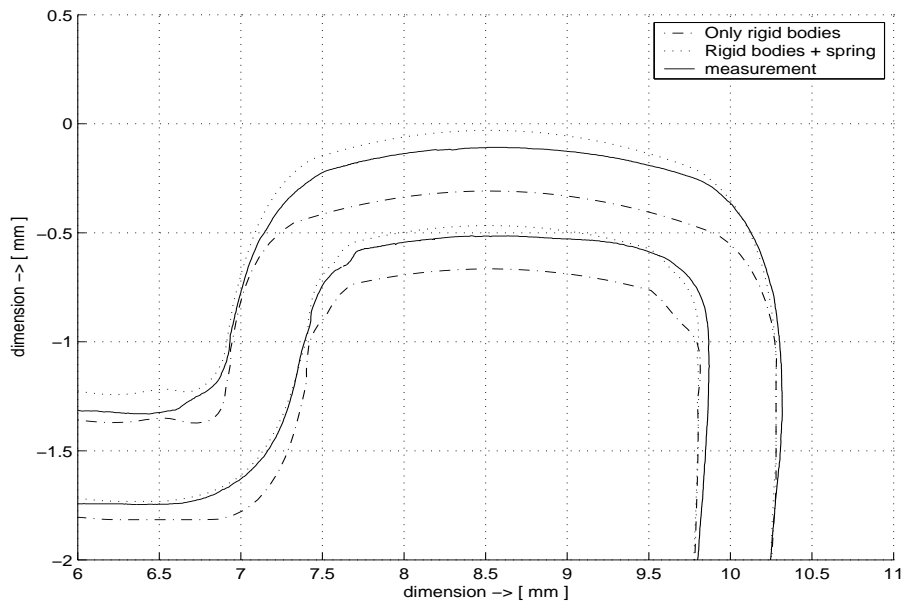

Figure 4.6: Influence of elastic tool deformation on the product shape.

Chapter 5

Application

5.1 Abstract

Sandvik Nanoflex™combines good corrosion resistance with high strength. It shows good deformability in austenitic conditions. This material belongs to the group of metastable austenites: i.e. during deformation a strain-induced transformation to martensite takes place. After deformation, the transformation continues as a result of internal residual stresses. Depending on the heat treatment, this stress-assisted transformation is more or less autocatalytic. Both transformations are stress-state and temperature dependent. The martensite phase of Sandvik Nanoflex™can be aged substantial (more then 1000 N/mm^2).

A multi-stage metal-forming process is simulated. Results of the transformation behaviour are presented together with the shape of the product during and after metal forming.

During the engineering process of high precision metal formed products, like the example product, questions often arise about the relation between the scatter on the initial parameters (like the strip thickness, Yield stress etc. and the product accuracy. This becomes even more complex as:

- The material is instable, which means that martensite formation occurs very easily;

- The transformation rate depends on the stress state, which is strongly related to friction;

- The transformation rate depends on the temperature, which is strongly related to deformation heat.

A possible way to obtain a greater understanding of these phenomena is by doing a process window study, using DACE (Design and Analysis of Computer Experiments). In this chapter an example is presented of how to perform a DACE study on a three stage metal forming process, using distributed computing. The method is shown, together with some results. The study focuses on:

- Two types of hardening (strain-induced and stress-assisted);

- The influence of metal forming parameters on the form accuracy and the hardness after stamping.

5.2 Introduction

Metastable austenites may transform to martensite during or after metal forming. These transformations depend on temperature and hydrostatic stress. The calculations described in this article have therefore been executed with a dedicated and robust FEM solver called CRYSTAL.

Because of the influence of temperature, the calculations need to be fully thermo-mechanically coupled. The calculations also have to incorporate the effects of friction, because it influences the stress state. This code has been specifically developed to describe multi-stage metal forming processes including complex materials behaviour. The material used for these calculations is a corrosion-resistant steel, referred to as Sandvik Nanoflex™[3].

5.3   Three-stage metal forming process

5.3.1   Introduction

The main purpose for developing the material model for Sandvik Nanoflex™was applications in simulations on multi-stage metal forming processes. These kind of processes are normally used for mass production of metal parts, using progressive tooling. To validate the model and its robustness a multi-stage process is defined, consisting of three different steps. The calculations are carried out together with experiments.
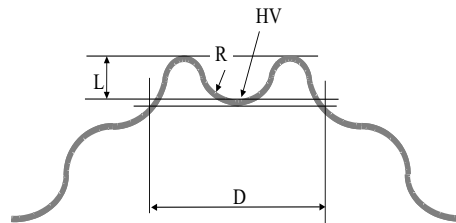

Figure 5.1: A sketch of the example product.

The example product is a combination of a spring and a bearing. The contact area of the bearing is the radius on the top of the product, see Figure 5.1. This radius part of the product must have a specific hardness (Hv) to avoid wear during operation. The other dimensions of the product are related to a specific stiffness in the vertical direction and to facilitate clamping.

The total production process consist of the following steps:

1. A stamping step, a simple deep drawing operation;

2. A waiting step which simulates the transport of the product from stamping step 1 to 2;

3. A stamping step, the second deep drawing step;

4. A waiting step, simulating the transport from stage 2 to stage 3;

5. A stamping step: biaxial stretching in the reverse direction;

6. A waiting step. this is the time from stamping up to austenitising;

7. Austenitising for 15 min. on 1323 K, quenching using 6 bar recirculating inert gas: during this time step the material becomes unstable;

8. An isothermal transformation step at 223 K for 24 hour;
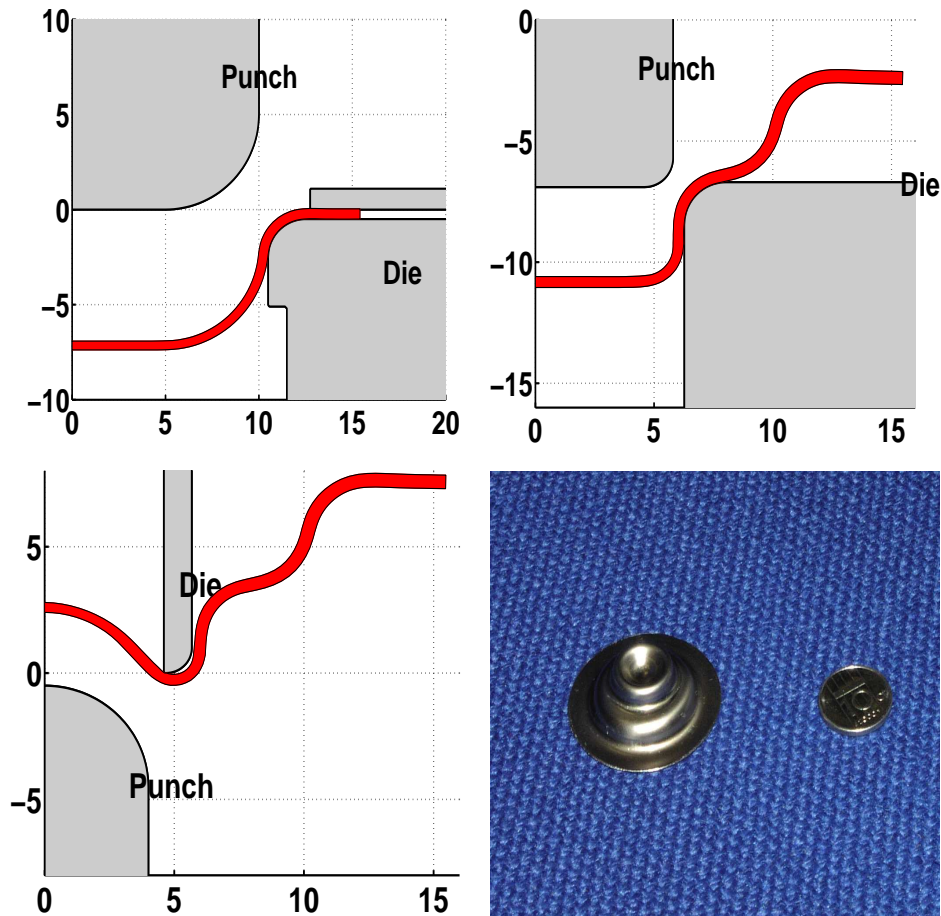
9. A precipitation step 15 min. at 773 K.

Figure 5.2: The example process. Top left: step 1; Top right: step 2; Bottom left: step 3. Dimensions in mm. Bottom right: photograph of the product. All cross-sections were made at the end of the process.

During the stamping process the product becomes partly martensitic, during waiting this transformation continues. After autenitising the product is fully austenitic and during isothermal transformation it becomes martensitic again at a level of about 60% to 80%. During this transformation, plasticity and dilation strain occur, resulting in dimensional changes of the product.
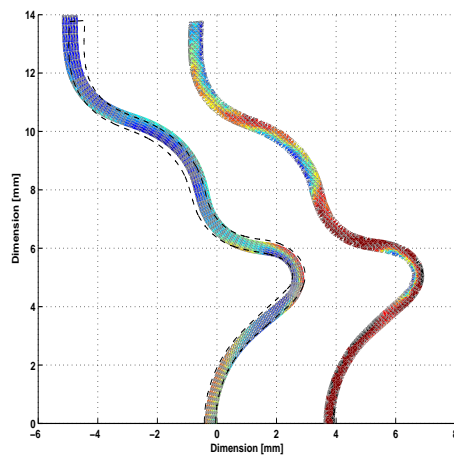
5.3.2   Implementation in the FEM code

All functions mentioned above were implemented in a dedicated metal forming code CRYSTAL defining 3 different models:
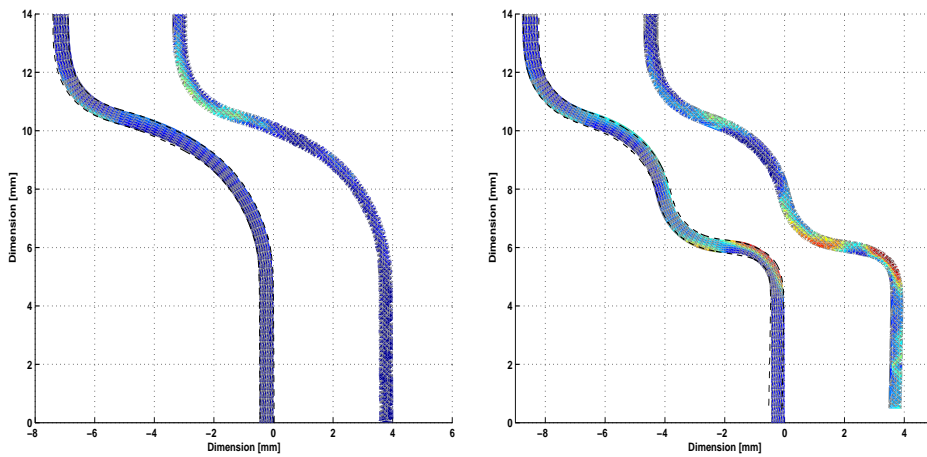
(a) After step 2: stamping

(b) After step 4: stamping

(c) After step 6: stamping

Figure 5.3: The example process. In the figures, the contours on the right are the calculated products, the ones on the left are the measurements. Martensite is represented in red and austenite in blue.

- One for stamping and waiting of stable material;

- One for austenitising;

- One for the transformation of instable material

All the calculations were fully thermo-mechanically coupled and the effects of friction were included because they influences the stress state. The tools were described as rigid bodies. The material properties after a calculation step were mapped on to the model for the next step to incorporate the cumulative effect of the transformation and work hardening during the different steps.

5.3.3 FEM simulations and verification

Figure 5.3 shows the results of the calculations after the different metal forming steps and waiting steps. In addition, the process was validated after steps 2, 4 and 6 using an automatic measuring method based on image processing [40]. The product contours and martensite profile were measured.

5.4   Process window studies

5.4.1   Introduction in Design and Analysis of Computer Experiments (DACE)
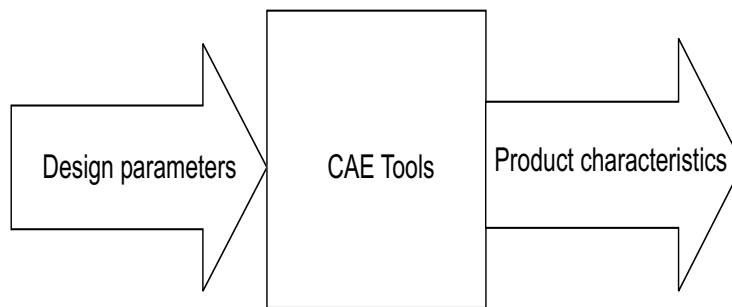

Figure 5.4: Design problem

The ever-increasing pressure on the development time of new products and processes has changed the design process during resent years. In the past, design merely consisted of experimentation and physical prototyping. In the last decade, computer simulation models such as FEM and CFD have become very popular in engineering design and analysis. The application described in this part is one of many examples. In many cases, only predicting the quality characteristics of a design is not enough. Usually, designers are confronted with the problem of finding settings for a number of design parameters that are optimal with respect to several product or process quality characteristics see Table 5.1. Since there are usually many possible combinations of design parameter settings, the crucial question becomes how to find the best possible settings with a minimum number of simulations. This new challenge has led to a new engineering discipline, often referred to as design and analysis of computer experiments (DACE). Surveys on this research area can be found in [44] and [45]. All methodologies that are suggested in the literature rely heavily on statistics and mathematical optimization theory. Generally, there are two types of approaches: iterative approaches [46]) and global modelling approaches [47]). Many papers have been published on applications of DACE in a wide variety of engineering disciplines. In this part, the DACE method 'Compact' and its application on optimizing the manufacturing process is presented. 'Compact' has already been used in several cases [48]), and is based on global modelling.

5.4.2   Methodology and application

In this Section, the 'Compact' methodology is presented. The approach consists of four steps: problem specification, design of computer experiments, 'Compact' modelling and analysis. Figure 5.5 gives an overview of the steps. Along with these steps, the implementation is described in the previous section.
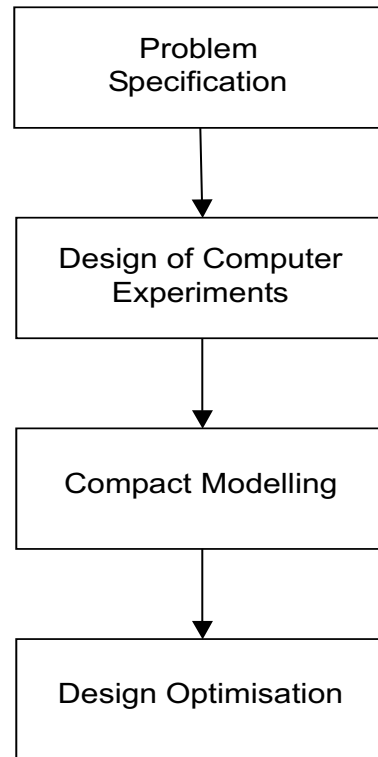
Figure 5.5: 'Compact' approach.

5.4.3 Problem specification

In the first step, the design optimization problem is defined. First of all, the definition is needed for the design parameters that are varied. Generally, two types of design parameters can be distinguished:

- Parameters for which the optimal settings with respect to the quality characteristics have to be found;

- Parameters that have significant influence on the quality of the design, which cannot (completely) be controlled in the physical reality.

In this case all the design variables of interest fall into the second category: we can not control the design parameters, see Table 5.1. The objective in this case was not to find the optimum setting of design variables but to gain insight into the robustness of several quality characteristics.

Table 5.1: The input parameters for the DACE analyses. ♣: Distribution: n=normal, u=uniform. ♡: S=Standard deviation

Number	Parameter	Low	High	Dimension	Dis.♣	3S♡
1	Initial temperature	288	298	K	n	5
2	Material thickness	0.49	0.51	mm	n	0.01
3	Influence Chemical composition (C_{strain})	280	420	K	n	25
4	Initial flow stress austenite	280	380	N/mm^2	n	50
5	Saturation value for martensite (f_{stress})	0.6	0.8	-	n	0.1
6	Time step between step1 and step2	0	600	sec	u	300
7	Time step between step2 and step3	0	600	sec	u	300
8	Waiting time after step3	100	10800	sec	u	5350
9	Ram depth step1 related to nominal	-0.02	+0.02	mm	n	0.02
10	Ram depth step2 related to nominal	-0.02	+0.02	mm	n	0.02
11	Ram depth step3 related to nominal	-0.02	+0.02	mm	n	0.02
12	Coulomb Friction	0.008	0.15	-	n	0.035

Next, definition is required of the quality characteristics that are important in evaluating the design. These quality characteristics are usually referred to as response parameters. In this case, response parameters are divided into three process steps. For every step, the response parameters are printed in Table 5.2.

Table 5.2: Dimensions and tolerances of the example process.

Symbol	Name	Nominal	Tolerance
D	Diameter	13 mm	±0.01 mm
L	Bearing high	3 mm	±0.01 mm
R	Bearing radius	4.06 mm	±0.005 mm
Hv	Bearing hardness	500 Hv0.2	±50 Hv0.2

5.4.4   Design of computer experiments

The second step in the 'Compact' methodology generates a set of suitably chosen combinations of design parameter settings or design points that must be located within the feasible design region, i.e., the part of the design parameter space that satisfies all bounds on the design parameters defined in step 1. The problem of choosing the design points is called Design of Experiments (DOE) [49]. Classical DOE mainly focuses on physical experimentation in which experiments are subject to noise as opposed to computer experiments in which the same calculation will always give the same results. Therefore, classical DOE schemes have a number of drawbacks when used for computer experimentation. In computer experimentation, a DOE should be:

- Space-filling, i.e. the minimal distance between any two design points should be a maximum. Compared to classical DOE, this means that design points will also be located in the interior of the feasible design space;

- Non-collapsing, i.e. when all design points are projected on to one (any) (design parameter) dimension, no two design point projections should be equal;

- Able to deal with non-box and integrality constraints: this means that the whole design matrix does not necessarily have to be filled with data;
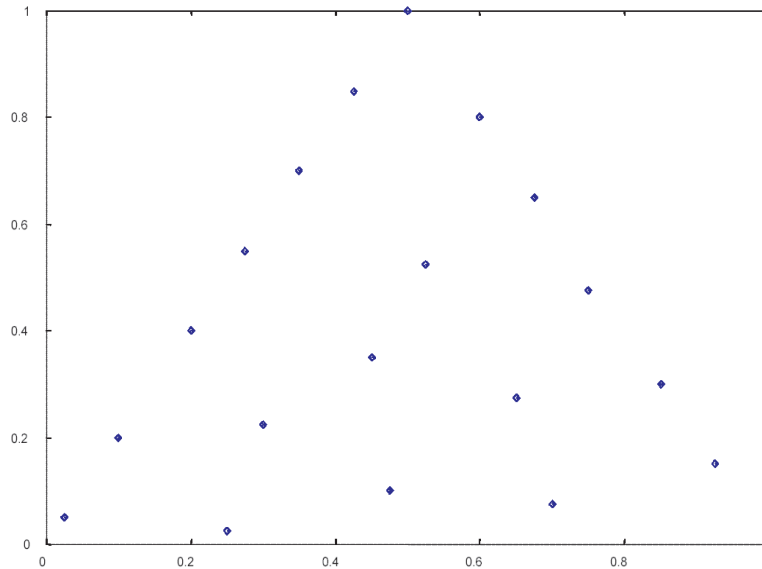
Figure 5.6: Computer generated space-filling LHD

- Expandable, i.e. it should be possible to add design points that comply with above mentioned criteria.

The approach used in 'Compact' satisfies all of the these criteria. It searches for the best space-filling simulation scheme within the class of so-called Latin Hypercube Designs (LHD) using a simulated annealing algorithm (Aarts and Korst [50]). Figure 5.6 gives an example of a constrained 2D simulation scheme generated by 'Compact'. (See Den Hertog and Stehouwer [48] for a more elaborate discussion on the 'Compact' LHD module). In the case described in section 3, a scheme was constructed consisting of 120 design points. Since simulation of one design point takes approximately 24 hours, all design points were simulated using distributed computing (taking a total calculation time of 3000 hours). See appendix B for details on the distributed computing technique used .

5.4.5 'Compact' modelling

The third step in the 'Compact' methodology consists of fitting a 'Compact' model for every response parameter in terms of the design parameters. The models are based on the simulation output generated after step 2. Other frequently used terms for 'Compact' models include; 'approximating model', 'Response Surface Model (RSM)' and 'meta-model'. For the purpose of predicting the results of a computer model, second order polynomial models, Kriging models (Sacks et. al. [51]) and Neural Networks [46] are frequently used. The 'Compact' approach supports both

polynomial models (using a step-wise term selection technique) and Kriging models. The first type is preferred, as Kriging models are more time-consuming to fit and harder to validate. Kriging may be necessary though, when the physics becomes so non-linear that a polynomial model of moderate degree cannot fit the data. Validation of the model is of course of great importance. There are several statistics that can be used for this purpose. Amongst these are e.g. RMSE, cross-validation RMSE and the error on an independent test set. For more information on model validation, see [52]. When a model is not accurate enough, two options exist. First, the design space can be decreased and a better model can be sought for this new region. This may imply that new simulations are needed in the new design space. Second, design points can be added to the original design space, simulated, and fitted to a new model. Eventually, this procedure will lead to an accurate 'Compact' model. In the case described in section 3, five 'Compact' models were fitted. As an example, the validation results based on step-wise second order polynomial models are presented in Table 5.3.

Table 5.3: Relative importance of the first 10 coefficients in the polynomial 'Compact' model for the radius after metal forming and waiting. These data are constructed using the intervals of the parameters from Table 5.1 (high-low) in combination with a second order normalized model, including the possible interactions.

Coefficient	Influence
$Mat.thickness * Friction$	0.043
$Friction$	0.031
$Ini.flowstress$	0.030
$Mat.thickness * Mat.thickness$	0.018
$Time2 \rightarrow 3 * Time2 \rightarrow 3$	0.016
$Mat.thickness * Ini.flowstress$	0.016
$Ini.temperature * Depthstep2$	0.015
$Depthstep1 * Depthstep1$	0.014
$Depthstep3$	0.013

5.4.6   Analysis

Steps 1 to 3 result in a 'Compact' model for each of the response parameters. In step 4, these models are exploited by four types of analysis:

- Prediction: since the 'Compact' models can be evaluated very quickly compared to a simulation run, prediction using a 'Compact' model is much more attractive. What-if scenario analysis can be performed by just changing a design parameter and evaluating 'Compact' models;

- Optimization: since prediction can be performed so quickly, traditional optimization techniques that usually require many function evaluations become

feasible. In step 1, the feasibility of the designs is defined and the preferability of the given design above another is determined using an objective function. These definitions can be exploited and the globally optimum design can be found using global Mixed Integer Non-Linear Programming (MINLP) techniques;

- Robust design: In step 1 it is determined which design parameters are controllable in reality and which are not. By defining a random distribution for each of the non-controllable design parameters, a Monte Carlo analysis is performed and the robustness of a design is evaluated;

- Sensitivity analysis: Usually, more than one conflicting objective exists. Using 'Compact' models and optimization techniques, it is easy to create a curve indicating all Pareto optimum designs.

In this case the robust design module was used to evaluate the spread of product characteristics in relation to the effect of the spread on the design parameters:

- Influence on the product accuracy of two types of hardening (strain-induced and stress-assisted);

- The influence of metal forming parameters on the form accuracy and the hardness.

Case 1: Hardening and accuracy

There are two possibilities to harden a product made from Sandvik Nanoflex™:

- Using the strain-induced transformation;

- Using the stress-assisted transformation.

It is interesting to compare the two. Hence, different Monte Carlo calculations were carried out to study the hardness after ageing and the accuracy of the example product.

The results of three Monte Carlo simulations are shown in the following figures:

- Figures 5.7-a and 5.7-b give the results directly after stamping;

- Figures 5.7-c and 5.7-d give the results after stamping and waiting for 10800 sec. It is assumed that after this time the stress-assisted transformation has stopped as the positive residual stress vanishes, because of the dilation strain. The results are very similar to that after stamping but there are some small dimensional changes;

- Figures 5.7-e and 5.7-f give the results after stamping, waiting, re-austenising and isothermal hardening. The graphs show that using this method the hardness increases, but the accuracy of the radius decreases. This is related to the dilation strain, and transformation plasticity.
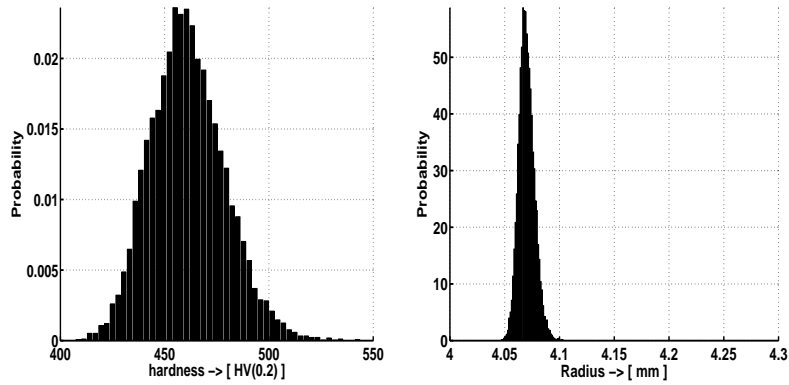
(a) The hardness distribution after stamping.

(b) The radius distribution after stamping.
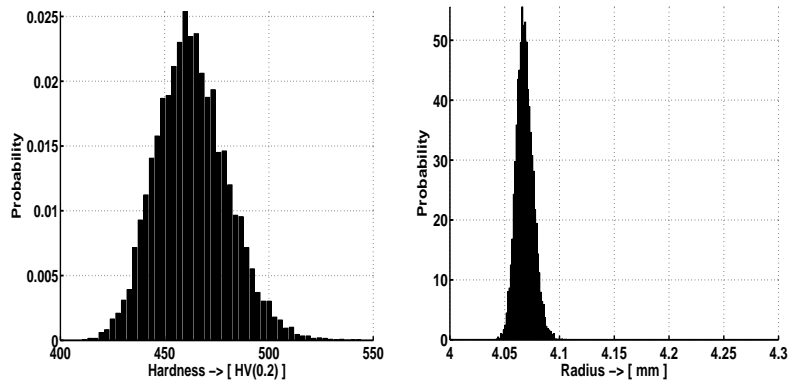
(c) The hardness distribution after stamping and waiting for 3 hours stamping.

(d) The radius distribution after stamping and waiting for 3 hours stamping.
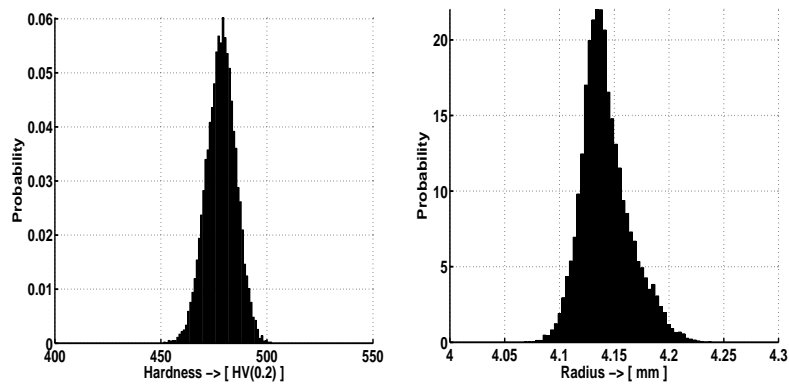
(e) The hardness distribution after stamping, waiting and re-hardening.

(f) The radius distribution after stamping, waiting and re-hardening.

Figure 5.7: Results of the Monte Carlo analysis on the accuracy and hardness (Hv0.2) of the final product.
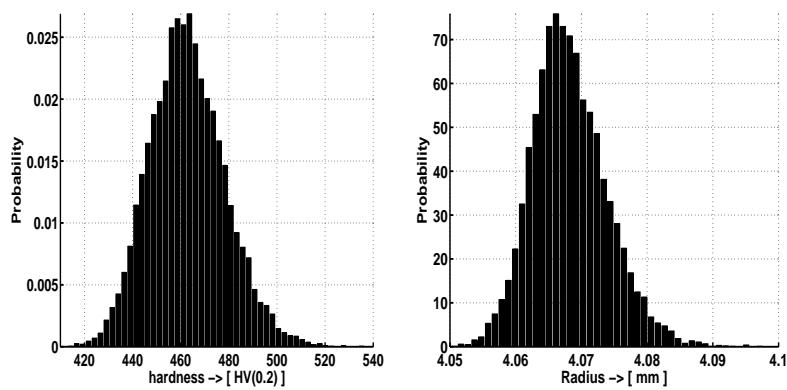
Case 2: The influence of metal forming parameters on the form accuracy and the hardness

A second Monte Carlo analysis was carried out on the product. The results for the hardness and the radius are shown in Figures 5.8-a and Figure 5.8-b. It can be seen that the expected hardness was 462.7 Hv with a standard deviation of 15.6 Hv. The radius was 4.068 mm with a standard deviation of 5.7 μm. The goal of the research was to investigate the influence of waiting time on the form accuracy and the hardness. Hence a Monte Carlo analysis is carried out with the nominal values from table 2, only the waiting times were varried. Note that the interactions between waiting times and other variations are excluded this way. The results are shown in Figures 5.8-c and 5.8-d. From these results can be concluded that the waiting times between the different steps do have an influence but are not the main factor for the accuracy of the product.

Table 5.4: Influence on the radius and hardness of different parameters by a Monte Carlo analysis. *: Material means thickness, flow stress and M_d temperature.

Variation on	Radius expected [mm]	Radius variation [mm]	Hardness expected [Hv0.2]	Hardness variation [Hv0.2]
All	4.0682	0.0057	462.7	14.86
Material*	4.0665	0.0045	465.6	14.86
Ram depth	4.0668	0.0013	465.3	0.99
Friction	4.0664	0.0024	465.4	3.32
Temperature	4.0664	0.0003	465.3	0.69
Waiting time	4.0677	0.0018	461.9	2.69

To determine where the spread in accuracy comes from, the same were carried out for the other parameters from table 5.4. The ram depths were all varied in one Monte Carlo analysis because the ram depths depend on the accuracy of the tools. The material parameters (material thickness, chemical composition and initial flow stress) were varied together because this is the input of the material in the process. Also the temperature and the friction were varied. The results can be seen in Table 5.4. From this table can be seen that variation in the material has the main influence on the deviation of the radius and the hardness.

(a) Spread of the hardness of the products.

(b) Spread of the radius of the products.
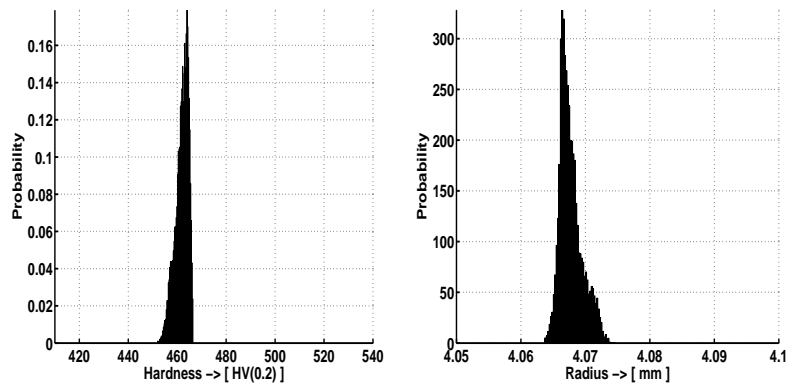
(c) Spread of the hardness due to waiting time.

(d) Spread of the radius due to waiting time.

Figure 5.8: Results of Monte Carlo analysis on the influence of metal forming parameters.

Chapter 6

Conclusions

6.1   Conclusions

6.1.1   Chapter 2:

- Sandvik Nanoflex™is a stainless steel belonging to the category of metastable austenites, i.e. strain-induced martensite transformation occurs during plastic deformation.

- Depending on the austenitising conditions, Sandvik Nanoflex™is so unstable that spontaneous stress-assisted transformation takes place. In stable conditions, this transformation only occurs as a result of positive hydrostatic residual stresses.

- The two types of transformation as well as a combination of these types can be measured with inductive sensors. It is necessary, however, to pay special attention to the calibration of these sensors.

- A macroscopic model provided which meets these requirements, which are necessary for full product simulations:

  - it is relatively simple and fast, compared to micro-mechanical models;

  - it is able to describe stress-assisted transformation and strain-induced transformation properly;

  - it is able to describe the hardening that takes place during plastic deformation and transformation accurately;

  - it covers the entire window regarding stress, temperature and deformation that is required for simulation of metal forming processes.

6.1.2   Chapter 3:

- The lookup/neural network implementation yielded a robust solver. The drawback of this approach is that it complicates implementation. The advantage is that the approach has a clear structure, which makes it easier to implement other material models;

- The model describes the transformation, including dilation strain and transformation plasticity, in a sufficiently accurate way, i.e. model and reality match, for 2 D situations;

- As regards to the stress-assisted transformation, the discrepancy between the model and reality falls short of the expectations. This is caused by the fact that the model is axi-symmetric, whereas measurements have shown that the transformation is three-dimensional, including direction-dependent strains.

6.1.3 Chapter 4:

- The measuring method described in this chapter may be a useful tool to check the results of simulations against reality;

- On top of that, this method also allows simulation of only a part or just one step of a multi-stage metal forming process, which may save a lot of time, depending on the number of steps in the process that need to be simulated.

6.1.4 Chapter 5:

- The DACE approach in combination with a robust solver is a powerful tool in optimising processes.

- This method can be very useful to determine the tolerances for parameters in the production process.

- about the forming process of the sample product:

  - The most accurate product is realized by using only the strain-induced hardening and ageing process;

  - The greatest hardness is realized by re-austenizing and isothermal hardening and ageing process;

  - The waiting times between two steps influence the shape accuracy and the hardness of the product due to stress-assisted transformation. Furthermore the strain-induced transformation in the next forming stage occurs at a different temperature. This combined influence is even larger than the influence of variation in the depth of the rams. The largest influence for this product lies in variation of the material parameters.

Chapter 7

Recommendations

- Although the model produces good results, it would be useful to gain more insight into the effects of temperature and stress state on the transformation behaviour. Micromechanical models may have added value in this respect;

- The measurements presented were all performed on ingot-cast material, whereas Sandvik Nanoflex™is currently produced by means of continuous casting. It therefore would be advisable to repeat the measurements on continuously cast material and to adjust the model on the basis of these results;

- The model used for transformation plasticity results in too much strain during strain-induced transformation. More research on this subject therefore seems useful;

- Directional dependence, i.e. anisotropy and texture, greatly influences stress-assisted transformation. Hence the simulation should be made three-dimensional to incorporate these 3D effects;

- It also would be useful to implement Estrin's original model with two dislocation quantities, including the inheritance of dislocations. This does require a solution of the stability of the coupled differential equations;

- By applying Estrin's work in more detail, the consequence of texture evolution and anisotropy can also be implemented.

Appendix A

Introduction to Neural Networks

A.1   Introduction

The field of neural networks covers a broad area: it is not possible to describe all types of neural networks in this paper. Hence the main focus of this paper is on the theory of multi-layered back propagation feed forward (MLBFF) neural networks and their application in the CRYSTAL solver.

Neural networks are inspired from biology. It is generally understood that all biological neural functions, including memory, are stored in the neurons and the connections between them. Learning is viewed as the establishment of new connections between neurons and of the modification of existing connections. It is possible to create a simple artificial abstracts these very complex biological systems. These simple abstracts are the neural networks that we use in our applications in various industries.

The MLBFF neural networks are used as function approximators. They are able to learn relationships between any different sets of data without knowing the mathematical relationships between these data sets. This makes these networks very flexible in their use. The learning is done through back propagation algorithms such as the Levenberg-Marquardt algorithm. These algorithms adapt the connections between the neurons in order to approximate the relation between the data sets. It is this universal function approximation behaviour that makes MLBFF neural networks very suitable for use within the CRYSTAL solver. During the development of the CRYSTAL solver we made use of the so-called lookup tables in order to store the relationship between different variables. The drawback of using this method is the amount of data used to store the relationships, which expands exponentially with the number of variables used. Therefore, an alternative method was required for storing multi-dimensional relationships. The solution was found in using MLBFF neural networks.

A.1.1   Multi-layer back propagation feedforward networks

Introduction

The multi-layer neural network is built up from simple components called neurons. The simplest neural network is a single-input neuron, which is extended to multiple inputs. These neurons are stacked together to produce a layer. Finally, we cascade these layers together to form a multi-layered network.

A.1.2   Single input neuron

The single scalar input p is multiplied by the scalar weight w to form wp, one of the terms that is sent to the summer. The other input, 1, is multiplied by a bias b, and then passed to the summer. The summer output, often referred as net input n, goes into the transfer function f, which produces the scalar output a.

The neuron output is calculated as:

$$a = f(\underbrace{wp + b}_{n}) \tag{A.1}$$

Note that w and b are adjustable parameters of the neuron. These parameters are adjusted from a given starting value using a training rule so that the input/output relationships meet some specific goal.

Transfer functions

Transfer functions can be represented by any linear or non linear function.

Note that in multi-layered networks the transfer must be differentiable in order to be used by a back propagation algorithm.

Multi-input neuron

Typically, a neuron has more than one input. The individual inputs $\mathbf{p}$ $p_1 \ldots p_r$ are weighted by corresponding elements $w_1 \ldots w_r$ of the weight vector $\mathbf{W}$. The bias is summed with the weighted inputs to form the net input n. This is then passed to the transfer function resulting in output a:

$$a = f(\mathbf{W}\mathbf{p} + b) \tag{A.2}$$

A.1.3   Network architectures

A one neural model even with multiple inputs is commonly not sufficient. The solution to this is to use multiple neurons operating in parallel, in what is called a layer. An architecture composed from one layer is called a single-layer network and an architecture composed from multiple layers is called a multi-layer network.

One-layer architecture

A single layer network of S neurons is connected to R inputs. Each of these inputs is connected to each of the neurons resulting in a weight matrix $\mathbf{W}$ of S rows and R columns. This is added by the bias vector $\mathbf{b}$ to form the net input vector $\mathbf{n}$, which is then passed to the transfer functions, see Figure A.1 for some example transfer functions, resulting in the output vector $\mathbf{a}$:

$$\mathbf{a} = f(\mathbf{W}\mathbf{p} + \mathbf{b}) \tag{A.3}$$

Note that generally the number of layers differs from the number of neurons (i.e., $R \neq S$).
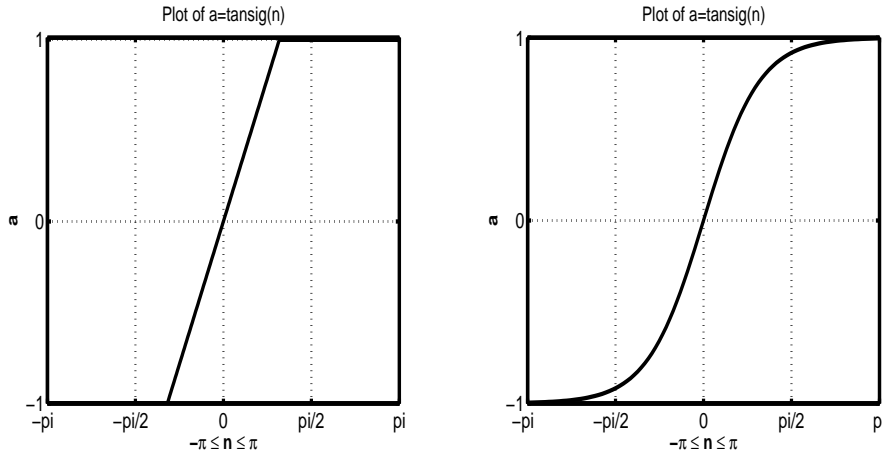
Figure A.1: Two example transfer function.

Multi-layer architecture

Consider a network with several layers. Each layer has its own weight matrix $\mathbf{W}$, its own bias vector $\mathbf{b}$, a net input vector. We will use a superscript to identify the layers. Thus, the weight matrix for the first layer is written as $\mathbf{W}^1$ and the weight matrix for the second layer is written as $\mathbf{W}^2$. To illustrate a multi-layer network we will use an example. Suppose we have R inputs and a network consisting of 2 layers with S^1 neurons in the first layer and S^2 neurons in the second layer. Then the weight matrix $\mathbf{W}^1$ of the first layer would have S^1 rows and R columns and the weight matrix of the second layer would consist of S^2 rows and S^1 columns. Hence, the net input vector $\mathbf{n}$ for the first layer is calculated using the following form: $\mathbf{n} = \mathbf{Wp} + \mathbf{b}$. This is then passed to the transfer functions resulting in the output vector $\mathbf{a}$. The output of the first layer is passed to the second layer as input and calculated accordingly. This results in the following form:

$$\mathbf{a}^2 = \mathbf{f}^2(\mathbf{W}^2\mathbf{f}^1(\mathbf{W}^1\mathbf{p} + \mathbf{b}^1) + \mathbf{b}^2) \tag{A.4}$$

This procedure can be expanded for networks with more than 2 layers by just continuing the procedure described.

Note that the layer whose output is the network output is called the output layer. The other layers are called hidden layers.

A.1.4   Training multi-layer networks

We know that multi-layer networks are universal approximators. However in order to use these networks we must first determine a procedure for adapting the network parameters ($\mathbf{W}$ and $\mathbf{b}$) to the best approximate given functions or relations between different data sets. The procedure for adapting the network parameters is called
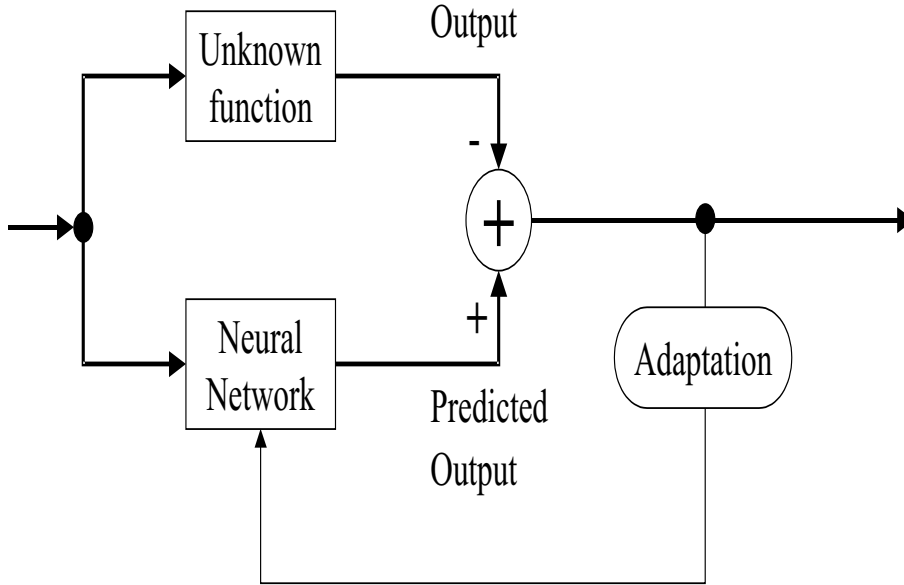
Figure A.2: Two-layer network

training the neural network. Specifically, the different procedures for training multi-layer networks are called back propagation algorithms.

For multi-layer networks the output of one layer is the input to the following layer. The equation that describes this operation is:

$$\mathbf{a}^{m+1} = \mathbf{f}^{m+1}(\mathbf{W}^{m+1}\mathbf{a}^m + \mathbf{b}^{m+1}) \tag{A.5}$$

for $m = 0, 1..., M - 1$ where M is the number of layers of the network. The neurons of the first layers receive external inputs : $\mathbf{a}^0 = \mathbf{p}$ and provide the starting point for the equation above. The outputs of the neurons in the layer are considered the network outputs: $\mathbf{a} = \mathbf{a}^M$.

Performance index

The back propagation algorithms are based on supervised learning. This means that the learning algorithm is provided with data sets of proper network behaviour:

$$\{\mathbf{p}_1, \mathbf{t}_1\}, \{\mathbf{p}_2, \mathbf{t}_2\}, \dots, \{\mathbf{p}_q, \mathbf{t}_q\} \tag{A.6}$$

where $\mathbf{p}_q$ is an input to the network, and $\mathbf{t}_q$ is the corresponding target output. As each input is applied to the network, the network output is compared to the target. The sum squared error is used as a performance indicator, which must be minimized in order to optimize the network performance. The generalized mean square error is given by the following equation:
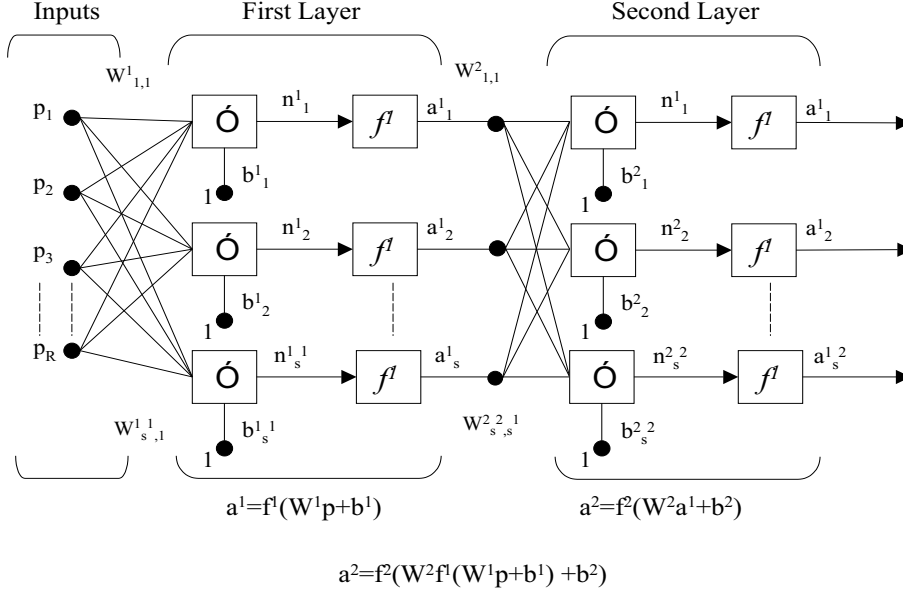
Figure A.3: Neural network as universal function approximator.

$$F(\mathbf{x}) = \sum_{1}^{q} \mathbf{e}_q^T \mathbf{e}_q = \sum_{1}^{q} (\mathbf{t}_q - \mathbf{a}_q)^T (\mathbf{t}_q - \mathbf{a}_q) \qquad (A.7)$$

Back propagation

In multi-layer networks the error is not an explicit function of the weight as is the case in single layer networks, but an indirect function of the weights of the hidden layers. Hence, the learning algorithms for multi-layer networks make use of a technique called back propagation. This technique derives its name from that its sensitivities **s** are back propagated from the output layer to the first layer.

$$s^M \rightarrow s^{M-1} \rightarrow \ldots \rightarrow s^2 \rightarrow s^1 \qquad (A.8)$$

The sensitivity at the output layer is calculated using the performance index:

$$\mathbf{s}^M = -2F'(\mathbf{n}^M)(\mathbf{t} - \mathbf{a}) \qquad (A.9)$$

This result is then used to calculate the sensitivities at the hidden layers using:

$$\mathbf{s}^m = \mathbf{F}'^m(\mathbf{n}^m)(\mathbf{W}^{m+1})^T \mathbf{s}^{m+1} \qquad (A.10)$$

where $\mathbf{F}'^m(\mathbf{n}^m)$ is a matrix in which the differentiates $f'^m(n_{S^m}^m)$ of the layer are on the diagonal.

Generalization

The multi-layer neural networks are universal approximators. The number of neurons, the number of layers and the data selected determine the accuracy of the approximation: the data must adequately represent the underlying functions and the number of neurons and layers must be able to capture the complexity without over-fitting the training data. There exist methods to improve networks interpolating capabilities thus avoiding over-fitting. such as early stopping. This method based on monitoring the performance during training. Another method is called regularization: here the performance index is modified by including a network complexity penalizing term. Neural networks cannot be expected to extrapolate. When a network receives input outside the network training data, the network output becomes unreliable.

Strategies

One can imagine that the performance index resembles a surface Ω in an n-dimensional space. The result of any training of a neural network ends with the mean square error stuck in a local minimum. Different strategies have been developed to deal with this problem which is inherent to multi-layer neural networks. These strategies can be divided into two groups: quantitative and qualitative. A quantitative approach to optimize the learning is to train multiple neural networks. Thus by training multiple networks each initiated with different weight and bias values. It is possible to determine the credibility of the network after training. A qualitative approach to optimize the learning process is to scale the data set to a more convenient domain and use this new data set to train the neural network. Obviously, the results of neural networks trained in this manner must be scaled back to the original domain.

Normally when using neural networks in an application a combination of both quantitative and qualitative strategies are used.

A.1.5   FEM implementation

Introduction

The CRYSTAL solver was developed in such a way that the materials scientist could instantly change the constitutive models, without the need of reprogramming the source of the solver. This was first obtained by using a flexible material formulation and with the use of the lookup tables principle. The drawback of this method is the amount of data used to store these lookup tables. Because the models used in CRYSTAL became more and more complex, with constitutive relations exceeding three dimensions. The need for an alternative method of storing the relations was desired. The multi-layer neural networks were chosen as a solution for storing higher dimensional relationships.

A.1.6   Neural network for FEM

Architecture

The constitutive relations used in the material models for CRYSTAL have the follo-wing functional prototype $f : \mathbb{R}^n \to \mathbb{R}$. Therefore the networks used for CRYSTAL must have one neuron with a purelin transfer ($a = n$) function in the output layer. In the hidden layers, neurons with tansig transfer functions ($a = \frac{e^n - e^{-n}}{e^n + e^{-n}}$) were used.

Scaling

The data used to train the neural networks is normalized in a [-1,1] domain, using the parameters T_{min} and T_{max}. An input was scaled using the following function:

$$I_{scaled} = 2 \frac{I_{unscaled} - T_{min}^i}{T_{max}^i - T_{min}^i} - 1 \tag{A.11}$$

The output was scaled back to its original domain using:

$$R_{afterscaling} = \frac{(R_{beforescaling} + 1)(T_{max}^0 - T_{min}^0)}{2} + T_{min}^0 \tag{A.12}$$

Training

Besides the qualitative approach of scaling the data we also used a quantitative approach. A number of k networks Net were varied with respect to: number of neurons, values of weight matrix, values of bias vectors and data used to train the networks. The actual training was done with the Levenberg-Marquardt back propagation algorithm using regularization to avoid over-fitting. These networks were then processed using the following form:

$$\bar{a} = \frac{1}{k} \Sigma_{i=1}^k Net_i(\mathbf{p}) \tag{A.13}$$

The aim of this exercise was to create a stable behaviour of the networks in order to be able to automate the training process by using a mean output value instead. The objective for the individual networks was to train the networks with a minimum number of layers and neurons and an optimum performance. The trained networks were then implemented in CRYSTAL using the flexible material formulation.

Implementation

The flexible material formulation in CRYSTAL was extended with the formulation of an extra 'nur' file. This 'nur' file replaces the 'lup' file for lookup tables and contained all the information that CRYSTAL needed to use neural networks such as: number of networks, scaling parameters, weight matrices, bias vectors, network architectures and so on.

A.1.7 Results

The implementation of neural networks in CRYSTAL was successful. The multi-layer neural networks were able to simulate the higher dimensional constitutive relationships with adequate accuracy. The quantitative and qualitative methods used guaranteed a stable behaviour and automated training was implemented. The simulation time of these neural networks when compared to the lookup tables increased dramatically resulting in increased computing time for calculations done with CRYSTAL. Nevertheless, multi-layer neural networks are a suitable alternative for lookup tables in higher dimensional relationships, and improved training strategies could increase computing efficiency.

Appendix B

Distributed computing

B.1   Introduction

Distributed computing is based on using the idle time within computer networks, by doing defined tasks within this time period. The design choices that were made concerning the structure and the protocols to build the distributed system are based on the scalability, robustness and controllability of the system.

B.1.1   Structure

The distributed computing structure can be divided into three sections:

- CRYSTAL users (CrystalUser), these are the users of the CRYSTAL solver organized on a LAN;

- the server (CrystalNet), the server that is connected to the same LAN;

- CRYSTAL clients (CrystalClient), these are the computers on the LAN that are used for the calcalations.

In general the (CrystalUser) is a subset of the (CrystalClient).

The user and the server sections can be grouped to form the input-output functionality. The server and the client section form the distributing functionality. The input-output functionality is to upload FEM-calculations to the server and to download the results of the FEM-calculations from the server.

The distributing functionality allows the distribution of the various calculations from the server to the clients, the computation of these calculations and returning these calculations back to the server.

The entire process is monitored and controlled through the use of three databases on the server section: the user, the calculation and the client database. The user database is coupled to the calculation database and contains information about the users for example the: number of calculations uploaded and downloaded. The client database contains information about the clients such as: number of calculations done, computer architecture and calculations being computed. The client database is also coupled to the calculation database. The calculation database contains the information about the calculation such as: calculation-id, status, calculation type, calculation size and owner.

B.1.2   Protocol

The relatively small scale, less then thousand clients, and the reliability of the network on which this distributed computing system is to function, allows us to implement an extensive protocol to maximize the controllability and robustness of the system.

The most basic protocol for the distribution function to work is to allow two requests to the server. The first request is a calculation to be executed and the second request is to return the executed calculation. We have chosen to extend this basic protocol with a few announcements and requests such as: an announcement
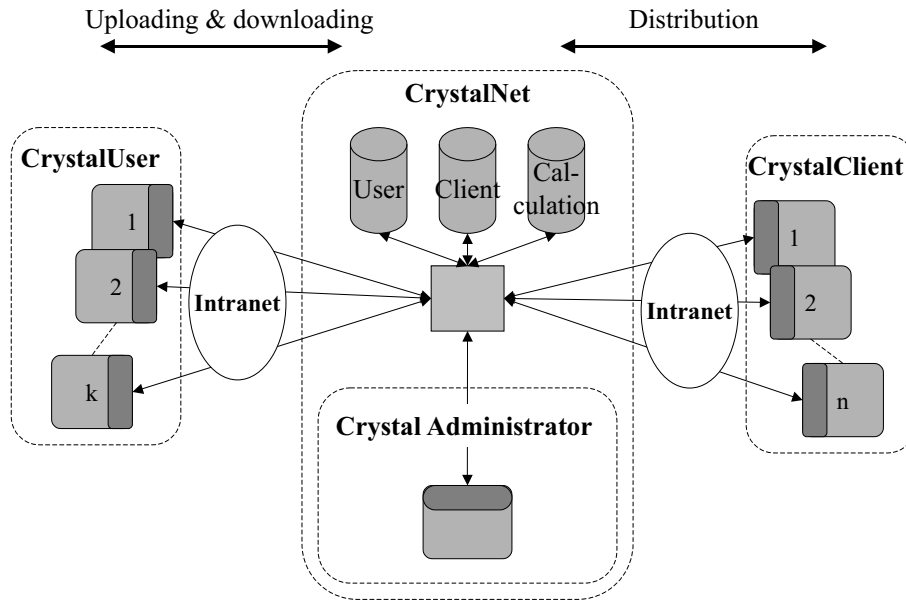
Figure B.1: The structure of the CRYSTAL distributive computing system. Showed are the three main components: CrystalUser, CrystalNet and CrystalClient.

that the computation has been interrupted and a request to cancel the current tasks. These extensions allow the server to anticipate on events that occur on the clients. For example in the case of the announcement that the computation is interrupted, the server could react by restarting this interrupted calculation on a different client. Hence, this leads to more control over the process, an increased robustness because long calculation interruption could be averted and better process monitoring.

The protocol for the input-output functionality consists of two basic request is the first request to upload a calculation to the server and the second request is to download results from the server. Furthermore the protocol consists of monitoring requests to determine the status of the distributed calculation.

Appendix C

Published articles relating to Sandvik Nanoflex™

1. Verification tool for 2D multi-stage metal forming processes involving small parts made of stainless steel

   J. Post, C. de Vries, J. Beyer, H.J.M. Geijselaers

   Shemet 2001, page 475-484

2. Inductive measurements of the stress-assisted and strain induced martensite transformations of Sandvik steel 1RK91 before, during and after metal forming.

   H. Nolles, J. Post, J. Beyer

   ICOMAT 2002, page 425-428

3. FEM simulations of a multi-stage forming process on Sandvik steel 1RK91 describing the stress-assisted and the strain induced martensite transformation.

   J. Post, J. Huétink, H. J. M. Geijselaers, R.M.J. Voncken

   ICOMAT 2002, page 417-420

4. A physically based model for the isothermal martensitic transformation in Sandvik steel 1RK91.

   S.O.Kruijver, H.S.Blaauw, J.Beyer, J.Post

   ICOMAT 2002, page 437-440

5. Constitutive behaviour of the metastable stainless steel: Sandvik Nanoflex™.

   J. Post, K. Datta, J. Huétink

   NUMIFORM 2004, page 1670-1676

6. FE calculations on a three stage metal forming process of Sandvik Nanoflex™.

   R.M.J.Voncken, O. van der Sluis, J. Post, J. Huétink

   NUMIFORM 2004, page 469-474

7. A DACE study on a three stage metal forming process made of Sandvik Nanoflex™.

   J. Post, G. Klaseboer, E. Stinstra, J. Huétink.

   NUMIFORM 2004, page 475-480

8. The constitutive behaviour of Sandvik steel Nanoflex™, part1: physical based model

   J. Post, K. Datta, H. Nolles, J.Beyer, H.R. Jousma

   Materials Science & Engineering A, Elsevier, submitted

9. The constitutive behaviour of Sandvik steel Nanoflex™, part2: FE Implementation and validation

   J. Post, R.M.J.Voncken, H.J.M. Geijselaers, O. van der Sluis, M. Hommes

   Materials Science & Engineering A, Elsevier, submitted

10. Validation tool for 2D multi-stage metal-forming processes.

    J. Post, C. de Vries, J.Huétink

    Materials Science & Engineering A, Elsevier, submitted

11. A process window study, using DACE, on a three stage metal forming process, including martensite transformation.

    J. Post, G. Klaseboer, E. Stinstra, T. van Amstel, J.Huétink

    Materials Science & Engineering A, Elsevier, submitted

12. Constitutive modelling of Sandvik 1rk91

    K. Datta, J. Post, J.Huétink,

    COMPLAS 2003, Barcelona, ISBN 84-95999-22-6, 2003

13. Finite Element Calculation of Local Variations in the Driving Force for Austenite to Martensite Transformations

    K. Datta, J. Post, A. Dinsdale, S. van der Zwaag,

    Acta Materialia, Elsevier, submitted

14. A study on the influence of waiting time between forming steps on the form accuracy of a three stage formed deep drawn product made of Sandvik Nanoflex™

    Gerrit Klaseboer, Jan Post, Erwin Stinstra and Han Huétink

    METAL FORMING 2004, to be published

15. A Method to Generate Constitutive Equations for Metastable Austenitic steels

    K. Datta, J. Post, H.J.M. Geijselaers, J.Huétink,

    Acta Materialia, Elsevier, submitted

16. Constitutive Modelling of Metastable Steels

K. Datta, M. Hommes, J. Post, H.J.M. Geijselaers, J.Huétink, J. Beyer,

ESAFORM 2004, page 147 - 150, ISBN 82-92499-02-04

Bibliography

[1] A.H. Maslow. *Psychologie van de wetenschap*. Lemniscaat ISBN 9060691881, Rotterdam, 1966.

[2] Questek Innovations LLC. www.questek.com.

[3] M. Holmquist, J.-O. Nilsson, and A. Hultin Stigenberg. Isothermal formation of martensite in a 12Cr-9Ni-4Mo maraging stainless steel. *Scripta Metallurgica et Materialia*, pages 1367–1373, January 1995.

[4] T. Narutani, G.B. Olson, and M. Cohen. Constitutive flow relations during strain-induced martensitic transformation of austenitic steels. *journal de physique*, december 1982.

[5] G.B. Olson and M. Cohen. A mechanism for the strain-induced nucleation of martensitic transformations. *Journal of the Less-Common Metals*, 28:107–118, January 1972.

[6] G.B. Olson and M. Cohen. Kinetics of strain-induced martensic nucleation. *Metallurgical Transactions A*, 6A:791–795, April 1975.

[7] S.R. Pati and M. Cohen. Nucleations of the isothermal martensic transformation. *Acta Metallurgica*, 13:189–199, March 1969.

[8] F.D. Fischer, G. Reisner, E. Werner, K. Tanaka, G. Cailletaud, and T. Antretter. A new view on transformation induced plasticity (TRIP). *International Journal of Plasticity*, 16:723–748, 2000.

[9] M. Cherkaoui, M. Berveiller, and X. Lemoine. Coupling between plasticity and martensitic phase transformation;: overall behavior of polycrystalline trip steels. *International Journal of Plasticity*, 16:1215–1241, 2000.

[10] I. Tamura. Martensitic transformations and mechanical effects in the book

martensite: A tribute to Morris Cohen, edited by G.B. Olson and W.S. Owen. *book*, 1992.

[11] J.-O. Nilsson, A.H. Stigenberg, and P. Liu. Isothermal formation of quasicrystalline precipitates and their effect on strength in a 12Cr-9Ni-4Mo maraging stainless steel. *Metallurgical Transactions A*, 25A:2225–2233, October 1994.

[12] G.B. Olson and M. Cohen. A general mechanism of martensitic nucleation: Part iii. kinetics of martensitic nucleation. *Metallurgical Transactions A*, 7A:1915–1923, December 1976.

[13] V. Raghavan. Martensite: A tribute to morris cohen. *ASM*, pages 197–226, 1992.

[14] R.G. Stringfellow, D.M. Parks, and G.B. Olson. A constitutive model for transformation plasticity accompanying srain induced martensitic transformations in metastable austenitic steels. *Acta Metall*, vol 40(7):1703–1716, 1992.

[15] S. Socrate. Mechanics of microvoid nucleation and growth in high strength metastable austenitic steels. *PhD thesis MIT USA*, 1995.

[16] Y. Estrin, H. Braasch, and Y. Brechet. A dislocation density based constitutive model for cyclic deformation. *Journal of Engeneering Materials and Technology*, 118:441–447, October 1996.

[17] Y. Estrin. *Unified Constitutive Laws of Plastic Deformation*. Academic Press, editor A.S. Krausz and K. Krausz, 1996.

[18] S.S. Hecker, M.G. Stout, K.P. Staudhammer, and J.L. Smith. Effects of strain state and strain rate on deformation-induced transformation in 304 stainless steel: Part i. magnetic measurements and mechanical behavior. *Metallurgical Transactions A*, 13A:619–626, April 1982.

[19] J.A.C. Cortés, T. Tsuta, Y. Mitani, and K. Osakada. Flow stress and phase transformation analyses in the austenitic stainless steel under cold working.(part 1, phase transformation characteristics and constitutive formulation by engineering criterion). *JSME International Journal*, 35(2):201–209, June 1992.

[20] V. Seetharaman and R. Krishnan. Influence of the martensitic transformation on the deformation behaviour of an aisi 316 stainless steel at low temperatures. *Journal of materials science*, 16:523–530, 1981.

[21] R.B. Goldfarb, R.P. Reed, J.W. Ekin, and J.M. Arvidson. Magnetic suscep-
tibility and strain-induced martensite formation at 4K in type 304 stainless
steel. *Advances in Cryogenic Engineering*, 30, 1984.

[22] F.D. Fischer, Q.-P. Sun, and K. Tanaka. Transformation-induced plasticity.
Applied Mechanics ReviewsF, 49:317–364, June 1996.

[23] V. Raghavan. Kinetics of martensite transformtions in the book martensite: A
tribute to Morris Cohen, edited by G.B. Olson and W.S. Owen. *book*, (ISBN
0-87170-434-X):197–225, 1992.

[24] J.C. Fischer. Application of nucleation theory to isothermal martensite. *Acta
Metallurgica*, 1:32–35, 1953.

[25] S.R. Patel and M. Cohen. Kinetics of isothermal transformationsin an iron-
nickel-mangenese alloy. *Acta Metallurgica*, 19:1327–1332, 1971.

[26] I.J. Garshelis, W.S. Fiegel, and S. Wade. Magnetic observations of austenite-
martensite transformations induced by torsional strain. *Journal of Applied
Physics*, 53(3):2407–2409, March 1982.

[27] L. Callegaro, E. Puppin, and A. Vannucchi. Magneto-optical measurements
on mechanically stressed thin ferromagnetic films. *Review of Scientific Instru-
ments*, 67(2):1065–1067, October 1995.

[28] Y. Estrin, A. Molinari, and L.S. Toth. Strain hardening at large strains as
predicted by dislocation based polycrystal plasticity model. *Journal of Engi-
neering Materials and Technology*, 124, January 2002.

[29] Y. Estrin, L.S. Toth, A. Molinari, and Y. Brechet. A dislocation-based model
for all hardening stages in large strain deformation. *Acta mater*, 46(15):5509–
5522, 1998.

[30] V. Raghavan and A.R. Entwisle. The physical properties of martensite and
bainite. *Special report Iron and steel institute*, vol 93:30, 1965.

[31] C.L. Magee. The nucleation of martensite. *Phase transformations, ASM*, page
115, 1970.

[32] J. Sestak and G. Berggen. Study of the kinetics of the mechanism of soli-state
reactions at increasing temperatures. *Thermochimica, Acta*, 3:1–12, 1971.

[33] Y. Estrin, L.S. Toth, Y. Bréchet, and A. Molinari. A dislocation based model

for all hardening stages at large strain deformation. *Acta Metallurgica*, 46:5509–5522, May 1998.

[34] B. Reichert, Y. Estrin, and E.H. Schuster. Constitutive modelling of the deformation behaviour of a precipitation hardened high temperature alloy. *Journal of the Mechanical Behaviour of Materials*, 9:69–82, 1998.

[35] S.O. Kruijver. A physically based model for the isothermal martebsitic transformation in a maraging steel. *ICOMAT 2002*, pages 437–440, 2002.

[36] V. Stolyarov J.M. Neto S.S. Tavaras, D. Gunderov. Phase transformation induced by severe plastic deformation in the aisi 304l stainless steel. *Materials Science & Engineering A358*, pages 32–36, 2003.

[37] J.A. Venables. The martensite transformation in stainless steel. *Acta Mat*, pages 35–44, 1961.

[38] J. Simo and T. Hughes. *Computational Inelasticity*. Springer-Verlag, New York, 1998.

[39] E. Atzema. *Sheet Metal and Sandwich Laminates*. FEBO ISBN 909006941-0, Rotterdam, 1994.

[40] J. Post, Beyer J. Vries, C. de, and H.J.M. Geijselaers. Verification tool for 2d multi-stage metal forming processes involving small parts made of stainless steel. *Shemet 2001*, pages 475–484, 2001.

[41] W.H. Press, B.P. Flannery, S.A. Teukolsky, and V.T. Vetterling. Numerical recipes in C. 1992.

[42] `http://members.ozemail.com.au/~comecau/index.htm`. *Computational Mechanics Australia Pty.Ltd.*, 2002.

[43] Romenofky. *Spaanloze vormgeving*. Springer-Verlag, New York, 1950.

[44] R.H. Myers. Response surface methodology - current status and future directions. *Journal of Quality Technology*, 31:30–43, 1999.

[45] J.-F.M. Barthelemy and R.T. Haftka. Approximation concepts for optimum structural design - a review. *Structural Optimization*, 5:129–144, 1993.

[46] H. Bakircioglo and T. Kocak. Survey of random neural network applications. *European Journal of Operational Research*, 126:319–330, 2000.

[47] A.J. Booker, J.E. Dennis, P.D. Frank, D.B. Serafini, V. Torczon, and M.W. Trosset. A rigorous framework for optimization of expensive functions by surrogates. *Structural Optimization*, 17:1–13, 1999.

[48] D. Hertog den and H.P. Stehouwer. Optimizing color picture tubes by high-cost nonlinear programming. *European Journal on Operations Research*, 140,2:197–211, 2002.

[49] D.C. Montgomery. *Design and Analysis of Computer Experiments*. John Wiley & Sons, New York, 2 edition, 1984.

[50] E. Aarts and J. Korst. Simulated annealing and boltzmann machine. *Wiley & Sons, Chichester*, 1989.

[51] D. Sacks, W.J. Welch, T.J. Mitchell, and H.P. Wynn. Design and analysis of computer experiments. *Statistical Science*, 4:409–435, 1989.

[52] A.R. Conn, N.I.M. Gould, and P.L. Toint. Trust region methods mps/siam series on optimalization. *SIAM Philadelphia*, 5:129–144, 2000.

Acknowledgements

As a large number of people have contributed to this thesis to a greater or lesser extent, I will mention them in chronological order.

The story started with M. Bliek, who stimulated me to embark on PhD research and write a thesis. In this early phase it was not yet clear what the research subject would be. At about the same time I had this discussions with M. Bliek and H. de Beurs Philips started using Sandvik Nanoflex™. In view of the complexity of this material, my activities gradually shifted towards the constitutive behaviour of Sandvik Nanoflex™.

Over the years there have been a number of people who have been of overriding importance for completing this thesis. R.M.J. Voncken made sure that the constitutive behaviour could be robustly implemented in our in-house Philips solver. Ruud and I both realised that the development of an in-house solver combined with the implementation of the complex behaviour of the Sandvik Nanoflex™material would probably take several few years. Hence Ruud suggested that this project would make an excellent PhD research subject.

Tj. de Vries always realised the importance of this research for Philips, which resulted in support from the people surrounding me at work and their willingness to take part in endless discussions on this subject until this very day.

C. de Vries and H. Nolles assisted me tremendously during the measurement of the transformations and the validation of the models.

T. van Amstel, who is always on the lookout for something new, was a great help during implementation of the model and with regard to the neural networks. This last together with T. Kessen

The Staff of the University of Twente (H.J.M. Geijselears, J. Beyer, K. Datta, J. Brinkman, J. Huétink and T. van Scherpenzeel) have also provided a great deal of assistance during the many discussions that have taken place over the years and that have helped to clarify the ultimate objective. During the trips from Drachten to Enschede, J. Beyer and I spent much time speculating about the behaviour of Sandvik Nanoflex™. The staff of the University of Twente mentioned above also played a large role in this research by supervising the various students who worked on the various subsidiary aspects of this research. Many students took part in the research: W.P Kikstra, C. de Vries, H Nolles, S.O. Kruijver, H. Veltkamp, B. Kleine dopke, R. Jousma, T. van Amstel, J. Diepstra, T. Kessen, B. Koopman, M. Groen, G. Engels and W.D. Purmer. They all made an important contribution and archiving their findings was quite a task.

I also required support regarding Latex, in which T. van der Boogaard, R. Jousma, R van Straaten and O. van der Sluis played an important part, I was and maybe I remain an outsider concerning Latex.

Dankwoord

Gezien het grote aantal mensen, dat in meer of mindere mate aan het tot stand komen van deze promotie heeft meegewerkt, zal ik mijn dankwoord geven in min of meer chronologische volgorde.

Aan het begin van dit verhaal staat M. Bliek. Hij heeft me gemotiveerd om aan een promotie te beginnen. In deze beginfase was nog niet duidelijk, wat het onderwerp precies zou worden. In dezelfde tijd, dat de discussies met M. Bliek en H. de Beurs liepen, begonnen we bij Philips ook met het toepassen van het Sandvik Nanoflex™. Gezien de complexiteit hiervan zijn mijn activiteiten gedurende de jaren steeds meer verschoven naar het constitutief gedrag van Sandvik Nanoflex™. In die jaren is er een aantal mensen geweest, die van doorslaggevend belang zijn geweest.

R.M.J. Voncken heeft er voor gezorgd, dat het 'constitutive' gedrag robuust geïmplementeerd kon worden in onze interne Philips solver. Ruud en ik beseften, dat de ontwikkeling van een eigen solver in combinatie met de implementatie van het complexe materiaalgedrag enkele jaren van ons leven zouden gaan kosten, waarop Ruud concludeerde, dat dit dan misschien een leuk onderwerp voor een promotie zou zijn.

Tj. de Vries heeft altijd het belang van het onderzoek ingezien voor Philips, hetgeen resulteerde in steun in de werkomgeving en de bereidheid om er eindeloos over te willen praten. Tot en met deze dag.

C. de Vries en H. Nolles hebben me geweldig geholpen met het inductief meten van de transformaties en de validatie van de modellen.

T. van Amstel, altijd op zoek naar wat nieuws, heeft veel geholpen bij de implementatie van het model en met het gebeuren rond de neurale netwerken. Dit laatste overigens samen met T. Kessen.

Daarnaast hebben de mensen van de UT (H.J.M. Geijselears, J. Beyer, K. Datta, J. Brinkman, J. Huétink en T. van Scherpenzeel) mij geweldig geholpen in de vele discussies, die hebben plaatsgevonden door de jaren heen. Het doel, waar we naar toe moesten, werd steeds duidelijker. Tijdens de ritten van Drachten naar Enschede, die ik samen met J. Beyer heb afgelegd, hadden we veel tijd om over het gedrag van Sandvik Nanoflex™te speculeren. Daarnaast hebben ze een grote rol gespeeld in de begeleiding van de diverse studenten, die aan de diverse deelaspecten hebben meegeholpen.

Studenten zijn er bij bosjes geweest. Ik noem: W.P Kikstra, C. de Vries, H Nolles, S.O. Kruijver, H. Veltkamp, B. Kleine Döpke, R. Jousma, T. van Amstel, J. Diepstra, B. Koopman, M. Groen, G. Engels en W.D. Purmer. Het moge duidelijk zijn, dat al dezen hun bijdragen geleverd hebben en dat alleen de archivering daarvan voor mij al een opgave op zich was.

Natuurlijk had ik ook de nodige ondersteuning nodig op het gebied van Latex, waarin T. van der Boogaard, R. Jousma, R. van Straaten en O. van der Sluis een belangrijke rol hebben gespeeld. Ik was en misschien blijf ik een leek op het gebied van Latex.

Mijn dank gaat ook uit naar M. Semmelink voor het gedeeltelijk vertalen en nakijken van de tekst. Zonder dit nakijken was het absoluut steenkolenengels gebleven.

In de eindfase moesten natuurlijk de puntjes op de i worden gezet. In deze fase hebben mijn directe collega's: M. Hommes, G. Klaseboer, R. Jousma en L. Vinkenvleugel (tevens mijn clusterleider) een grote rol gespeeld door me te ontzien dan wel direct te helpen bij het doen van de uiteindelijke simulaties. G. Klaseboer heeft zelfs een deel van de Philipsbureaucratie op zich genomen als een soort firewall. Mijn dank daarvoor. Een aantal collega's van de materiaalkundegroep en analysegroep heeft mij altijd bijgestaan. H.S. Blaauw speelt natuurlijk een grote rol door alle discussies rond Sandvik Nanoflex™en zijn werk op het gebied van de stress-assisted transformatie. Ook J. ten Hoor, R. van der Linden, A. Punter, H. de Boer, S. de Vries en R. van der Werf verdienen dank voor hun hulp bij al het meetwerk.

Niets had natuurlijk gekund zonder materiaal van Sandvik. Ik dank A. Sjöberg, S. Olsson, F. Sandberg en J.-O Nilsson voor het leveren van proefmateriaal en de nuttige discussies.

Graag bedank ik G.B. Olson voor zijn commentaar op mijn model, waardoor het een stuk vollediger is geworden.

E. Stinstra van CQM wil ik bedanken voor de hulp bij het doel van de 'process window study', een geweldige opsteker aan het eind van het traject.

Het ATC/MT team van het ATC en met name A. Gehring wil ik bedanken voor de ruimte, die is gecreëerd om deze promotie mogelijk te maken.

De leden van de leescommisie: O. Hoitinga, R. Mulder, L. Vinkenvleugel en Tj. de Vries wil ik bedanken voor hun bereidheid het geheel door te lezen en van commentaar te voorzien.

Als laatste wil ik mijn vrouw Marianne en mijn kinderen Dirk en Koen bedanken voor de ruimte, die ze geboden hebben, om me een aantal jaren te kunnen concentreren op dit promotiewerk.